A FEASIBILITY STUDY OF THE SPATIO-TEMPORAL ANALYSIS OF CARDIAC PRECORDIAL VIBRATIONS

A thesis submitted for the Degree of

Doctor of Philosophy

in the University of London

by

Ying-Sheung Cheung

November, 1977

Engineering in Medicine Laboratory
Department of Electrical Engineering
Imperial College of Science and Technology
London SW7.

ACKNOWLEDGEMENTS

I am greatly in debt to my supervisor, Professor B. Mac Sayers, not only for his continuous supervision, but also for the advice and encouragement he provided throughout this project. His patience and good humour have made my three years in the laboratory not only a rewarding but also an enjoyable time.

I am also grateful to the staff and many of my colleagues in the laboratory for their assistance in various ways. In particular, I wish to thank Mr. M.W. Ellis for his advice on the transducers, Dr. D.M. Monro for the use of his Fourier Transform and contouring programs, Mr. W.C. Cutler for his technical assistance and Dr. G. Lo for the many hours of fruitful discussion. I am also grateful to Dr. J. Verburg for sending me a copy of the manuscript of his work before it is published.

I extend my gratitude to my friends, Roy and Hazel McClelland, for their encouragement and support during my writing up of the thesis in Belfast, and to Miss. M. Burns for taking up the burden of typing the final thesis. The constant support of my twin brother, Peter, throughout the past four years has meant much to me.

Finally, I wish to express my gratitude to my dear friend, the late John Branch, by dedicating this work to him for his companionship and assistance during the first two years of this work.

This project was carried out during the tenure of the University of London Postgraduate Studentship.

TO:

JOHN

ABSTRACT

The present work attempts to develop an adequate procedure for the measurement of cardiac vibrations over the entire precordium, to study the vibrations thus measured using various spatio-temporal presentations and signal analysis techniques and to determine the likely value of such techniques in this field. A significant purpose of the work has been to develop (or extend) signal processing methods that can be used not only in this and other spatio-temporal studies, but in processing other kinds of biological signal to which they are relevant.

These objectives were achieved. An adequate method has been developed which gave a set of reliable and reproducible measurements of cardiac vibrations over the entire precordium of a normal subject. A spectral averaging procedure devised for the pre-processing of the measurements represents a significant contribution to the understanding and handling of phase spectra of signals. A series of spatio-temporal presentations and analysis of the measurements demonstrates how such signals can be investigated and studied. The analysis suggests that the observed precordial vibrations are contributed from waves generated by multiple sources and transmitted to the precordium through multiple pathways. These pathways can have different frequency characteristics resulting in different groups of frequency components being spread differently over the chest wall.

Detailed investigation into the possibility of obtaining a set of 'inverse sources' which could have produced the measured vibrations were made based on an oscillating-sphere model in an infinite viscoelastic medium. The inversion was obtained by the conventional least square and a constrained least square method. The latter was found to give more satisfactory results. The likely value, the limitations and the associated difficulties in solving the 'inverse problem' in precordial cardiac vibrations were discussed.

The findings of the work suggest that 2-dimensional recording and analysis of precordial cardiac vibrations can be of possible value and warrant further investigations. The methodology developed offers a convenient starting point for further studies into the interpretation of the 2-dimensional measurements in normal and pathological cases.

CONTENTS

CHAPTER 1

INTRODUCTION

1.1 Background

A well established method in vibration engineering to investigate the condition of a mechanical system utilizes the measurement of vibrations of the structure at suitable locations in the system; any deviation of these vibration measurements (usually characterized by their spectral content) from the normal indicates a possible fault in the system.

The vibration measured on the precordium due to cardiac activity can contain frequencies from about 1 Hz to 1000 Hz. In the infrasonic range the pattern is usually known as a vibrocardiogram, which is mainly appreciated by inspection and palpation. In the audible frequency range the vibration is known as a phonocardiogram. The audible vibrations are often attributed to the hydraulic pressure transients associated with abrupt acceleration and deceleration in blood flow as in the case of heart sounds and to the turbulence in blood flow as in the case of murmurs.

Information about the functioning of the heart is contained in:- (i) the timing, (ii) the amplitude and (iii) the wave pattern of the precordial vibration in relation to the locations where the observations are made

on the thoracic surface. Any malfunctioning of the system can vary one or more of these factors. Therefore maximum information should be obtained if all these factors are taken into consideration. To achieve this, one has to measure the precordial vibration at a certain number of sites over the area of interest in order to produce an adequate spatial picture of the vibration. The present work attempts to study the precordial vibrations in the spatio-temporal context.

1.2 Earlier Investigations

A number of workers have measured the precordial vibrations at multiple sites for different purposes. Very few, however, had considered the four variables: timing, location, amplitude and wave-shape simultaneously.

As early as 1952, Dunn and Rahm (1952) recorded the precordial vibrations using three identical microphones at a time and the results were plotted on a radiograph of the subject's chest. It was found to be useful to clinical studies of heart diseases. Faber and Burton (1962) recorded the heart sounds at 4 to 7 locations on the chest wall and measured accurately the arrival time delay of the first heart sound between each pair of points. From these delays, they established the estimated velocity of propagation of heart sound to be about 15 m/sec for the 100 Hz component over the chest surface. They also located the 'secondary source' for the mitral component of the first sound assuming that the vibration had been transmitted from the source of

generation to the 'secondary source' and then spread over the chest wall surface. Shah et al., (1964) repeated the experiment on subjects with Starr-Edward valve and obtained a different conclusion. Zalter et al., (1963) studied the acoustic transmission characteristics of the thorax by measuring the intra-cardiac and pre-cordial heart sounds and estimated the mechanical transfer impedance of the thorax for frequency between 40 and 500 Hz. In another paper Faber (1963) studied the damping of sound on the chest surface by applying an external sound source to the sternum and concluded that the damping is proportional to the distance, d, from the surface source rather than d^2 as previously believed. The damping due to the viscosity of the structure depends on the square root of the frequency.

In a study of the modelling of transmission of cardiac vibrations, Verburg (1975) measured vibration across a row of twelve locations simultaneously and observed a phase reversal of vibration pattern for the second heart sound across the chest wall. Three models for the mode of transmission of the vibration:- (i) a pulsation model, (ii) a surface wave model as proposed by Faber (1962) and (iii) a mechanical dipole model suggested by Verburg himself were investigated. From the measurements, he concluded that the dipole model gave the best description of the transmission of heart sounds.

The study of sound (or vibrations) distribution on

the human chest wall was not only confined to the physical characteristics of the chest wall and the transmission pathways, but also had been considered to be very useful in enhancing and guiding clinical diagnosis. Shah et al., (1964) suggested a revision of the classical areas of auscultation based on clinical experience and knowledge supplied by intra-cardiac phonocardiography and physiological principles. Sainani et al., (1967) confirmed their conclusion by systematically measuring the amplitude of different components of the heart sounds at different sites on the precordium and established the corresponding areas of auscultation. In a further study (1968), they documented the best location for recording abnormal heart sounds and murmurs.

Hayashi (1973) recorded the first, second heart sounds and murmurs at 98 to 140 sites on the chest wall using QRS complex of the ECG as time trigger. Best beats of vibrations were then visually selected and maps of equal intensity contours were plotted for the maximal integral of the vibration patterns at each location using linear interpolation.

1.3 Proposed Investigations

Although multi-site measurements and investigations of precordial vibrations had been explored extensively, we could not find any record of previous work where the precordial vibrations are measured and studied in spatio-temporal terms. In majority of the studies, except in the

work of Hayashi (1973), measurements were made at a few sites where 'useful signals' were expected. Hayashi's study was, however, limited to the contouring of the maximal value of intensity of activities at each measurement location and the temporal relationships between signals at different sites were not considered. Moreover, we believe that the measurement of as many as 140 sites on the chest wall can be rendered unnecessary if a more efficient method is employed for interpolation. It should be feasible to determine from the spatial spectrum how many observation points are required.

As indicated by previous works, the value of spatio-temporal measurement and analysis of precordial vibrations, both in the study of the physical and physiological mechanism of transmission of cardiac vibrations and in the assessment of clinical diagnostic procedure, is at least a possibility. The main obstacle in such a spatio-temporal study had been the vast amount of data needed to be measured stored and analysed. With the present day advances in digital computers, ~~there~~ this is no longer a limiting factor. However, before any extensive study can be explored, an engineer would seek to answer the following questions:-

(1) Is there any procedure for the measurement of precordial vibrations which is both practical and capable of giving representative, time-synchronised signals over the entire chest wall?

(2) Are there any positive indications that spatio-temporal measurement and analysis of precordial vibrations can be more informative than just temporal measurements?

(3) How can such spatio-temporal signal be handled?

The present study can be divided into three phases:-

(1) The design of an adequate measurement scheme for the measurement of vibrations over an area of the precordium where signals of substantial strength can be detected.

(2) Study the signals thus measured using various spatio-temporal signal analysis methods.

(3) Investigate the possibility of solving the inverse problem of precordial vibrations based on a variable orientation multiple 'dipole' model as a means of condensing the information in the spatio-temporal signals.

CHAPTER 2

DATA ACQUISITION AND PRE-PROCESSING

2.1 Introduction

Prior to the detailed discussion of the experimental design, data acquisition procedure and pre-processing techniques, it is necessary to clarify what we intended to measure.

The complex vibratory phenomenon produced by the motion of the heart and transmitted to the precordium is far more than what is perceived by the auditory system of man in auscultation. The heart sounds and murmurs are but only part of this vibration. This leads some investigators (LUISADA, 1972) to rename 'phonocardiography' as 'acousticardiography' or 'mechanocardiography'. Although how such vibration is transmitted to the chest wall is not exactly known, there are clear indications that vibrations in living tissues are transmitted both as shear waves and compression waves (von GIERKE, 1952; FRANKE, 1951). The vibrations due to cardiac activity are likely to be dominated by shear waves especially at the low frequency end of the spectrum. Therefore heart sounds are sounds as such only up to the point that the vibrations transmitted to the chest surface set the air at the skin-air interface to vibrate and produce sound waves. For this reason, we shall use the term 'vibrations' instead of 'sound' to describe the measured phenomenon.

This vibratory phenomenon covers a frequency range from less than 1 Hz to over 1 kHz. However, as a feasibility study, we confine our signal of interest to the most energetic band of the spectrum. Earlier investigators had found that most of the energy in precordial vibrations (except for murmurs) is contained in frequencies less than 100 Hz (RUSHMER, 1970; BURTON, 1971; LUISADA, 1965; McKUSICK, 1958). We therefore choose 100 Hz as our upper frequency limit of our signals.

The objective of the data acquisition procedure is to obtain a representative spatial set of precordial vibrations of the prescribed frequency range at many sites over an area on the chest surface where substantial signal can be detected.

2.2 General principles of the experimental design

There are generally two different approaches in the measurement of temporal signals at multiple sites. In principle, such measurements should be made simultaneously but serial measurements should also be feasible.

Simultaneous measurement offers the convenience that all signals measured are already time synchronised and can be interpreted directly as a spatio-temporal signal. This advantage, however, is accompanied by a number of problems. First, the transducers have to be identically matched to allow sensible comparison to be made between signals from different sites. Many costly transducers are needed. Because the number of spatial sites usually outnumber the

the data channels in most data acquisition computers, a separate channel scanning and multiplexing unit is required to scan all the transducers. A large number of transducers attached to the subject can cause unacceptable loading on the chest surface and distort the measurements. As a feasibility study and with limited resources, we therefore chose the alternative approach.

Serial measurement, however, implies that measurements at different sites have to be synchronised. The on-set of the cardiac electrical activity as indicated by the QRS complex can only serve as an approximate time reference. The delays between the QRS complex and the onsets of the first and second vibrations are mainly dependent on the ventricular filling of the preceding cardiac cycle, which, in turn, is affected by various factors like heart rate and changes of intra-thoracic pressure at different phases of respiration. (LUISADA et al., 1941; MESSER et al., 1951; WAYNE, 1973). A long diastolic interval in the preceding cycle shortens the on-set of the first vibration with respect to the QRS complex, as less time is needed to build up the pressure in the ventricle and close the atrio-ventricular valves, but prolongs the delay of the onset of the second vibration because more blood needs to be emptied. The reverse is true for a short preceding diastolic interval. Since no accurate time reference is available, a pre-processing method which does not require a time reference is needed. In addition, the signals obtained from different

sites, even if they are synchronised, are individually subjected to variabilities in waveshape and amplitude. These statistical variations have to be removed by suitable methods before the data can be studied as a set of spatio-temporal signals.

Preliminary studies indicated that the main source of variability in the measurements was respiration. Directly, respiration causes low frequency movements of the chest wall close to the frequency of the heart beat as well as high frequency vibrations produced by turbulence of air in the airways. Indirectly, it changes the geometry of the thorax, the position and orientation of the heart with respect to the precordium, and other conditions (e.g. thoracic pressure and heart rate) of the whole haemodynamic system. Some workers had asked the subject to halt breathing for a few seconds during which measurements were taken. We found that this interruption of the respiration cycles not only caused discomfort but also introduced unacceptable changes in the haemodynamic system.

These problems were eliminated very satisfactorily by asking the subject to synchronise his breathing to a respiration indicator - a defocused spot on an oscilloscope. With the time base turned off, the y-amplifier of the oscilloscope is driven by a respiration waveform generated by a low frequency function generator. Figure 2.1 is an example of the respiration waveform. This method

not only allows vibrations from the same phase of respiration to be selected, but also has the desirable effect of greatly reducing all the other variabilities.

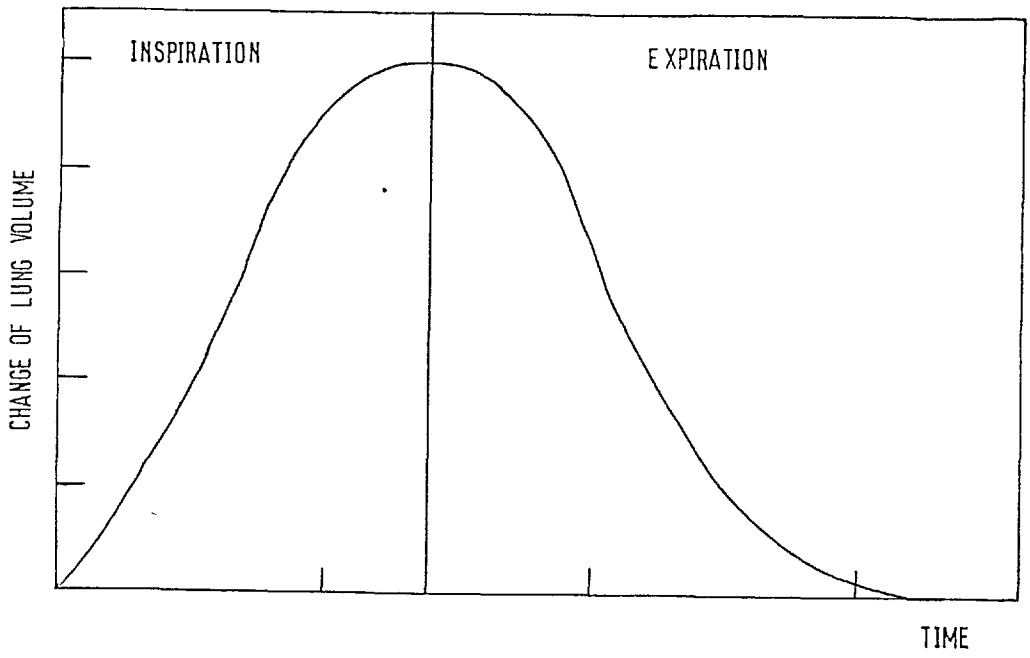

Figure 2.1 An example of the respiration waveform used for synchronization

2.3 Transduction

The basic technical problem concerning the transduction of chest wall vibration is the one of loading, that is, the alteration of the vibration at the measurement site due to the presence of the transducer. If the loading is significant, tedious calibrations would be necessary. This problem is realised by many researchers (TAKAGI et al., 1964; ROTTERDAM et al., 1967; VOLLENHOVEN et al., 1968, 1971; IKEGAYA et al., 1971). Since the

idea of mechanical impedance of body tissues was employed by von GIERKE and FRANKE (1952, 1951), different methods were developed to calibrate the transducers. The calibration procedures often require tedious measurements of the mechanical impedance of the transducer and the tissue at the locations where the transducer is placed, as well as the mechanical coupling between the body surface and the transducer. These measurements are not possible with the equipments available to us. Indeed, even if the suitable equipment were available, it would be necessary to do the calibration over many sites since the mechanical impedance of the chest wall changes over the precordium. Therefore one of the most important criteria for our choice of transducer is to achieve minimum loading.

The transducers generally employed in phonocardiography can be catagorized into (a) non-contact type, (b) contact type and (c) absolute method. A number of transducers were tried. The following is a brief survey of different possible transducers. A miniature accelerometer type of transducer was identified as most suitable for our purpose.

Non-Contact Type

The two common transducers are air-contact microphone and the capacitor transducer. In the air-contact microphone, a closed air chamber separates the skin surface and the diaphram. The displacement at the skin surface is converted into a pressure which acts on the diaphram. The

shape, volume and size of the air chamber are important because cavity resonance of the chamber can cause distortion. Methods had been developed to calibrate them when used as phonocardiographic transducers (Van VOLLENHOVEN et al., 1970). This type of transducer, however, is very vulnerable to ambient noise and usually gives poor S/N ratio unless it is used in a sound proof room. Another example of non-contact type of transducer is the capacitive transducer where the skin surface is used as the movable plate of a condenser element. Although this method eliminates the problem of ambient noise, it is very difficult to calibrate. The circuitry involved in the measurement is very complex. The area of the plate has to be large for a reasonable reading and the fixed plate must be very close to the skin without touching it. The separation between the skin and the fixed plate is difficult to control.

A new air-contact type transducer using the hot-wire anemometer principle was developed by LAUGHLIN et al., (1972). The movement of the skin is amplified hydraulically by sealing a plastic cup over the area of interest. The plastic cup opens into a narrow plug where a sensing element of hot tungsten wire with gold flash coat is mounted at the centre. The tungsten element could be replaced by a thermister for low frequency measurements. The movement of the skin, in this case, is converted into variation of air flow rate over the sensing element. This

changes the temperature, and therefore the resistance, of the hot-wire. The advantage of such a device over the conventional air-contact devices is its high sensitivity due to the hydraulic amplification and its insensitivity to ambient noise. However, the device is very difficult to calibrate and the plastic cup has to be heavy enough to avoid its own movement and may, therefore, introduce substantial loading.

Contact Type

The direct contact transducers usually consist of an element such as a button or a bar which is in direct contact with the body surface. The other end of the contact is connected to a sensing element. The moving coil transducer is an example. But nowadays piezoelectric crystals, which are much cheaper and lighter, are most widely used. It is sensitive and easy to use. However, the loading presents a problem. In all non-absolute measurement methods the whole transducer is resting on the body and the displacement measured is actually the relative displacement of the skin inside the transducer with respect to its frame (figure 2.2). Therefore for both contact and non-contact type transducers the frame of the transducer must have a minimum weight so that it does not bounce up and down with the vibration. This indirect loading could disturb the whole transmission pattern. In the case of contact type transducer, a certain amount of energy is required to drive the contact before any reading can be

obtained. This causes a direct loading in addition to the indirect loading. In addition to the loading problem, another objection in using piezoelectric transducers is that its amplitude and phase response are too dependent on the static pressure applied to it (Van VOLLENHOVEN, 1971). This is even worse if the transducer is kept in place by a rubber strip because the pressure of the rubber strip on the transducer is very variable and is very difficult to measure. A piezoelectric microphone built for such purpose was found to be unsatisfactory in this respect.

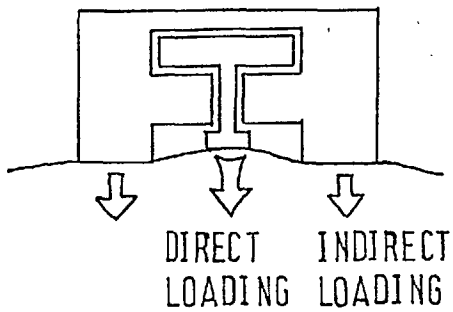

Figure 2.2 Direct and indirect loading

Absolute Methods

The preceding methods actually measure precordial movement relative to the chest wall where the transducer is mounted. In absolute methods, the movement of the chest wall is measured relative to a rigid reference external to the body. A transducer using a photopotentiometer (Photain Control Ltd.) was developed. A light plate with a narrow horizontal slit was attached normal to the body surface such

that any vibration of the chest wall will cause the slit to move accordingly. The plate is made to intercept the light illumination on the photo-potentiometer which, therefore, register any movement of the slit (figure 2.3). This method, although eliminating the problem of loading as the plate can be made lighter than 1 gm, was found to be impractical in an experimental situation. The main difficulty was the optical alignment of the device which was very tedious, time consuming and very often inaccurate. Other unwanted non-cardiac movements also caused unacceptable artefacts.

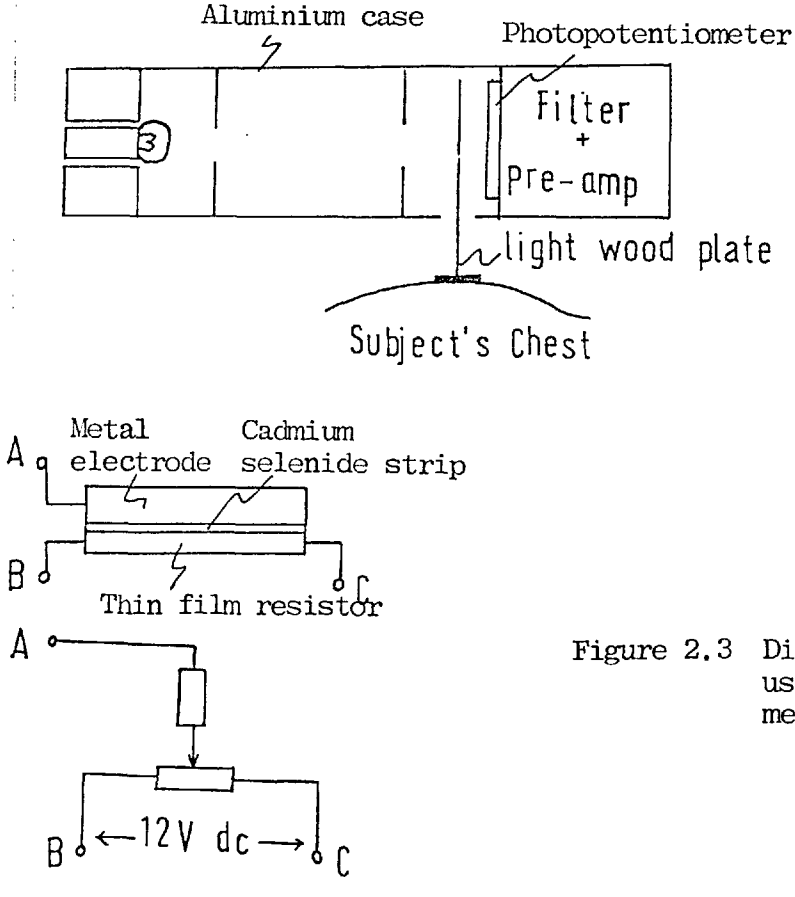

Figure 2.3 Displacement measurement using photopotentiometric method

An alternative way of achieving absolute measurement without the need of tedious alignment with a rigid reference is by accelerometers. BEW (1971) and VERBURG (1974) had used miniature accelerometers to measure precordial movements. A similar accelerometer (J. Langhan Thompson, BLA-1) developed for the RAF institute of Aviation Medicine was available to us, which meets our requirements. It consists of a double-arm piezoresistive strain gauge actuated by a damped cantilevered mass (fig. 2.4). Acceleration of the base structure of the device causes bending on the cantilever, the magnitude of which depends on the mass, the stiffness of the cantilever and is proportional to the acceleration of the base. The change of resistance of the strain gauge can be measured using a Wheatstone bridge. The accelerometer weighs less than 2.5 gm and has a sensitivity of 0.4 mV/g with a bridge voltage of 5 Volts. It has a flat response (fig. 2.5) up to about 100 Hz with resonance at about 140 Hz. The calibration procedure and the strain gauge amplifier circuit are given in appendix A. Higher sensitivity and resonance frequency can be achieved if necessary, but the JLT-accelerometer appeared to be satisfactory for our purpose.

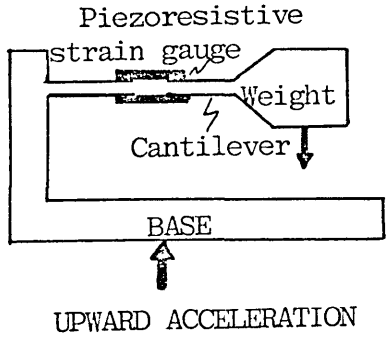

Figure 2.4 Basic principle of cantilever accelerometer

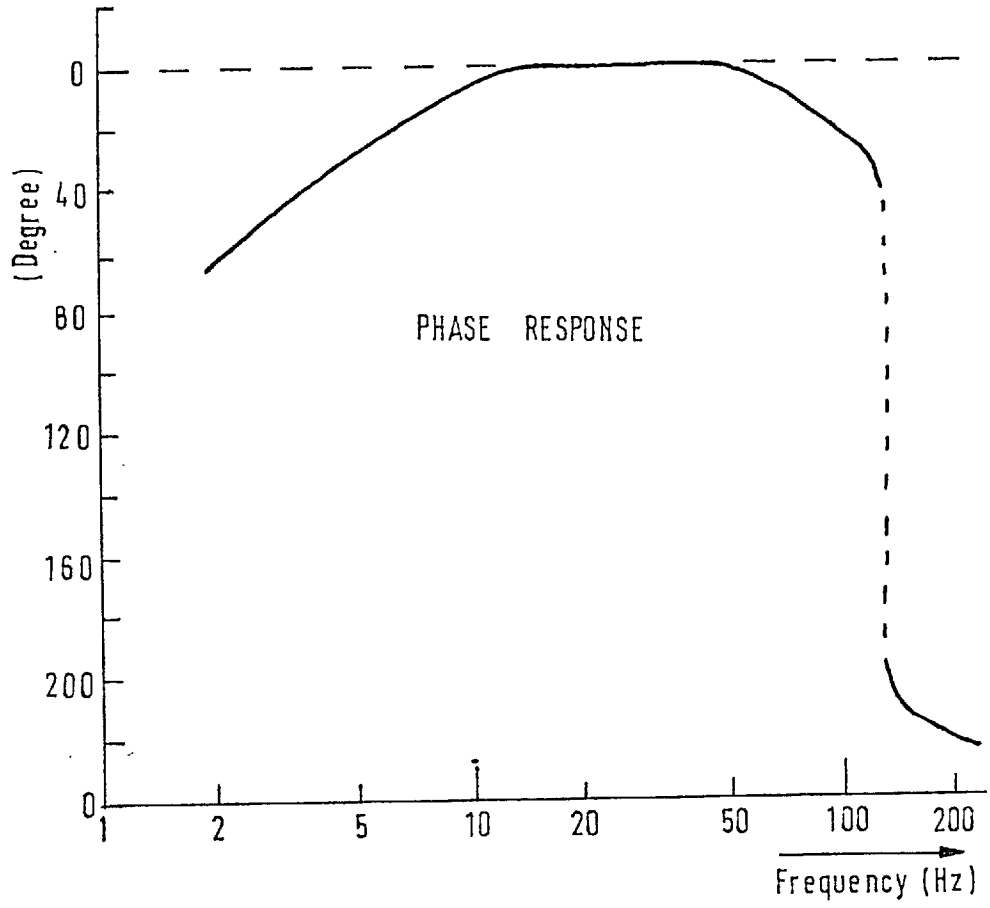

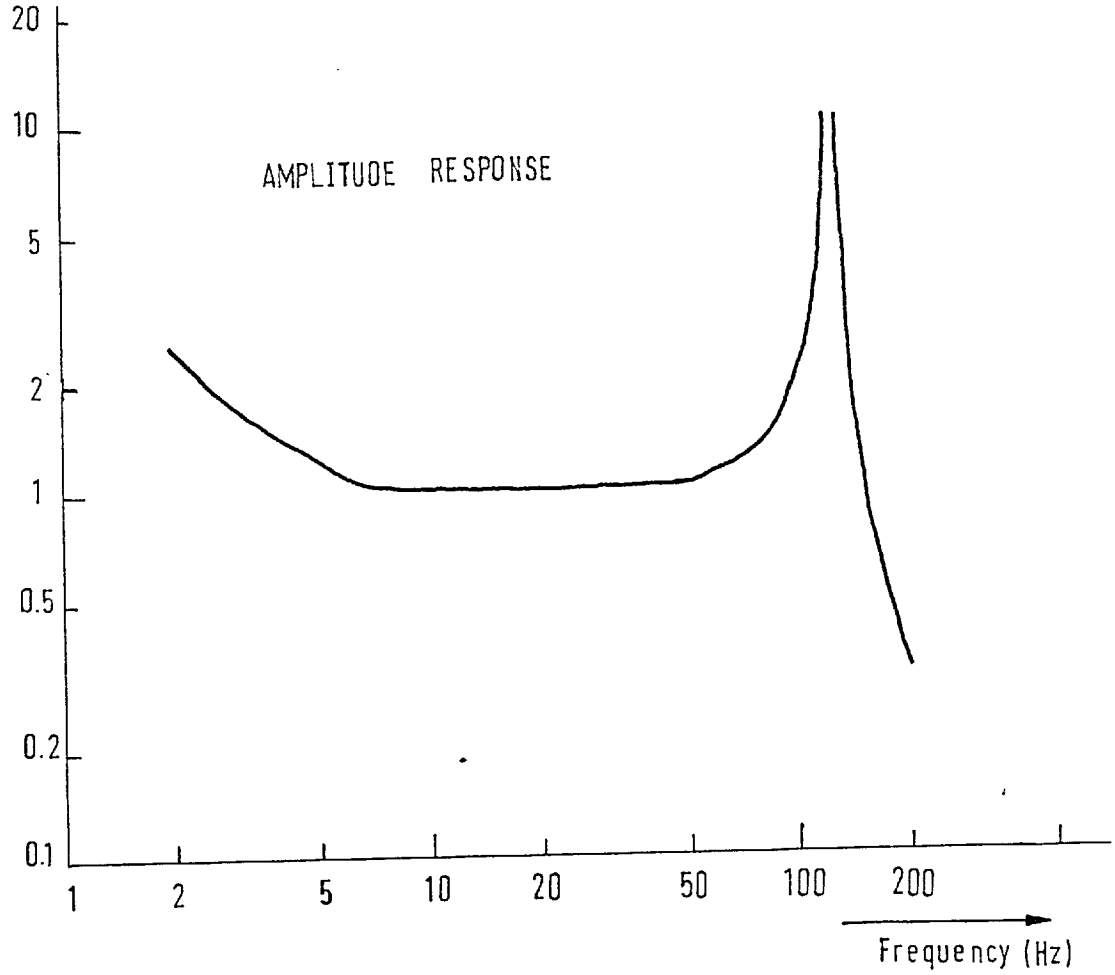

Figure 2.5 Amplitude and Phase characteristics of the BLA-1 accelerometer

The miniature accelerometer has the following advantages over other devices described:-

(i) Light weight and therefore small loading on the chest wall.

(ii) Gives 'absolute' measurement of the vibration.

(iii) Convenient and comfortable to use.

(iv) Gives emphasis on high frequency vibration (since acceleration increases with square of frequency for the same displacement) while preserves the displacement information (BEW et al., 1971).

The effect of loading caused by the weight of the accelerometer was assessed by an indirect method. Vibrations at a precordial site were measured with small weights added on the accelerometer in steps of 1 gm. The observations were compared for different amount of loading. Figure 6 shows examples of observations taken at the same phase of respiration (end of expiration) for 0 to 3 gm of additional load. If the loading of the accelerometer is significant, the measurements are expected to alter if the weight of the accelerometer is doubled. Little change of the measurement was noted even with an addition of 3 gm added on the accelerometer. Therefore it was concluded that the loading was insignificant.

2.4 Experimental Procedure

The vibration was measured serially over 49 sites in a 7 x 7 equally spaced grid from a normal 17-year-old healthy

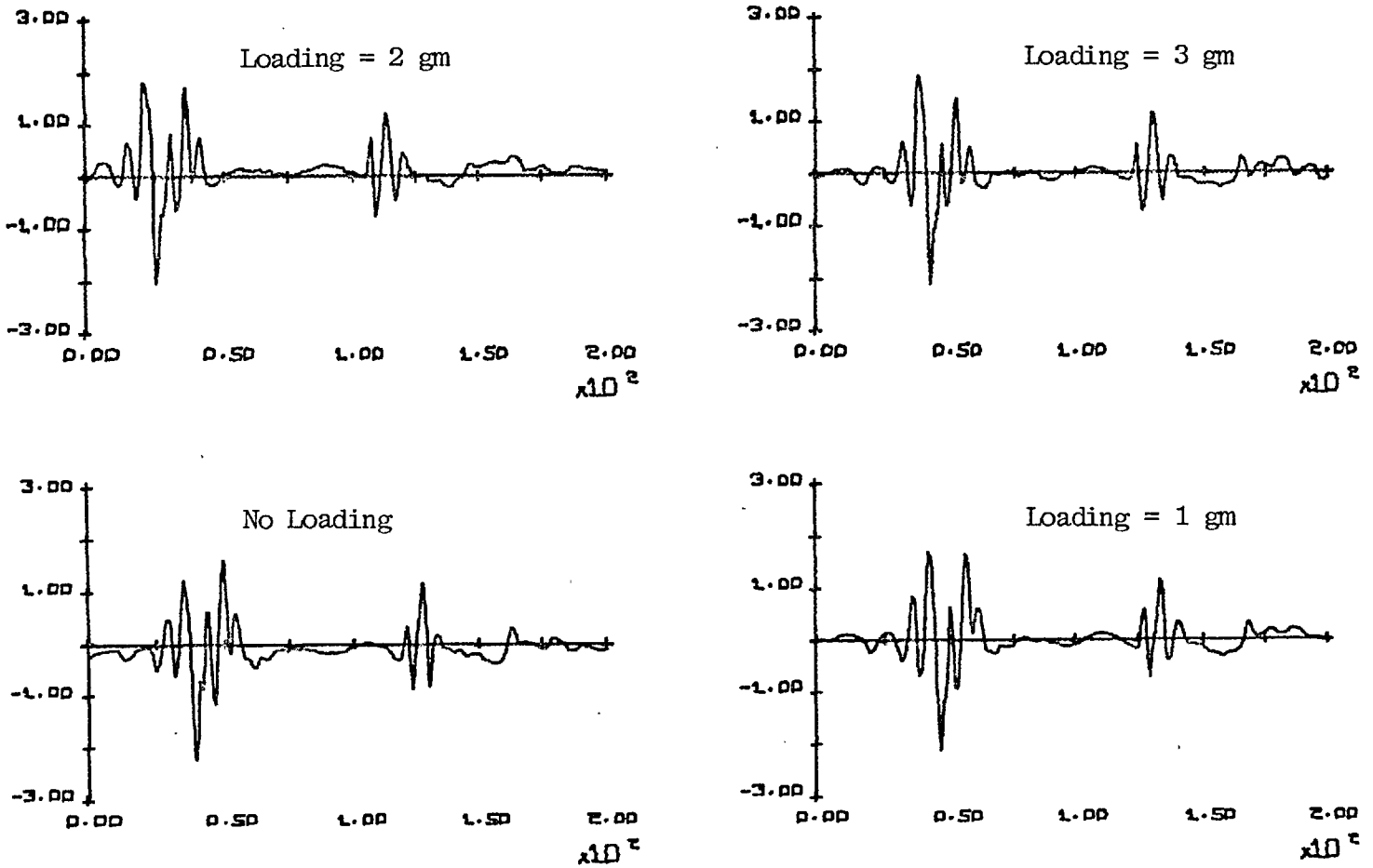

Figure 2.6 Acceleration waveforms at the same site with different loading; the abscissa is sample number = 200 x 1/256 sec maximum

male subject (without any previous heart or chest complaint). The measurements were taken at 3 cm spatial intervals covering an area of 18 x 18 cm^2 immediately above the heart, biased to the left, with the subject lying in the supine position. The third column from the left corresponds to the sternum and the fifth row from the top corresponds approximately to the fifth intercostal space.

The precordial vibration, the ECG and the respiratory synchronous waveform were recorded simultaneously on a FM recorder (Precision Instrument) and later digitized by an IBM 1800 data acquisition system. The digitized data were stored on digital magnetic tape for further processing and analyses. The vibration was low pass filtered at 100 Hz with 30 dB/octave roll off (Alison passive filters) and were digitized at a rate of 256 sample/sec. A two minute recording was taken from each recording site. The experimental procedure is summarized in figure 2.7. Figure 2.8 shows an example of the digitized signal.

The very low frequency movement of the chest wall caused by respiration was removed by filtering in the frequency domain. The vibration signal was divided into 16 second segments (4096 data points) and tapered to zero from 10% of each end by a raised cosine bell. Their spectra were computed using the Fast Fourier Transform Algorithm (FFT) and all frequency terms less than 0.8 Hz

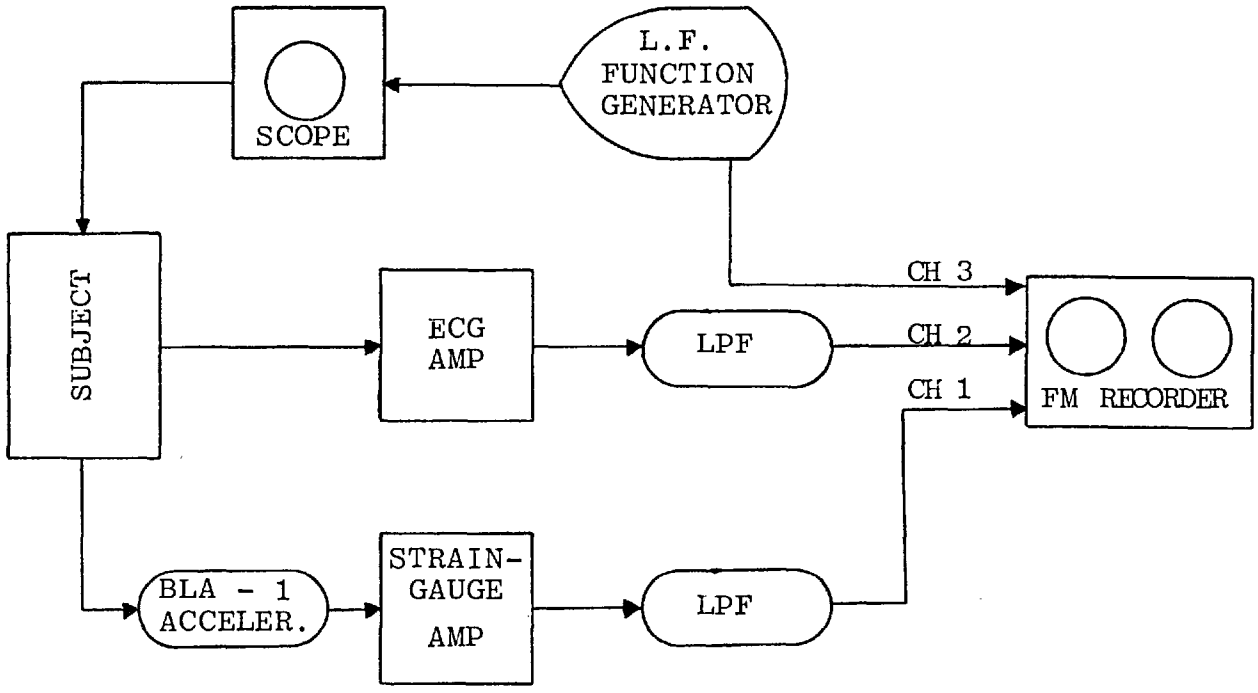

Figure 2.7 Block diagram of the experimental set-up

were set to zero. The time domain signal was reconstructed from the filtered spectrum. The displacement signal was also derived from the acceleration spectrum at this point by dividing each spectral component with minus the square of the corresponding frequency in Hz. This has the same effect as integrating the signal (acceleration) twice with the integration constant set to zero, that is, assuming the subject's body as a whole was not moving and can be taken as a fixed reference. ' An alternative approach using phaseless recursive filtering method was employed by VERBURG (1974) but we found that the frequency domain method is simpler to use and gave

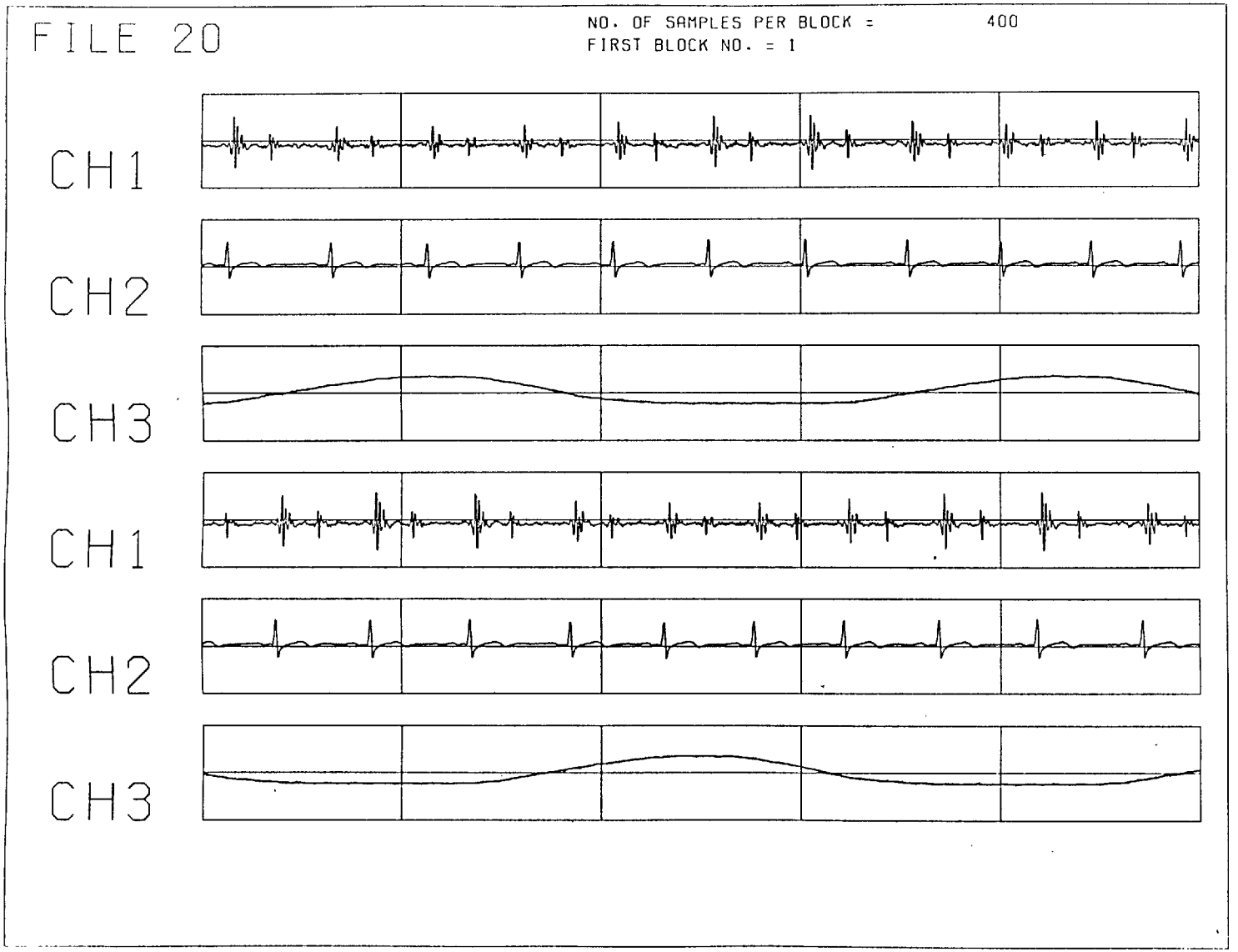

Figure 2.8 An example of the digitized data, CH 1 - precordial vibration; CH 2 - ECG; CH 3 - respiration synchronizing waveform

satisfactory results. Figure 2.9 demonstrates the effect of the filtering procedure.

Individual beats were isolated from the record using the R-peak of the ECG as time markers. This constituted 117 msec (30 samples) pre- and 664 msec (170 samples) post-R-peak of the vibration signal. This period was selected so that all the activities in the first and second vibrations were included without any overlapping from the proceding and subsequent beats. In this way, each vibration record can be conveniently divided into equal halves (100 samples, 390 msec) for the two vibrations with little activities occuring near the edges of the signal so as to minimize truncation effect when the signal is divided into the two components. Only those beats which satisfied the following criteria were selected for processing and analyses: (1) the ~~best~~ beat occurred at the end of expiration when the chest was in a resting position; (ii) the preceding R-R interval fell within $\pm$ 1 SD of the average interval. These criteria were set to reduce the undesirable variability caused by respiration and different degrees of ventricular filling.

In this way, 25-35 beats were obtained for each measurement site. An example of such an ensemble of vibration is shown in figure 2.10. Each of these beats could be thought of as a sample taken from a population of beats for that particular location with certain statistical variabilities. The variabilities mainly manifested in

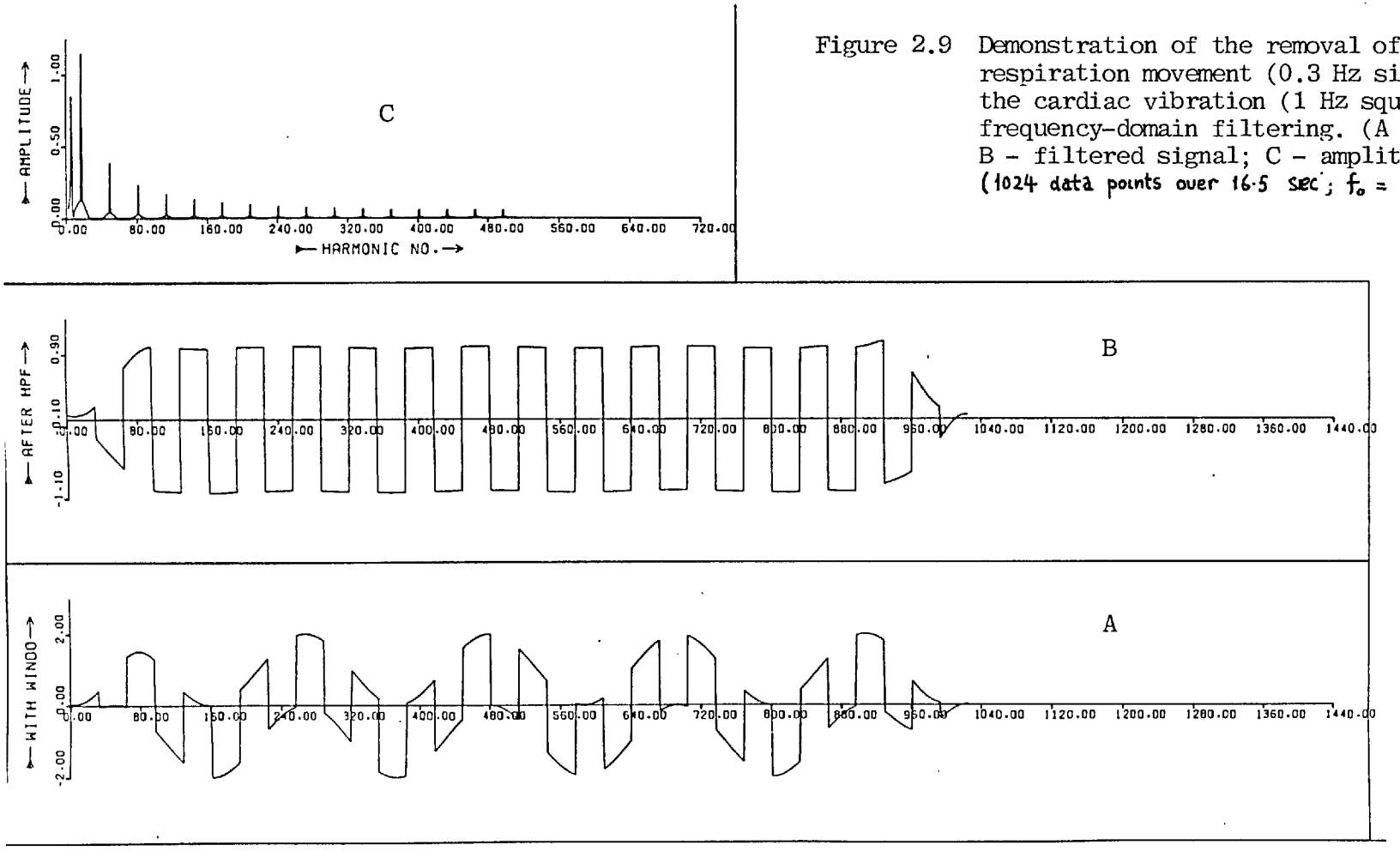

Figure 2.9 Demonstration of the removal of low-frequency respiration movement (0.3 Hz sine wave) from the cardiac vibration (1 Hz square wave) using frequency-domain filtering. (A - original signal; B - filtered signal; C - amplitude spectrum of A) (1024 data points over 16.5 sec; f_o = 0.06 Hz)

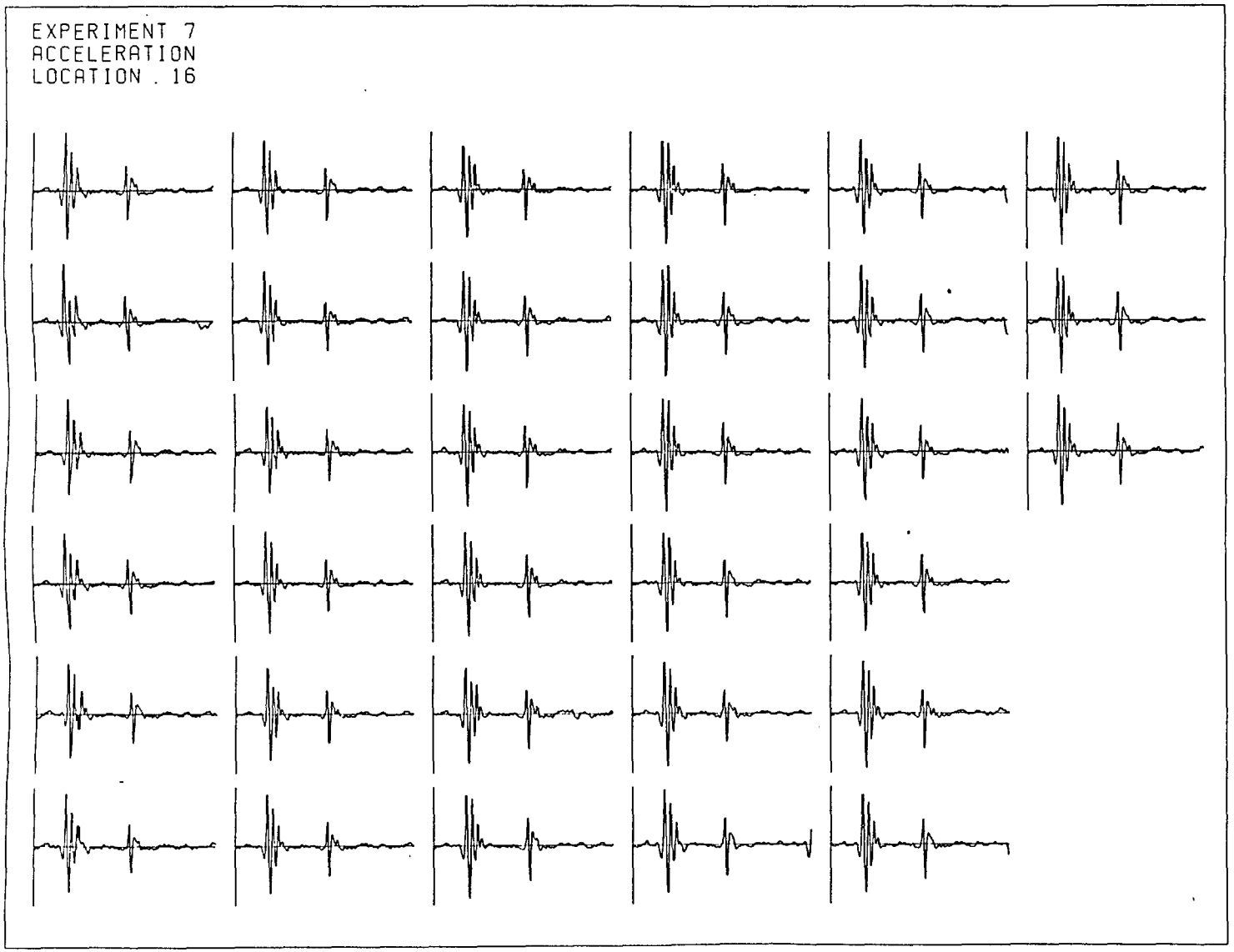

Figure 2.10 An example of an ensemble of selected vibration beats from one measurement site (Location (3,4))
(220 data points over 0.78 sec)

three signal features, namely: (i) the signal amplitude; (ii) the time of onset of the vibrations with respect to the electrical activation and (iii) the wave pattern of the signal. In order to obtain a reasonable representation of the vibration at each site so that comparison of signal from different sites could be meaningful, these variabilities have to be assessed and, if possible, reduced by suitable means.

2.5 Pre-processing Procedure

The variation of the onset of the vibrations with respect to the QRS complex discussed in section 2.2 render the coherent averaging method unsuitable for our purpose. Adding a number of time-jittered signals is equivalent to convoluting the true mean signal (figure 2.11a) with a series of dirac pulses symmetrically distributed about zero time. If a large number of such signal are to be added, the series of pulses can be represented by its distribution curve (figure 2.11b). The convolution is equivalent to filtering the signal spectrum by a low pass filter the severity of which depends on the degree of dispersion. This is usually known as the 'smearing effect'.

A spectral averaging procedure was developed which was found to be most appropriate for the signal concerned. Firstly each selected beat of vibration from the ensemble of the same site was separated equally into its corresponding first and second vibrations. The two signals were then tapered at 10% of its length at each end by a half cosine

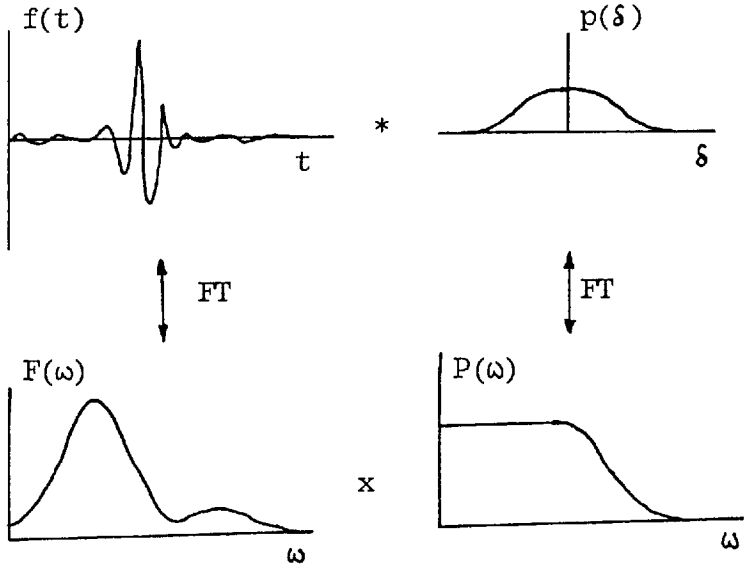

Figure 2.11 The smearing effect of time jittering in coherent averaging

bell to reduce the effect of truncation on their spectra. It was noted that none of the main activities in both vibrations were affected by the tapering because the time window was chosen such that the main vibratory activities occurred well away from the edges. The amplitude and phase spectra of the vibrations were then computed by FFT and subsequently averaged. The equivalent averaged singals were finally reconstructed from the averaged amplitude and phase spectra.

The principle that this averaging method employed becomes obvious once we recognize that the effect of any time jitter in a signal is to cause a linear trend being added to its radical phase spectrum, the gradient of which

is proportional to the time shift. This additional linear trend would have a positive or a negative slope depending whether the vibration comes forward before or after the mean onset time (see equation B.2). Hence by averaging the phase spectra one tends to reduce the variability of the time delay of the onset of the vibration with respect to the time reference. In other words, the latency of the 'averaged' signal would be closer to the expected latency for that location. In this way, synchronization between measurement sites was achieved. A detailed discussion on spectral averaging can be found in appendix B. It is also shown that the procedure reduces the effect of any additive noise component from the average noise level

$$\frac{1}{n} \sum_{i=1}^{n} |N_i(\omega)|$$

to

$$\frac{1}{n} \sum_{i=1}^{n} \left(\tfrac{1}{2} \sin^2 \theta_i(\omega) \left| \frac{N_i(\omega)}{S_i(\omega)} \right| \right) |N_i(\omega)| \qquad \ldots\ldots\ldots\ldots\ldots \quad (2.1)$$

Provided that $|N_i(\omega)| \ll |S_i(\omega)|$.

The computation of the mean phase value from a sample of phase angle was complicated by the wrap around nature of phase angle. For instance, the arithemetic mean of two phase value 175° and -175° is zero while we know that the true mean phase value should be 180°. This difficulty was

overcome by a simple algorithm which calculated the mean phase value by finding the phase angle of the resultant of n unit vectors each with the corresponding phase value to be averaged. Hence,

$$\bar{\theta} = \tan^{-1}\left(\frac{\sum_{i=1}^{n} \sin\theta_i}{\sum_{i=1}^{n} \cos\theta_i}\right) \quad \ldots\ldots\ldots\ldots\ldots \quad (2.2)$$

There is an additional problem with the spectral averaging procedure. Since the amount of phase shift caused by a given time shift increases proportionally with frequency, the average phase angle estimate for the high frequency components could be 180^{o} out of phase with its actual mean value due to the wrap around effect of phases, if the amount of time jitter of the signal exceeds a certain limit. This is best demonstrated by the circular histogram plot of the phase distribution in figure 2.12. Note that as the amount of phase scatter increases up to a certain limit, the mean phase estimate becomes 180^{o} out of phase with the true mean phase value. This effect, however, was found to be insignificant in our signal as will be shown in later section.

Before the averaged data can be analysed as a representative set of spatio-temporal signal, a few aspects of the averaged signal and the averaging procedure need

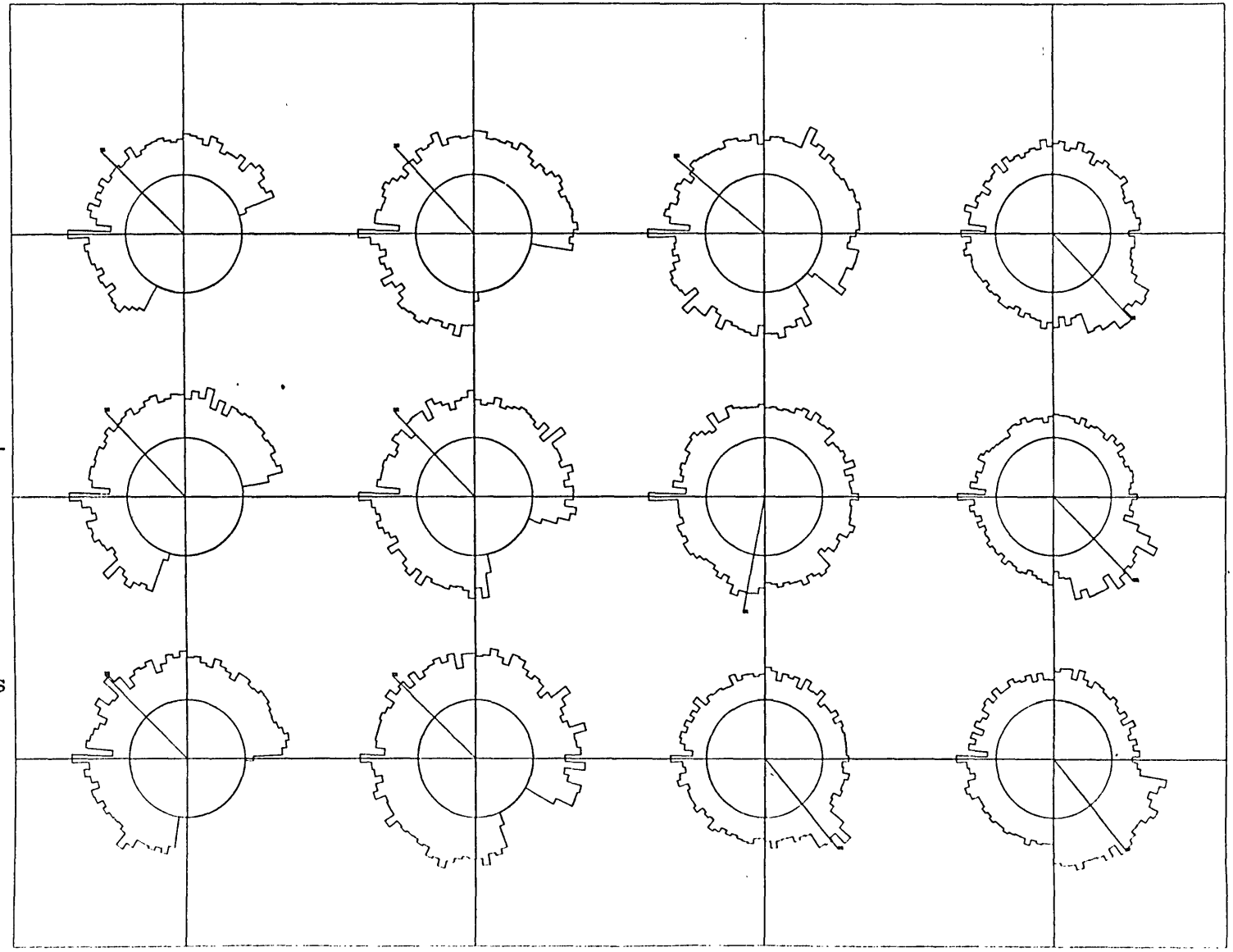

Figure 2.12 Circular histograms of the distribution of ensemble of uniformly distributed phase values with different amount of scatter. The true mean phase is 135^{o}. Note how the mean phase estimate become 180^{o} out from the the true mean as the scatter increases beyond a limit due to the wrapping of phases (Amount of scatter increases gradually as one moves downward from the left.)

to be investigated. How effective is the procedure in synchronising and averaging the ensembles of time-jittered signal? Are the observations reproducible? How much does the averaging reduce the variability of the observations at each recording site? The following sections are accounts of various investigations carried out to attempt to answer those questions.

2.6 Assessment of the averaging method

The effectiveness of this spectral averaging procedure was tested by comparing its result with that obtained by coherent averaging an 'alignment' ensemble of records from the same site. The alignment was achieved by the following procedure. (i) The spectra of each record were calculated by FFT. (ii) A least square line was fitted to a portion of each unwrapped phase spectrum near the low frequency region of the spectrum where it could be adequately represented by a linear phase trend. (The method of unwrapping is described in a later section). (iii) The average slope of the least square lines were calculated and each phase spectrum was adjusted to have the same average slope. (iv) The 'aligned' signals were reconstructed from the amplitude and the adjusted phase spectra. The two averaged signals were found to be nearly identical with a cross correlation coefficient better than 0.99. On the other hand the smearing effect of a direct coherent averaging without alignment was obvious. (Figure 2.13). Therefore, the spectral averaging method

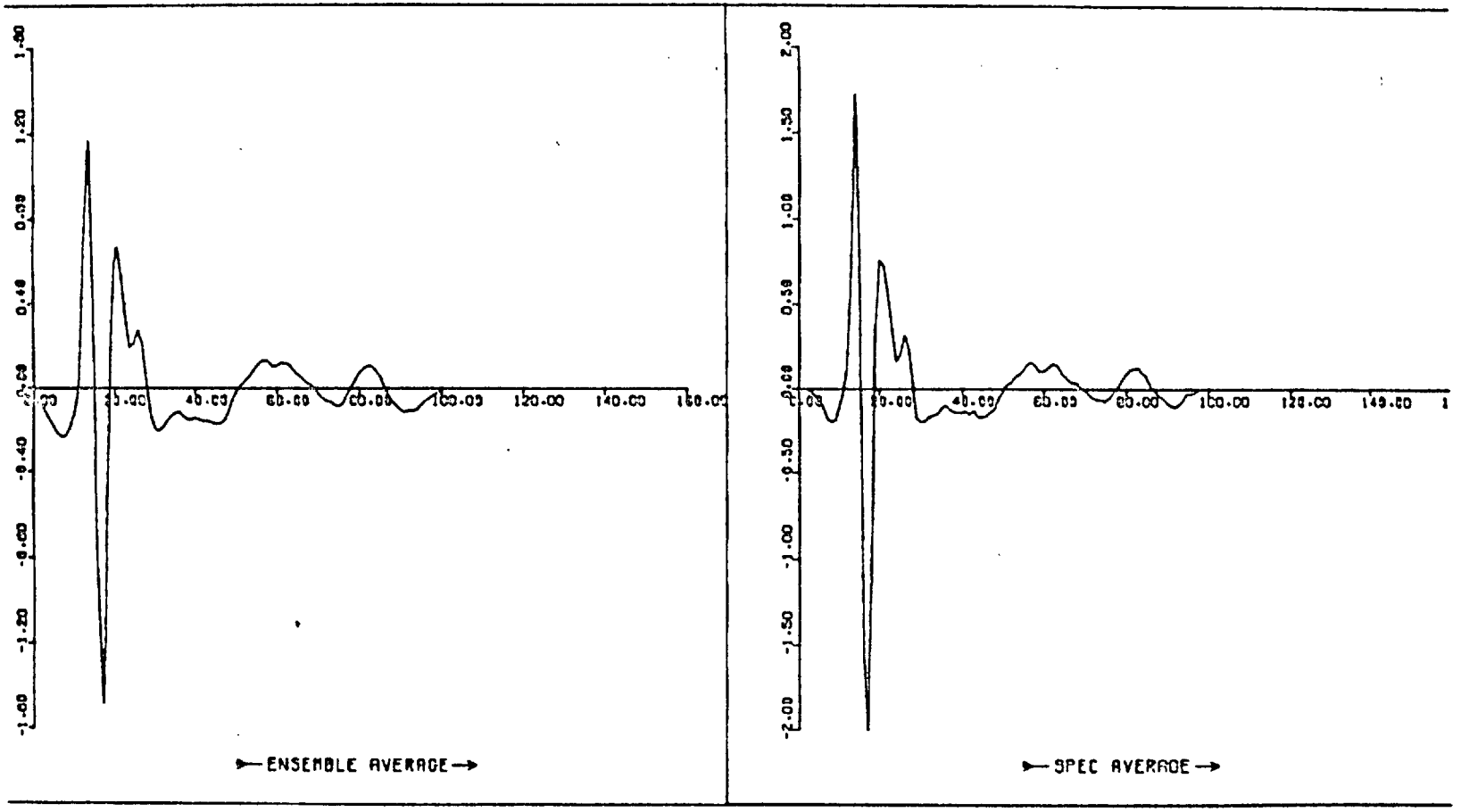

Figure 2.13 Comparison between a spectral averaged waveform (right) and a coherent averaged waveform (left). The second vibration of location (3,4)). The smearing effect is evident. Note the ordinate scales.

achieves similar results to averaging an aligned ensemble of signal without the tedious phase unwrapping and least square regression or other alignment method using correlation techniques.

2.7 Reproducibility

The spectral averaged vibration of the entire 49 sites are shown in figure 2.14. The reproducibility of the measurements was investigated by repeating the measurements on the same subject two months after the previous experiment. In the second experiment the vibrations were measured at sites as close to those in the first experiment as possible. Half minute recordings were taken for each site which gave three to five beats falling into the resting expiration phase of the respiration cycle. An extra row near the head, an extra column on the right, and one extra site near the centre of the gird were recorded. The spectral averaged data from the second experiment are shown in figure 2.15. A visual comparison of figure 2.14 & 2.15 showed that the measurements were very reproducible for the same sites despite the possible misplacement of transducer and long term variability of the signal. The similarity of the vibration patterns between the two experiments is best assessed by the auto- and cross-correlation functions of the signals. (Figure 2.16 shows the auto-correlation functions of the averaged first vibrations for the first experiment and figure 2.17 shows the cross-correlation functions of the same vibration components at different

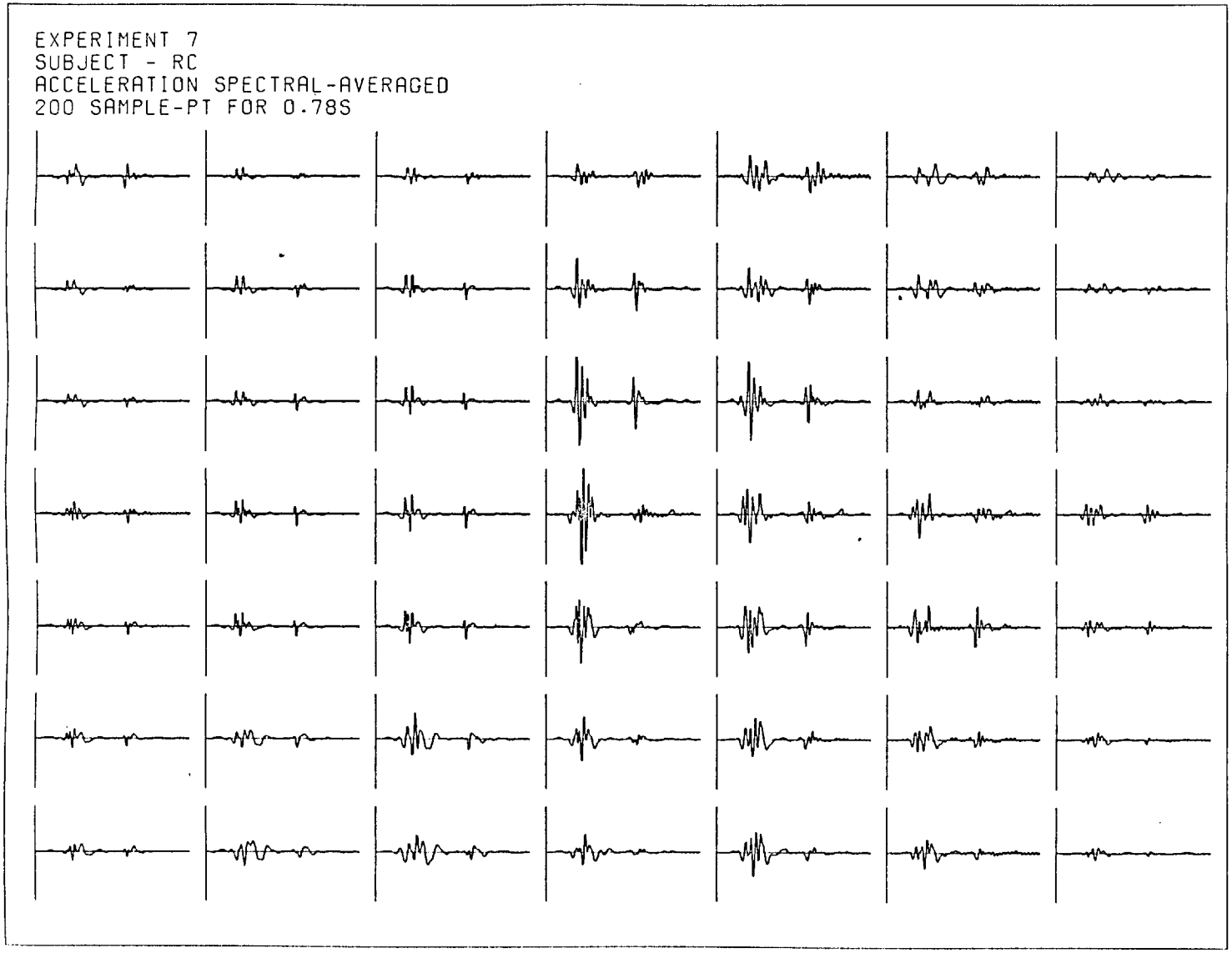

Figure 2.14 The spectral averaged vibration over the precordium at 49 sites for Experiment 1
(200 data points over 0.78 sec)

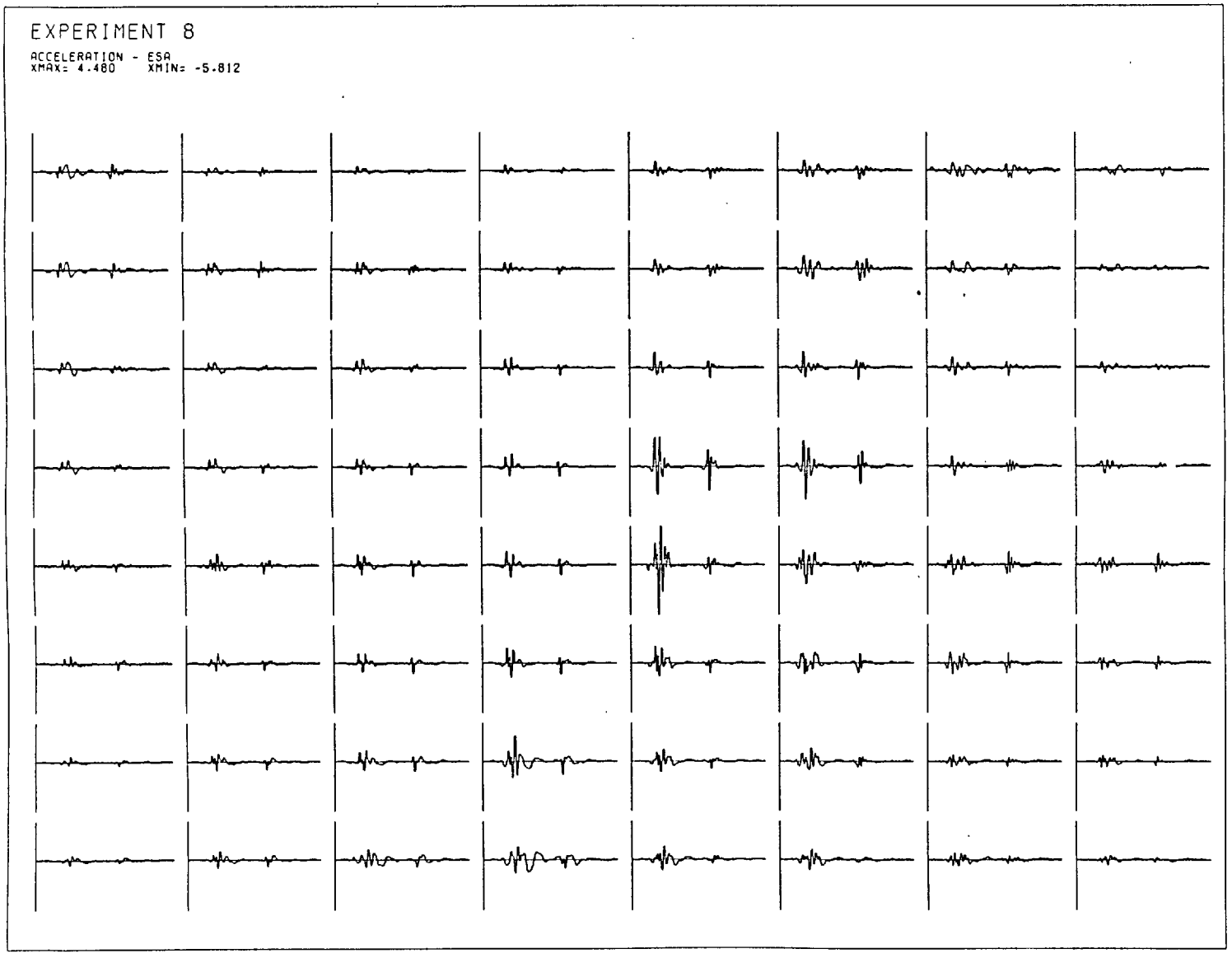

Figure 2.15 The spectral averaged precordial vibration measured in Experiment 2. The first row and column are additional to the measurement sites in Experiment 1.
(200 data points over 0.78 sec)

Figure 2.16a The normalized auto-correlation function (ACF) of the first vibration at the measurement sites. (Ordinate normalized to ± 1, abscissa shows ± 20 point shift.)

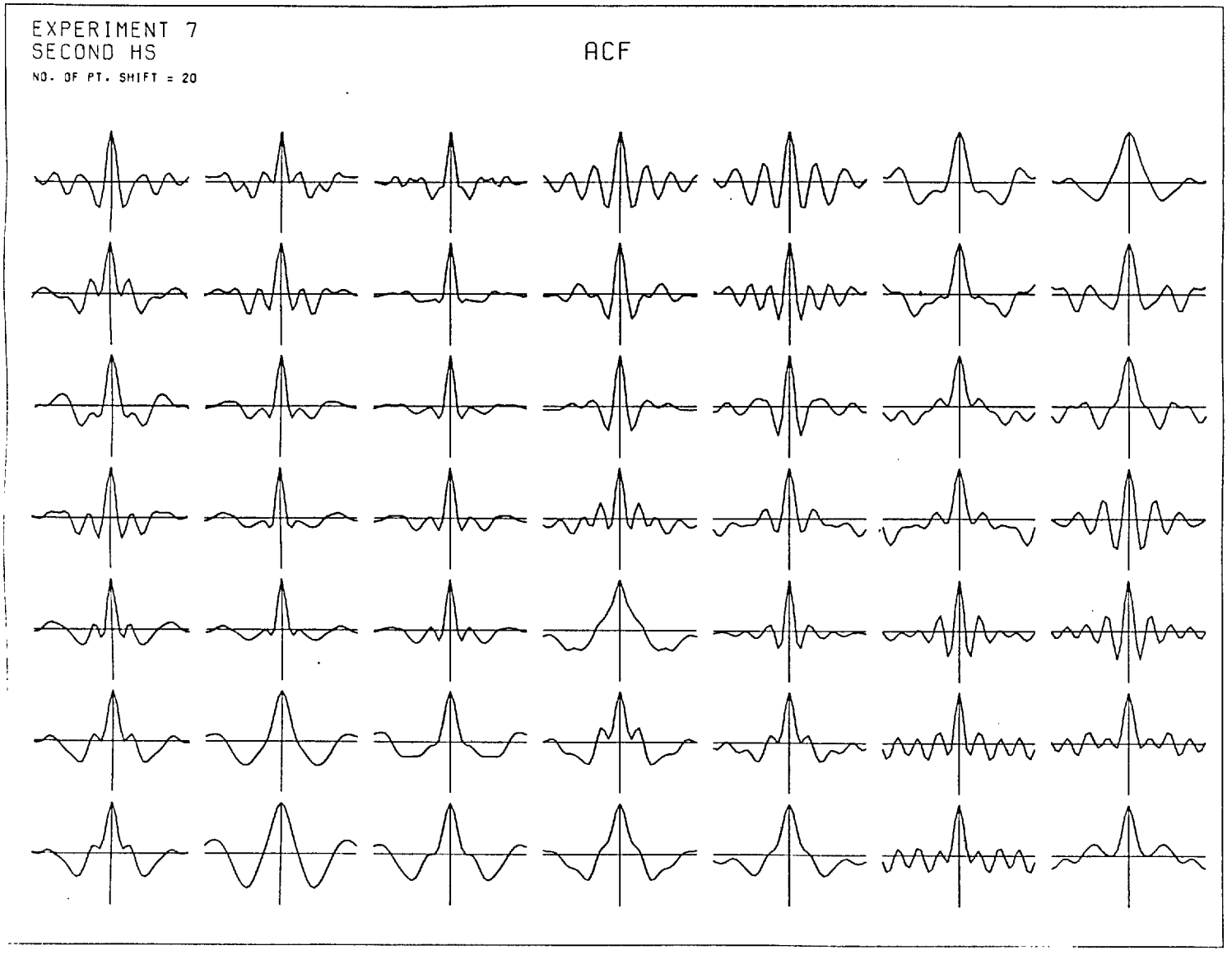

Figure 2.16b The normalized auto-correleation function (ACF) of the second vibration at the measurement sites.

Figure 2.17a The normalized cross correlation function (CCF) of the averaged measurement between the two experiments. (First vibration)

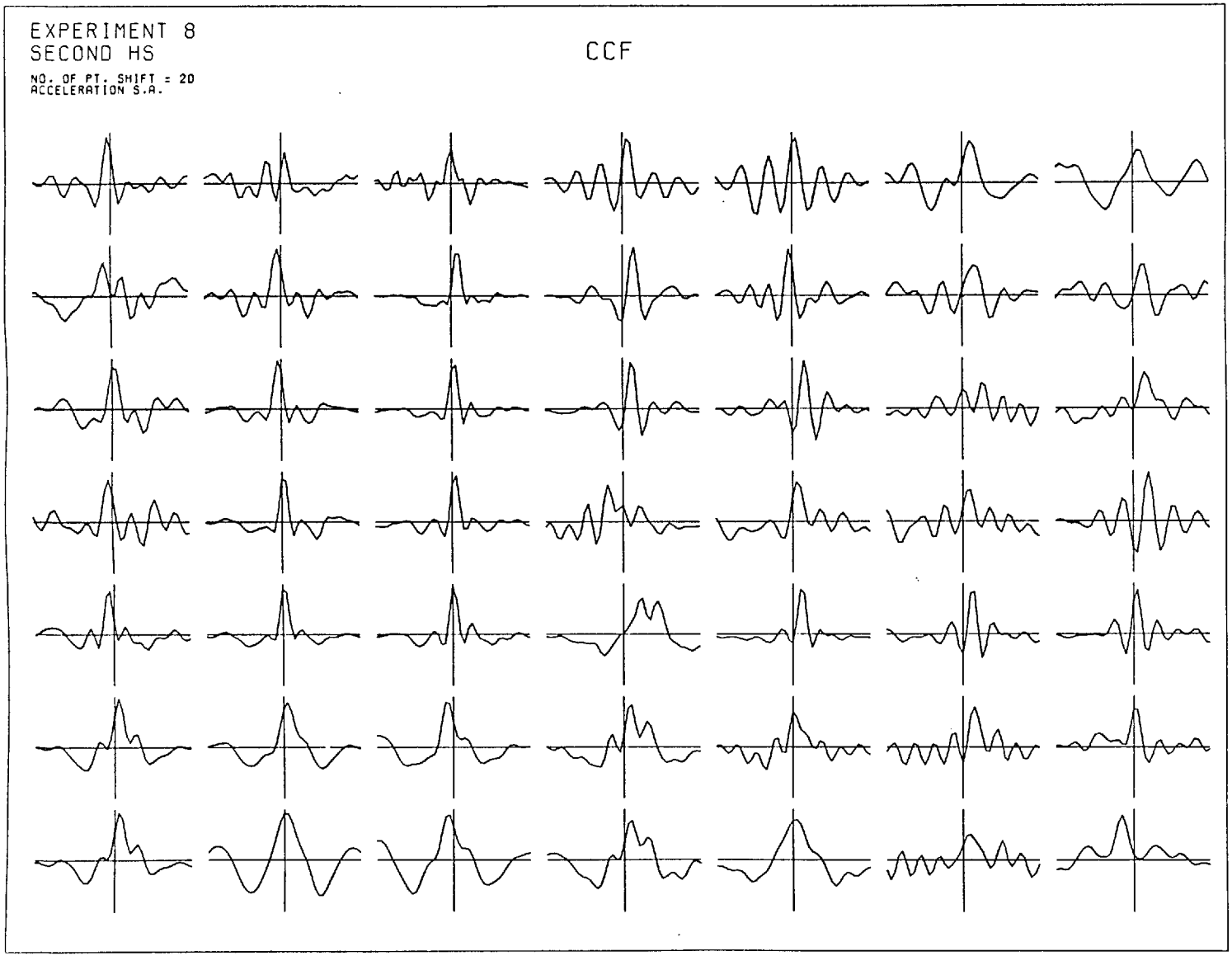

Figure 2.17b The normalized cross-correlation function (CCF) of the averaged measurement between the two experiments.(Second Vibration)

sites between the two experiments.) Table I and II are the maximum values of correlation coefficients (normalized to $\pm$ 1.0) between the two experiments for both vibrations at the measurement sites.

2.8 Statistical Studies

A very useful and concise visual display of the spectra of an ensemble of signals is shown in figure 2.18. The diagram shows the complete amplitude and phase spectra of an ensemble of 33 observations taken from location (3,4) (third row, fourth column). Each circle is the phasor diagram of each harmonic component of the observations. Individual crosses in the circle represent a member of the ensemble with its appropriate amplitude (distance from the centre) and phase (angle from the positive x-axis) value. The square symbol shows the vector of the mean amplitude and phase values for that component. The two circular arcs represent the 1 S.D. limits of the amplitude spectral values and the two thickened radii represent that of the phase spectral values. Hence the 'window' enclosed by the thickened lines shows the 1 S.D. variation of that particular frequency component. Because the radius of each display (outer, dotted, circle) is normalised to twice the mean amplitude spectral value, the thickness of the annular 'ring' bounded by the 1 S.D. circles reflects the coefficient of variation of the amplitude spectra. (A ring enclosing the whole diagram implies that the CV=1.)

The variability of the harmonic components are shown

TABLE I

.96	.87	.93	.92	.89	.74	.78
.95	.94	.88	.87	.83	.83	.42
.96	.88	.88	.91	.98	.60	.76
.99	.81	.81	.87	.87	.62	.89
.87	.88	.83	.88	.83	.65	.83
.92	.76	.92	.80	.90	.85	.85
.82	.77	.86	.81	.92	.79	.97

TABLE II

.91	.61	.66	.87	.88	.81	.63
.65	.91	.82	.94	.90	.59	.60
.82	.96	.86	.90	.94	.50	.70
.83	.85	.91	.72	.78	.61	.96
.85	.89	.93	.72	.88	.83	.87
.95	.88	.88	.82	.69	.78	.75
.93	.91	.88	.77	.79	.50	.88

TABLE I,II The maximum values of correlation coefficients (normalized to $\pm$ 1) between the averaged vibrations obtained from the two experiments at the measurement sites. (Table I - first vibration: Table II - second vibration).

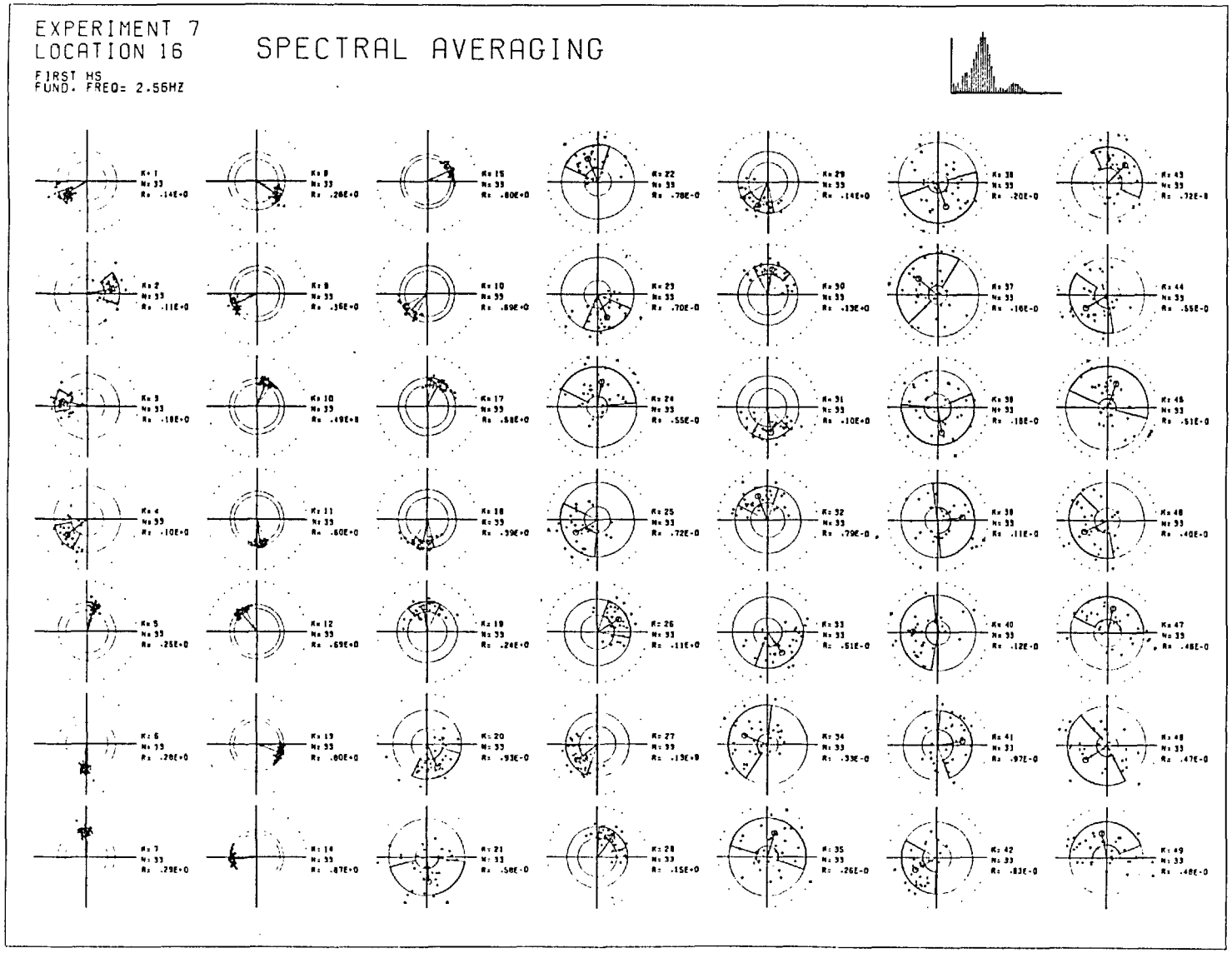

Figure 2.18a A display of the the spectra of an ensemble of signal and their statistics. Each circular phasor plot corresponds to one frequency harmonic and proceeds from the left downward. K = harmonic no.; N = total no. of sweeps in the ensemble; R = magnitude of the mean amplitude component.

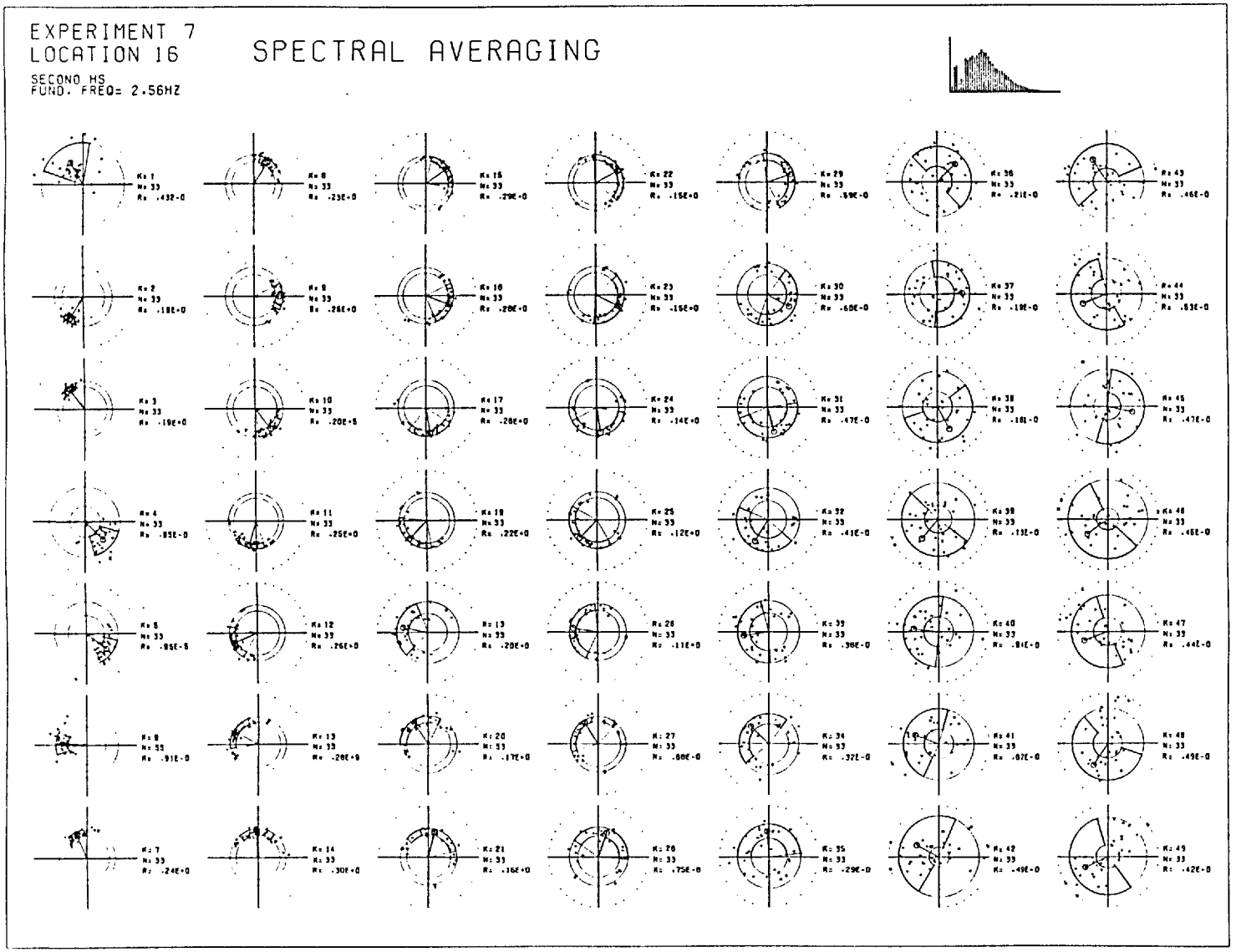

Figure 2.18b (See figure 2.18a)

in the figure. The variability of the amplitude spectra depended generally on the signal strength. A strong component was found to be less variable than a weak one. The variability of the phase spectra, however, tended to increase with frequency due to the 'ramp' effect caused by time jitters. (The exceptionally large phase variability for K = 21, 24 and 25 were due to their small signal strength). However, it was noted that for all components at frequency less than 80 Hz (K=34) the mean amplitude and phase values were good estimates of their expected mean values.

Two basic questions need to be answered before one can interpret the effectiveness of the pre-processing method in the reduction of variability. They are: (i) whether the samples taken from the population are normally distributed, and (ii) whether they are statistically independent samples. The amplitude and phase spectral components of the vibrations for a few measurement sites were tested for normality by the Kolmogorov-Smirnov one sample test. (The Chi-square test was found to be unsuitable because of the small sample size.) Figure 2.19 is an example of the maximum deviation between the observed and hypothetical Gaussian cumulative probability distribution vs harmonic number for one location. There is no reason to believe that the data are not normally distributed even at 20% significant level (D = 0.185 for N = 33). The samples, however, show obvious dependence. When the phase (or amplitude) spectra

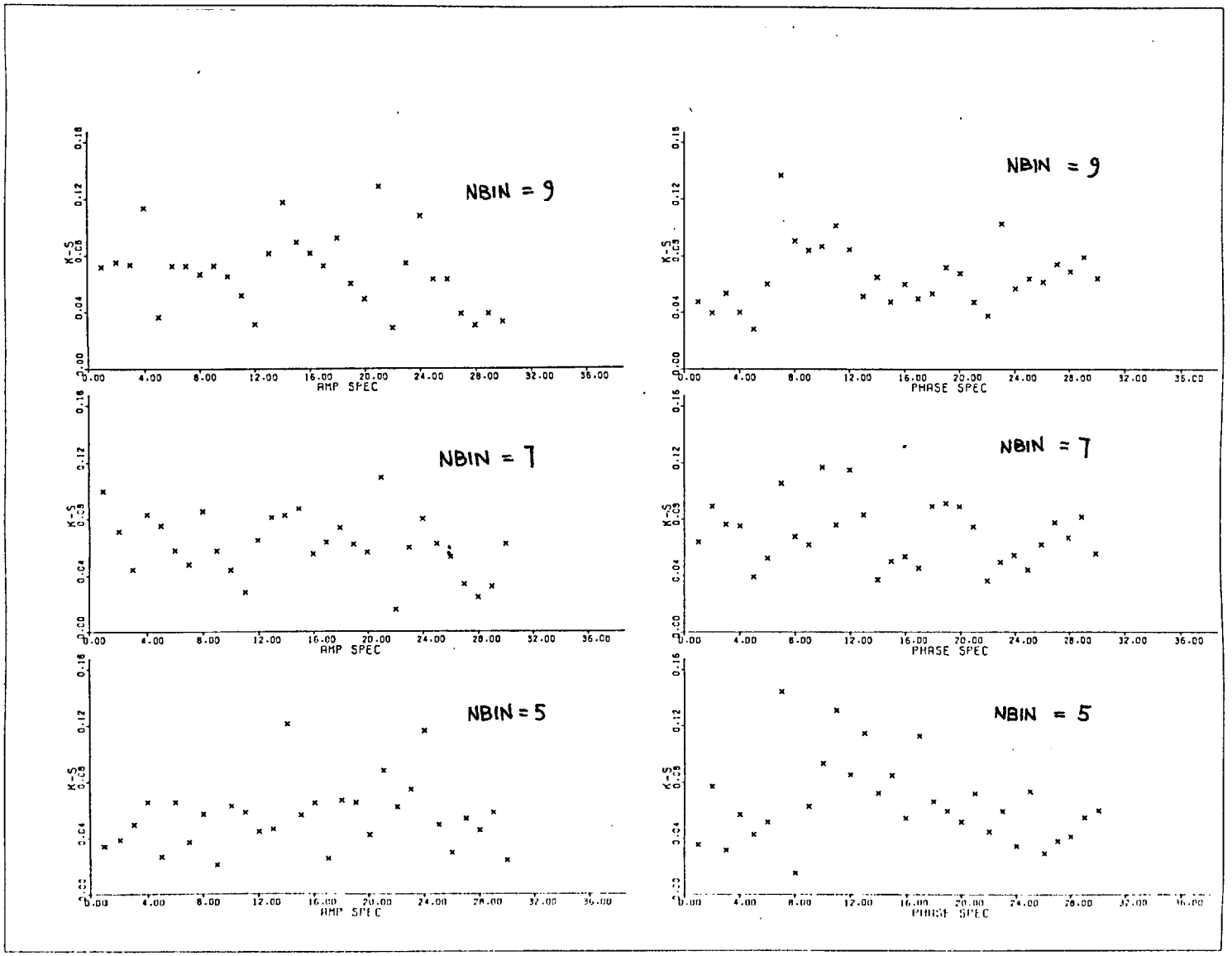

Figure 2.19 Maximum deviation between the cumulative distribution of the observed spectra (amp & phase) and a hypothetical Gaussian distribution with the same mean and variance. The deviations (Kolmogorov-Smirnov one sample test) are not significantly different from normal for all harmonic components. (D=0.185 for N=33 & p=20%)

for each harmonic are arranged in sequence of their occurrence and low pass filtered, obvious low frequency trends, which change characteristics in different frequency bands, can be observed (figure 2.20). This ensemble correlation has the effect of reducing the degree of freedom of the sample and hence the effectiveness of averaging.

2.9 Conclusion

The analysis of many 2-dimensional signals require the measurement of simultaneously occurring signals and in many cases, simultaneous recording is not feasible either due to technical or economical reasons. The signals then have to be measured asynchronously and later synchronised by some pre-processing procedure. This situation applies in the present case, because the choice of transduction scheme requires serial measurements. A technique was therefore needed that would produce an equivalent simultaneous representation of a set of serially measured data where a definite time reference is not available. (Another example requiring this approach is in the analysis of chest movement caused by respiration.)

As a result of these detailed investigations it was concluded that the methods described constitute a reliable method of measurement and pre-processing, from which a satisfactory set of signals for further investigation can be derived.

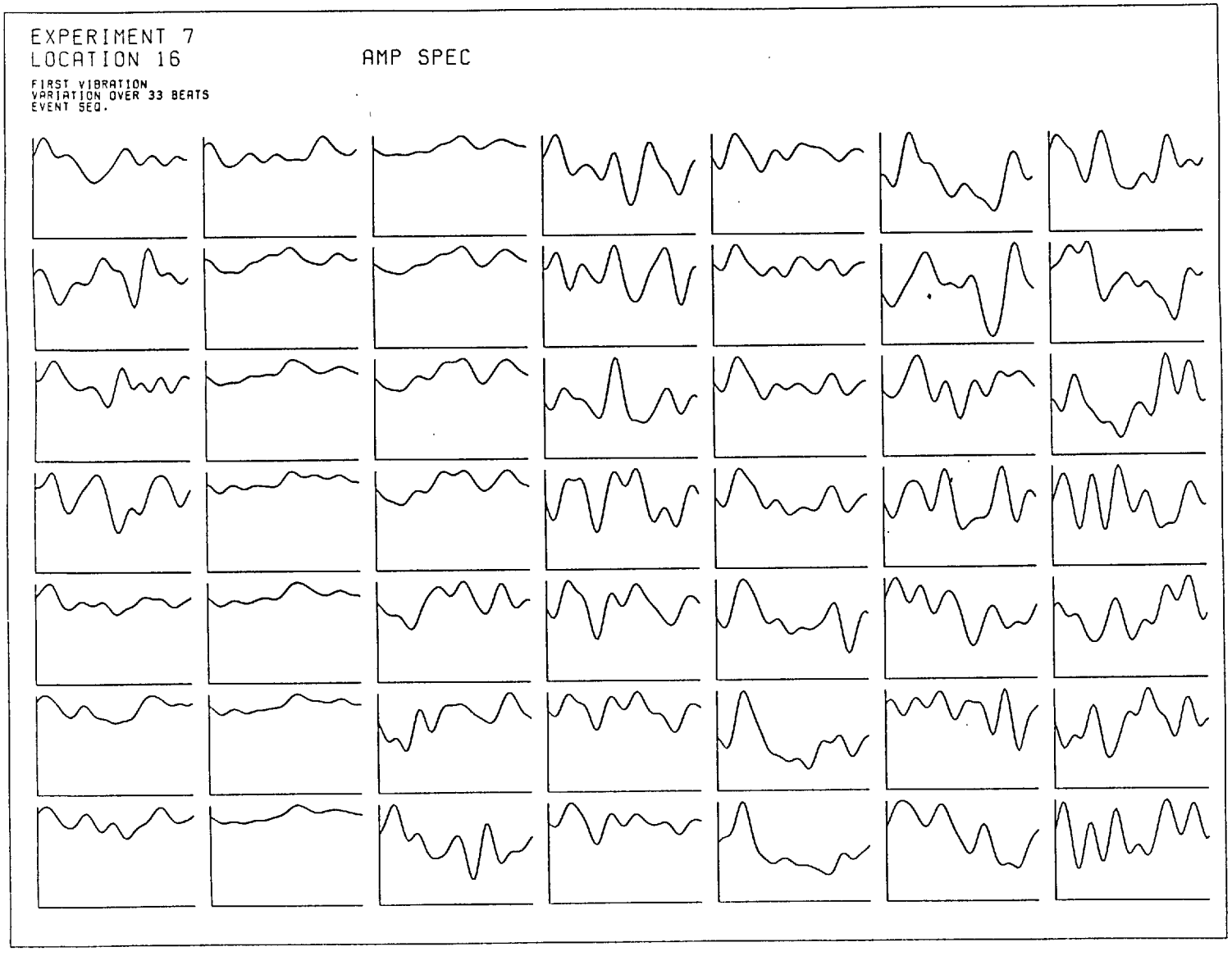

Figure 2.20a Low-pass filtered version of the sequence of spectral values (fig. 2.20a - amp spec; fig. 2.20b - phase spec) for each harmonic. Each graph corresponds to one frequency harmonic starting from the left and proceeds downward. Note the l.f. trends exhibited in the signals and the variation of the trend with frequency harmonics. (Relative Amplitude)

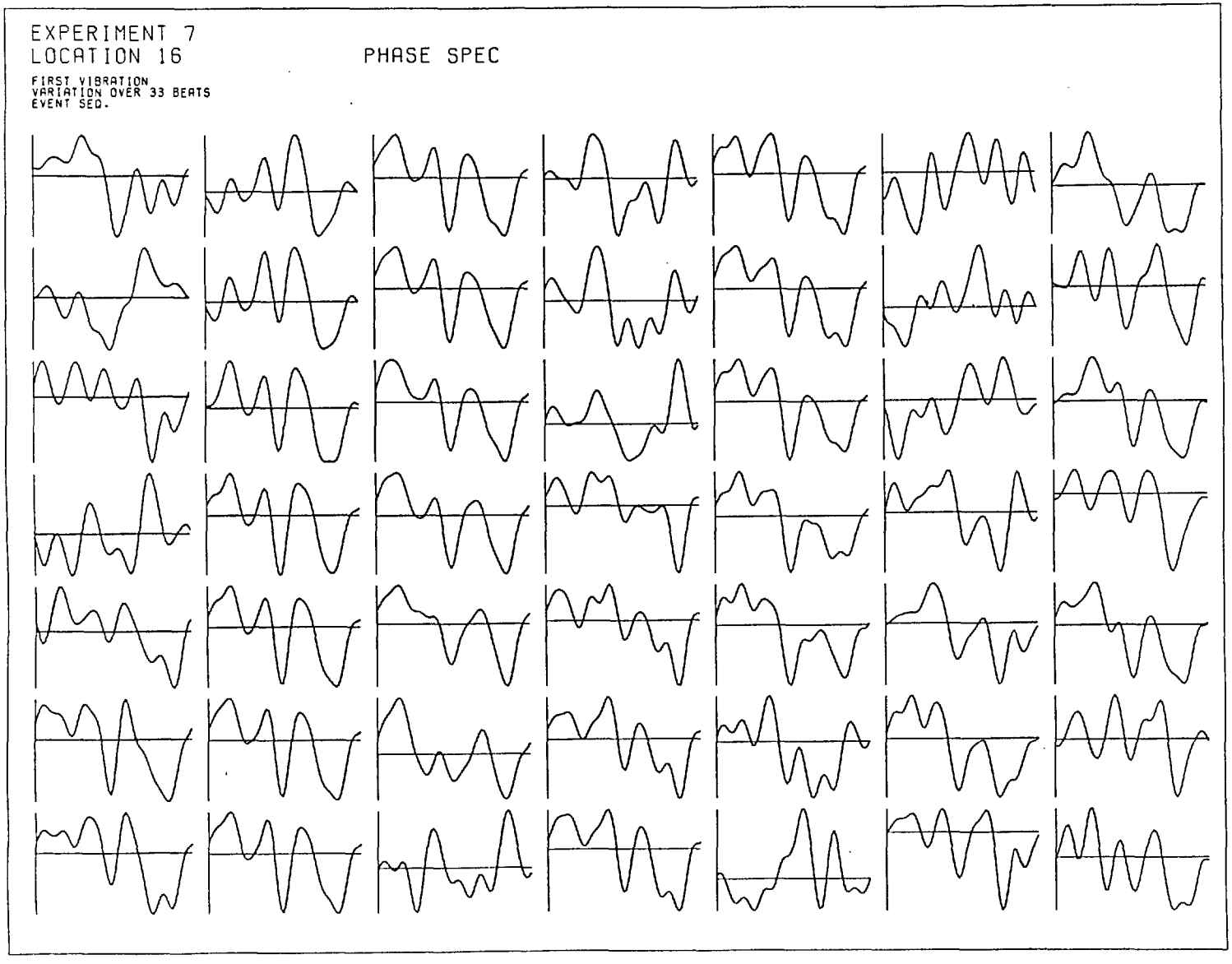

Figure 2.20b (See figure 2.20a)
(Relative Phase)

CHAPTER 3

SPATIO - TEMPORAL ANALYSIS

3.1 Visual Presentations

The spectral averaged observations for the entire 49 sites are shown in figure 2.14. The third column in the figure corresponds to the sternum and the fifth row corresponds approximately to the fifth intercostal space. For ease of reference, the locations will be referred as (row, column). The vibration pattern was found to vary significantly across the precordium with the exception of the sternal region where the underlying structure is rather uniform. The phase reversal phenomenon reported by Verburg (1974) is very obvious in our records (between location (3,4) and (5,5) for example). However, there is another phase reversal observed between the top right hand region (1,1) and the left parasternal region (3,4). In order to confirm this observation an extra row and column were measured in the second experiment session. This double phase reversal was clearly reproduced (figure 2.15). The significance of these observations will be discussed in a later section.

The amplitude spectra for the first and second vibrations are shown in figure 3.1 and 3.2. The spectra roll off rather sharply from about 60 Hz, confirming the adequacy of the sampling rate. The first vibration has the strongest contribution at about 30 Hz and the second vibration has a

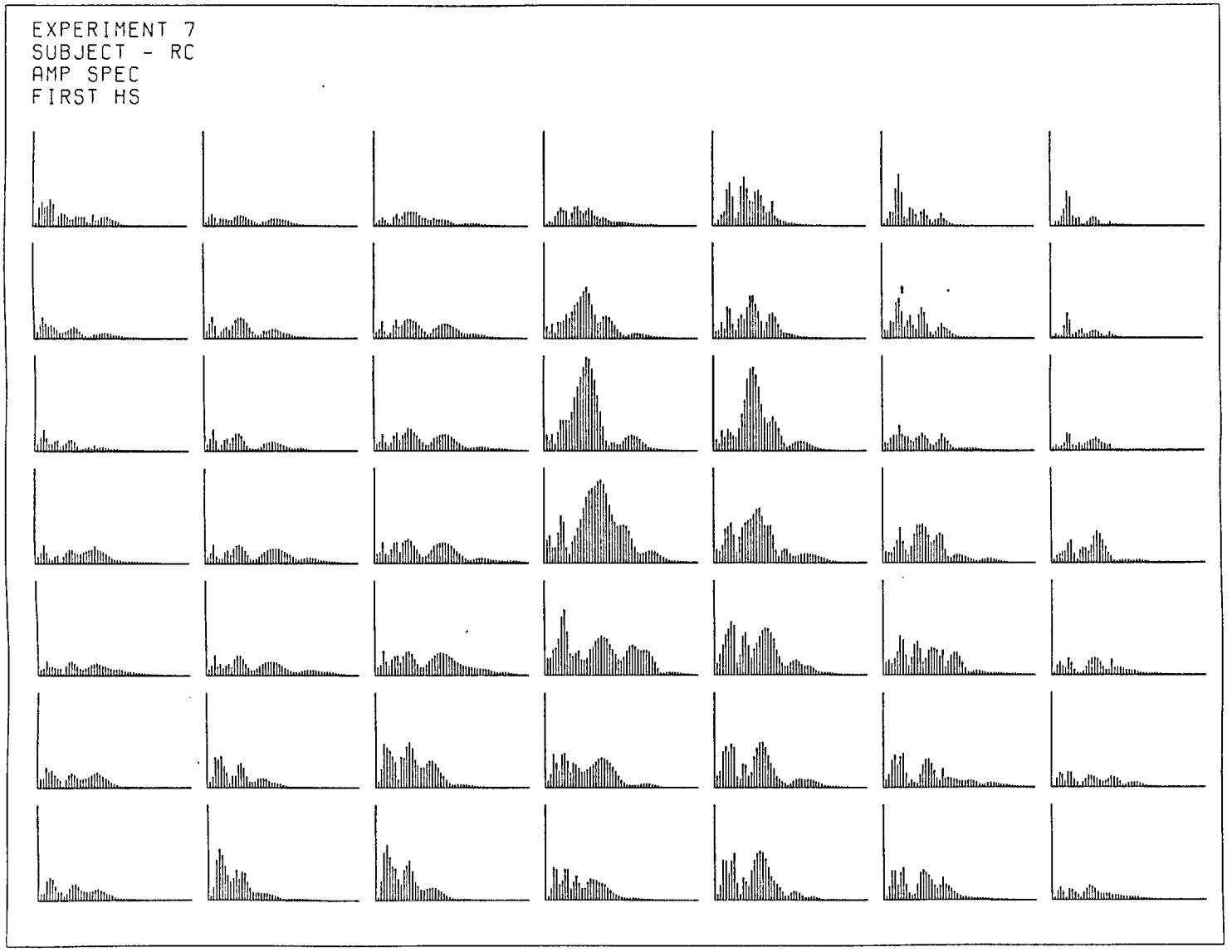

Figure 3.1 The amplitude spectra of the averaged signal for the first vibration at various sites.

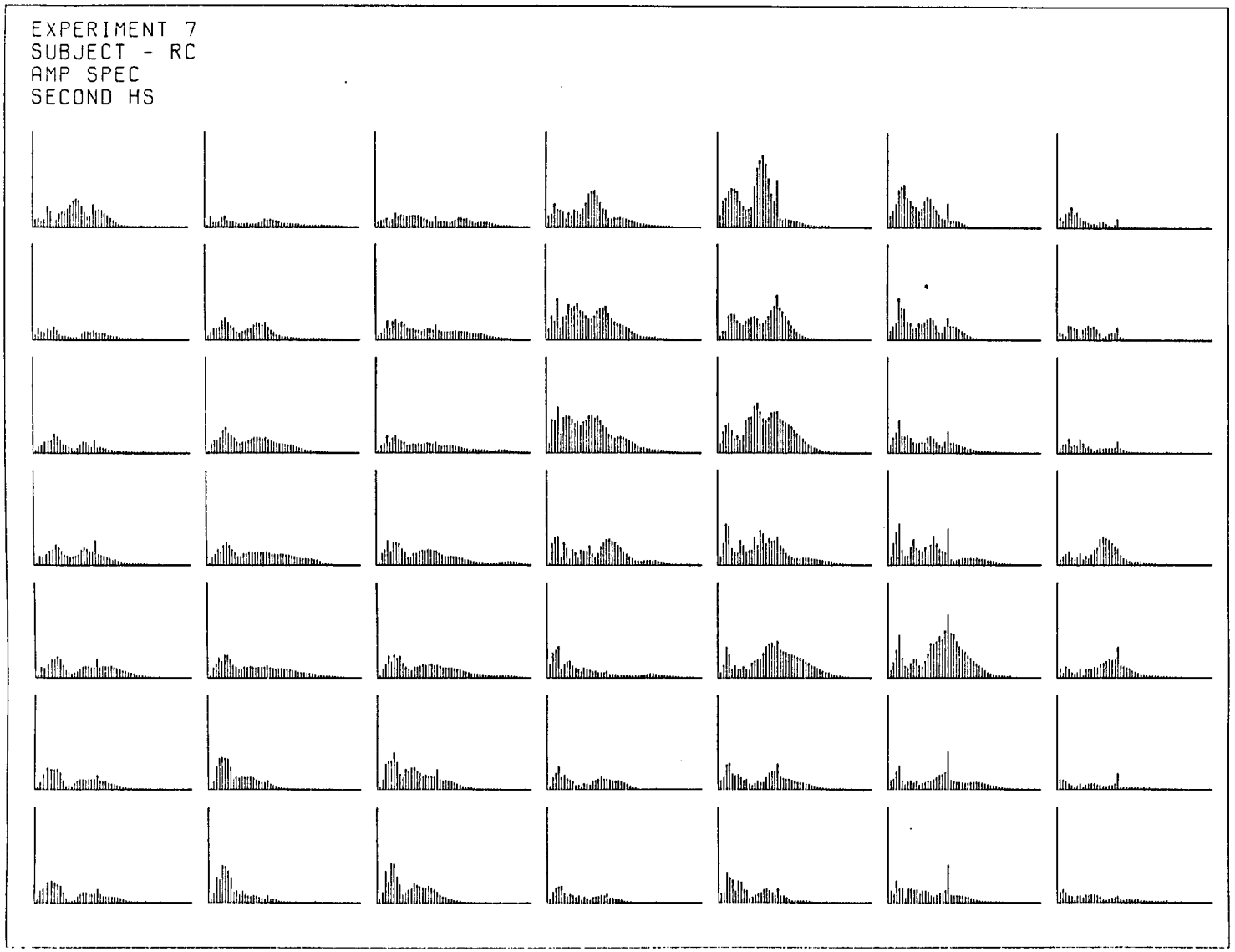

Figure 3.2 The amplitude spectra of the averaged signal for the second vibration at various sites.

broader band spectrum with the main frequency contribution at about 50 Hz. In regions where the underlying structure was formed from soft tissue (e.g. below the sternum) the signal showed proportionally stronger low frequency components.

The spectra show that the measurements were slightly contaminated by mains interference. Investigation in the experimental environment and the measuring equipments revealed that it was caused by the fact that the structure where the subject lay was vibrating at the mains frequency. However, this interference was not significant.

3.2 Spatial Interpolation

Visual inspection of the signals and their spectra is rather restricted. Various spatio-temporal analysis procedures could help to highlight any consistent features in the signal which might not be so obvious to visual inspection. However, the signals are available only at a limited number of sites, and, therefore, have to be interpolated spatially before one can form presentable pictures, for example, contour maps, of the spatial distribution.

Similar problem had been encountered in the surface mapping of ECG. Guardo (1972) treated the torso as a spherical body and used the Fourier 'band-limited' interpolation method which was conveniently implemented by the FFT algorithm in two-dimensions. However, because of the non-repetitive nature of our spatial measurements, we found that an alternative method using cubic spline functions

seemed to be more suitable.

The cubic spline functions are actually mathematical analogues of the thin flexible beam of small stiffness used by draftmen to trace curves. Suitable weights are loaded on the beam at points called knots or joints so that the deformation of the beam approximates the curve. It can be shown that (BIRKHOFF, 1964) the third derivatives at the joints are actually discontinuous but the first and second derivatives of the curve are continuous. Mathematically such a deformation can be represented by a set of piecewise cubic polynomial functions passing through the functional values and have continuous slope and curvature at each joint. In addition to the smoothness, the cubic spline function has the desirable property that it minimizes the 'strain energy' needed for the given deformation. Intuitively, vibrations on the chest wall can be thought of as 'deformation' of the surface tissue caused by forces transmitted from inside the body. Cubic spline (sometimes called linearized spline) therefore appeared to us to be a good choice for our purpose.

Detailed formulation and discussions on the properties of cubic spline functions can be found in the literature (BIRKHOFF, 1964; AHLBERG et al., 1967; GREVILLE, 1967, 1969). The summary of the formulation given here is for the clarification of our application. A more comprehensive account of the mathematics employed can be found in appendix C.

For a given set of (n+1) sample values, $(u_o, u_1, u_2 \ldots\ldots, u_n)$, of one independent variable, say x_i for i=0,1...,n, the cubic spline functions are cubic polynomials $u_i(x)$ between each interval $x_{i-1} \leq x \leq x_i$. The continuity condition of u, u' and u'' at each joint provides the following (n-1) difference equations.

$$u'_{i+1} + 4u'_i + u'_{i-1} = (3/h)\,(u_{i+1} - u_{i-1})$$

for i=1,2 ....., (n-1) ...(3.1)

assuming equal intervals, $x_i - x_{i-1} = h$.
The derivative u'_i are the unknowns to be solved. Since there are n+1 unknown and only n-1 equations, two additional equations defining the 'boundary condition' are needed. There are three possible choices for the boundary condition. The most trivial one is when u'_0 and u'_n are known (as in the case of 'clamped ends'). The other alternatives are assuming that $u''_0 = u''_n = 0$ (corresponds to the 'free ends' condition) or that the end segments have continuous third derivatives as well, i.e. $u'''_0 = u'''_1$ and $u'''_{n-1} = u'''_n$. In our case the first spatial derivatives of the boundary rows and columns are not known and are obviously not 'free-end'. Therefore the last alternative was chosen. This gives the the two additional equations as

$$u'_0 - u'_2 = -2/h\,(u_2 - 2u_1 + u_0)$$

$$u'_{n-2} - u'_n = -2/h\,(u_n + 2u_{n-1} - u_{n-2}) \quad \ldots\ldots\ldots\ldots (3.2)$$

Once u_i, u_{i+1}, u'_{i+1} are known for the segment $x_i \leq x \leq x_{i+1}$, interpolation within the segment is trivial.

Although our measurements were taken at equal spatial interval, this is not a limitation. Indeed it is obvious that, instead of sampling at equal spatial interval, better representation of the spatial distribution can be achieved by the same number of measurement sites if the measurements are more concentrated in regions of larger variation of the distribution and more spread out in regions where the distribution is relatively flat. This is another advantage of this method compared with the Fourier interpolation which is applicable only to equally spaced data.

To expand the linearized spline interpolation to two dimensional variables, three different approaches can be used. The most comprehensive one is the bicubic spline method developed by de Boor (1962). For a given set of observation u_{ij} on a rectilinear gird of points, piecewise bicubic polynomials

$$u_{ij}(x,y) = a_{00} + a_{10}x + a_{01}y \ldots\ldots + a_{33}x^3y^3$$

are fitted to each rectilinear mesh such that the polynomial surfaces has continuous first, second and cross derivatives (that is, continuous u_x, u_y, u_{xx}, u_{yy}, and u_{xy}) along the boundaries of each mesh. Birkhoff (1950) proposed a somewhat different approach. He first calculated the values u_x and u_y for each mesh point by fitting cubic splines along individual rows and columns (i.e. keeping x and y constant in turn) of the grid. Hence he obtained a set of 12-para-

meters for each mesh bounded by four mesh points (u, u_x and u_y for each corner of the mesh). He then fitted a surface constituting a linear combination of twelve basic functions F_1, F_2.....F_{12} which assume linear independent values of u, u_x and u_y at each corner, and have linearly varying $\partial u/\partial n$ along each edge. The algebra of this method is even more complicated than that of the bicubic polynomials because four of the 'basic functions' are rather elaborate. We adopted a much simplier variation of the bicubic spline method by interpolating along the rows first using cubic spline functions and repeat the procedure on the interpolated values along the columns. This procedure effectively fits surfaces which have continuous first and second derivatives along the boundaries of the rectilinear mesh but the cross derivatives are not necessarily continuous. However, for contour mapping of the spatial distribution, this method should be adequate. The differences in values obtained by reversing the order of interpolation (columns first, then rows) was found to be as small as the truncation error of the computer (the order of 10^{-14}). If irregular sampling is used, however, these differences can be considerable. This non-uniqueness of the method can be easily eliminated, if necessary, by taking the average of the two values obtained by the different order of interpolation, although this implies a doubling of computation time.

3.3 Assessment of the Spatial Sampling Rate

The sampling theorem is the time domain applies equally

to data in the spatial domain. If a spatial distribution is to be represented by discrete observations at a limited number of spatial sites, the sites should be closer to one another than twice the highest Fourier spatial frequency necessary to describe the distribution. The sampling interval of 3 cm was chosen arbitrarily since no record of any previous investigation in this aspect could be found. Therefore it seems necessary to enquire whether the chosen spatial sampling rate is adequate to represent the underlying distribution. This is best studied by the spatial spectrum of the distribution. Although one cannot be absolutely certain that aliasing does not occur once the signal is sampled (unless it has been appropriately filtered in its analogue form), the spatial spectrum provides indications whether the spectra is running down towards the folding frequencies (and therefore the sampling rate is likely to be adequate) or whether the proportional power in the higher spatial frequency components are appreciably large in magnitude suggesting that aliasing might have occurred.

The spectral averaged signals at the 7x7 gird were formed into 'frames' of spatial signal at the sampling time instants. Each frame was reflected along the edges to form a 14 x 14 grid. This was necessitated by the fact that the data was inherently non-cyclic in space and the discontinuity at the edges would distort the spatial spectrum when it is calculated by two-dimensional DFT. The use of

Hanning or other windowing was rendered unsuitable because of the few data points available and the reflection method was used instead. The spatial frequency spectrum was calculated for each time frame. The power spectrum P_{ij}, i,j = 0,1 ...., 6, was computed from the complex spatial spectrum (i,j =7 correspond to the nyquist terms and are equal to zero due to the symmetry of the data). The spatial power ratio R_k, expressed as a percentage of the total power, was calculated as the higher spatial frequency terms were stripped away. That is,

$$R_k = \sum_{i=0}^{k} \sum_{j=0}^{k} P_{ij} \Big/ \sum_{i=0}^{6} \sum_{j=0}^{6} P_{ij}$$

for k = 1,2 ......,6

These ratio were calculated for each time instant and were plotted as a series of curves as shown in figure 3.3. It is noted that majority of the spatial power is contained in the first few spatial harmonics and the spectral terms run down rapidly towards the folding frequency. By removing the d.c. term (P_{00}) before calculating R_k, one obtains a more sensitive picture of the contribution of various spatial harmonics to the total a.c. power in the signal (figure 3.4). It is, therefore concluded that the spatial smapling rate at 1 sample per 3 cm is likely to be sufficient for the signal concerned.

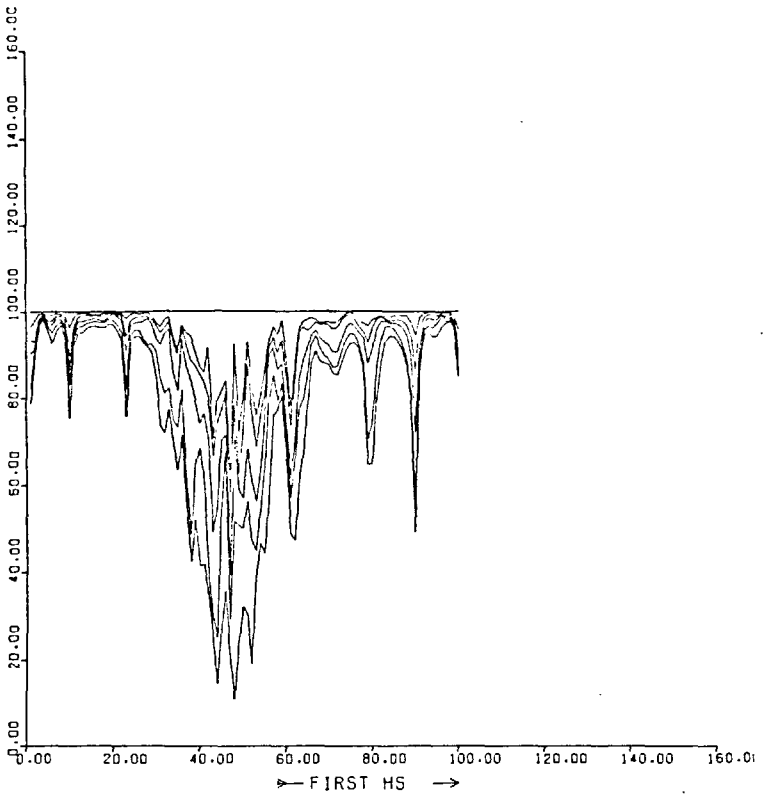

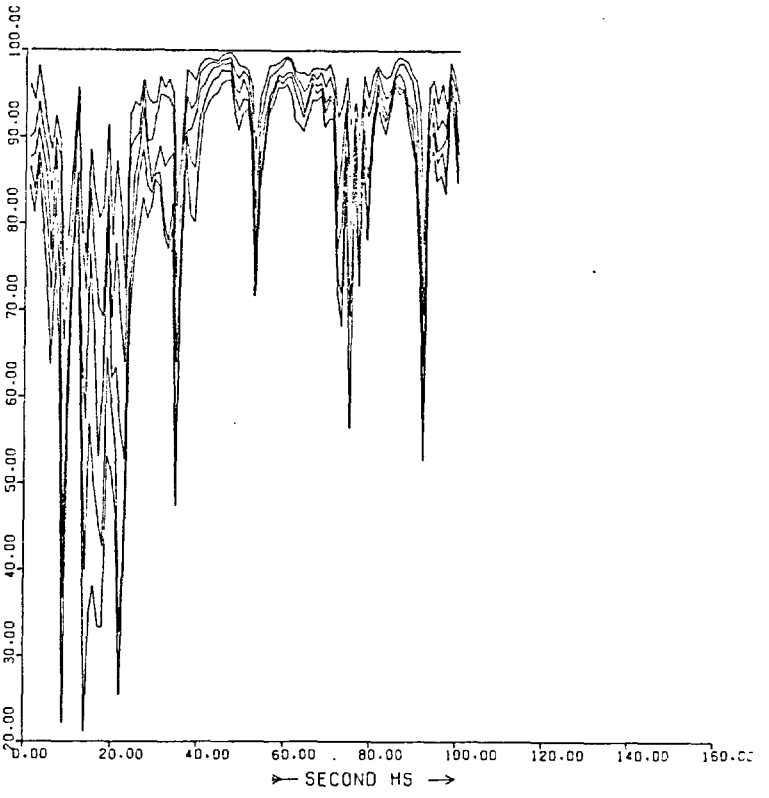

Figure 3.3 Decrease in percentage of spatial power in the spatial distribution of the vibrations plotted against time as spatial harmonic components are stripped off. Note that most of the spatial power is concentrated in the first few spatial harmonics.

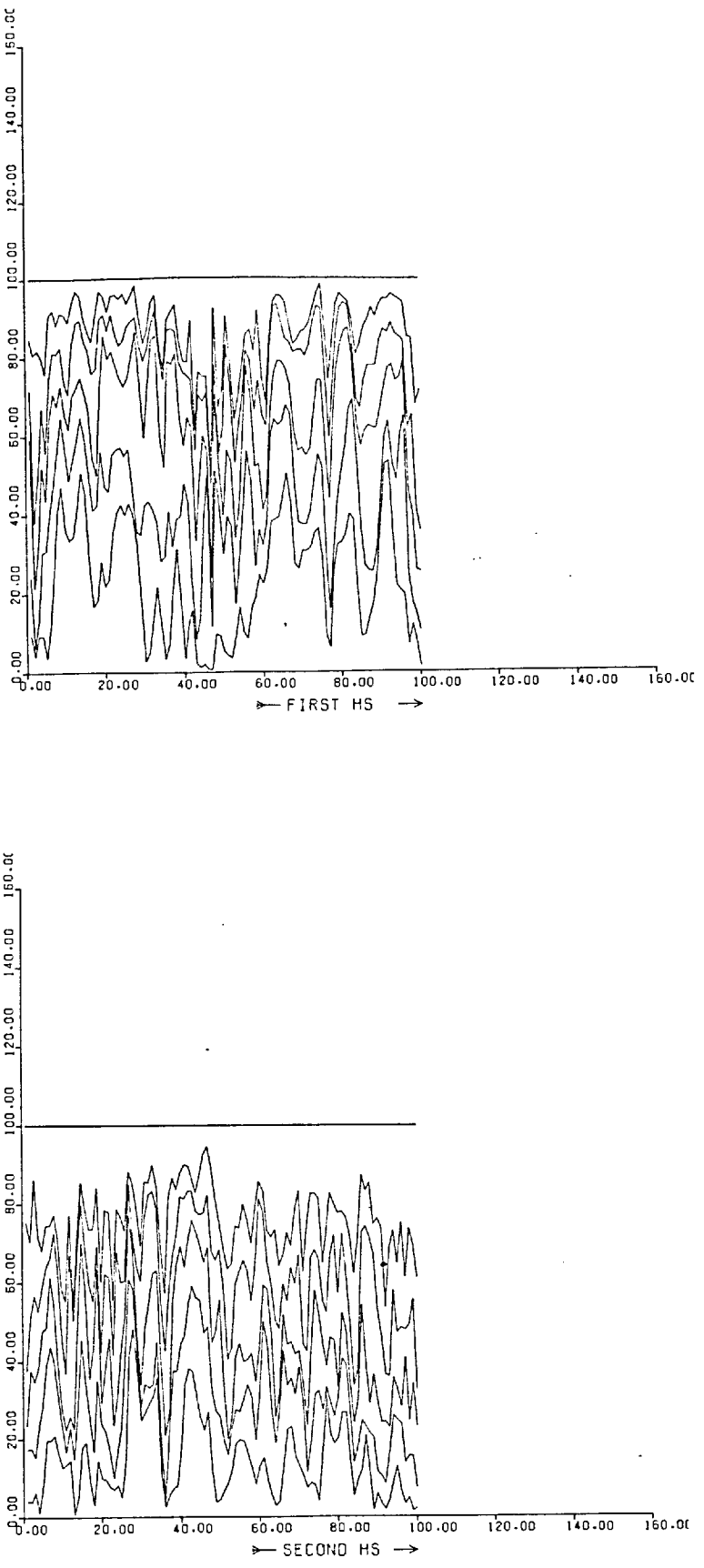

Figure 3.4 Same as figure 3.3 but with the percentage a.c. power plotted (i.e. with P_{00} set to zero)

3.4 Time Domain Spatial Contouring

A very straight-forward but useful way of studying a time varying spatial signal is by plotting a contour map of the spatial disturbution at each instant in time and examining how features in the spatial distribution (e.g. local maxima and minima) change from time instant to time instant.

The signal was first interpolated by five times in the time domain using the Fourier interpolation method. This was found necessary in order that the spatial distribution changed gradually between time frames. The interpolation procedure was implemented by calculating the complex spectrum of the signal by FFT, inserting zeros as higher frequency terms above the folding frequency and inverse transforming the expanded spectra. Instead of plotting the spatial distribution of the whole time course of the time-interpolated signal (consisting of 1000 time frames), it was decided to select a portion of the signal which included at least one complete oscillation complex (namely, the first large oscillation complex) of the first and second vibrations. For each instant in time of these selected signals, the 7 x 7 grid was interpolated to 55 x 55 points (an addition of 8 points between samples) using the 'double cubic spline' method described in section 3.2. Contour maps of the spatially interpolated data were then plotted on microfilms by the College CDC 6400 computer.

The 'effectiveness' of interpolation was investigated by a simple method. The vibrations that would have been observed at a location shown in figure 3.5 was reconstructed by interpolating spatially at this location the vibration obtained from the first experiment for each time frame. The vibration at the same location was measured in the repeated session with the same subject. The measured and the interpolated signals are shown in figure 3.6 a,b. The cross-correlation function (normalised), for the first and second vibrations, between the measurements and the reconstructions are shown in figure 3.7. (In order to obtain a more accurate correlation function, the CCF was actually interpolated to twice the data length using the Fourier interpolation method). The correlations were found to be satisfactory. When the exercise was attempted using the observations from the second experiment for the interpolation, the reconstructed signal was very different from the observation (figure 3.6). This is probably due to the fact that the averaged signals for the second experi-

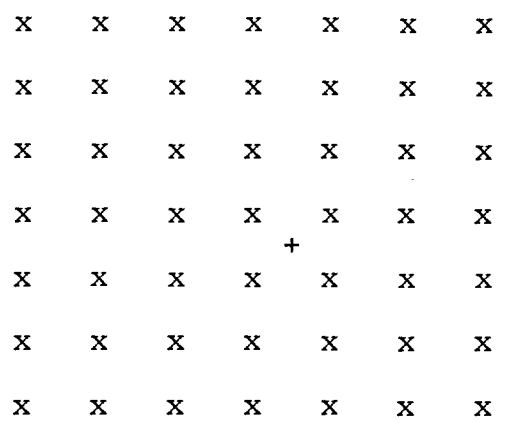

Figure 3.5 Location of the spatially interpolated vibration

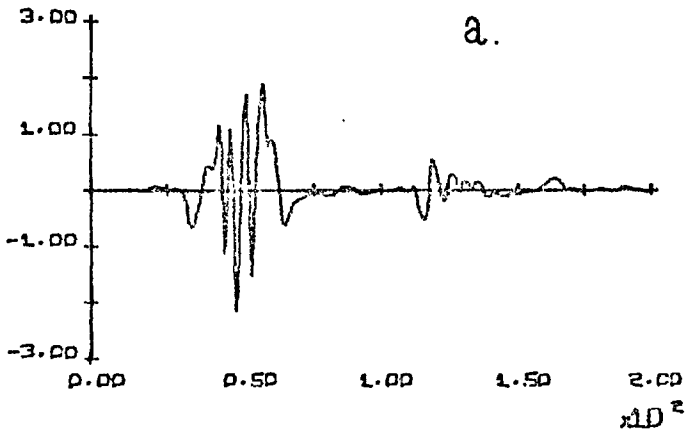

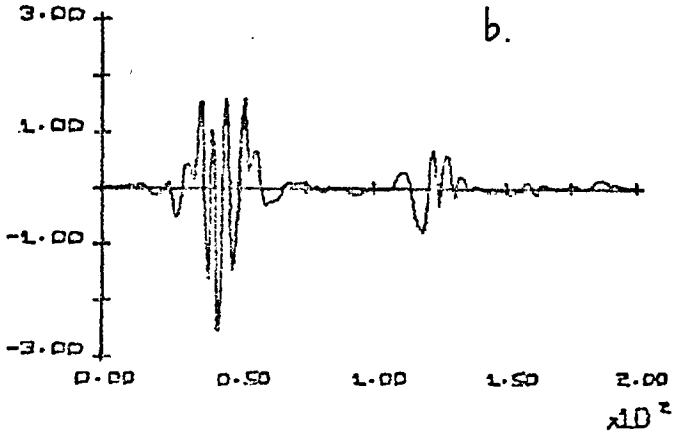

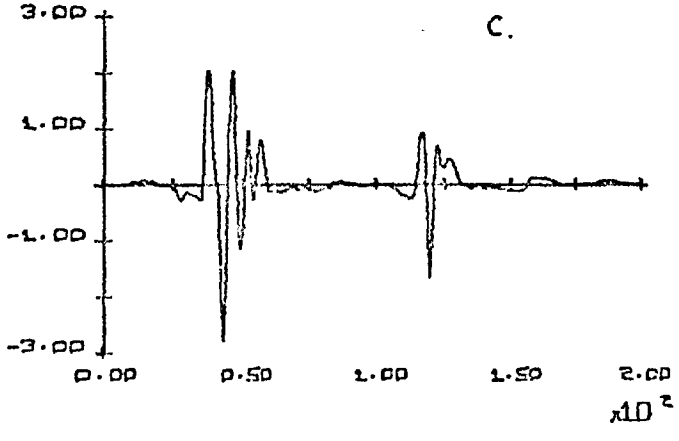

Figure 3.6 a) The observed signal; b) Signal reconstructed from spatially interpolating at the same site using bi-cubic spline method on the averaged measurements taken in Experiment 1. c) same as b) but reconstructed from measurements taken in Experiment 2.

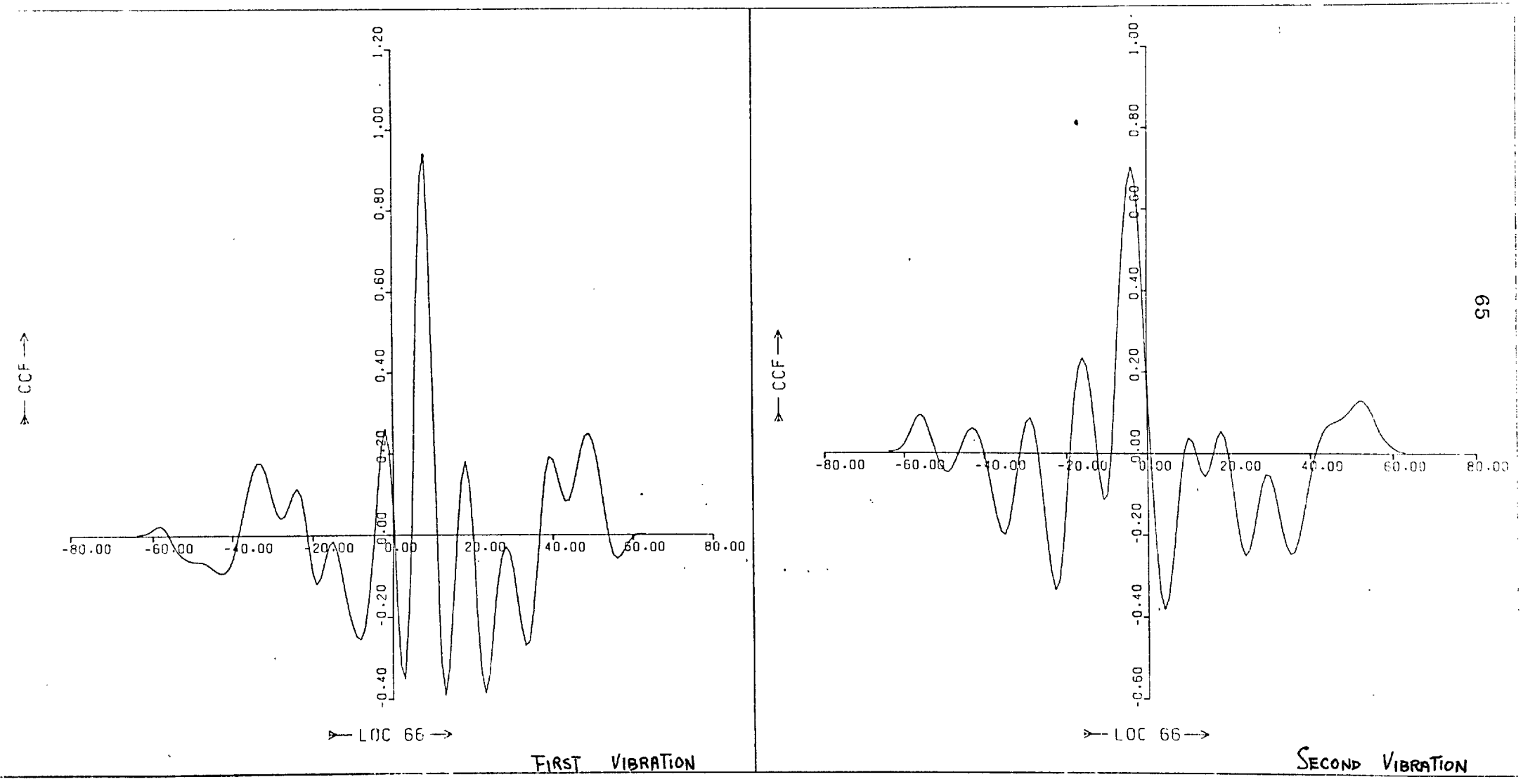

Figure 3.7 The normalized CCF between the observed and the spatially interpolated signals; abscissa is in units of half a sampling interval shift; total shift = $\pm$ 64 x 1/512 sec.

ment were obtained from a very small ensemble at each site (3-5 beats) and were therefore not properly time synchronized.

Figure 3.8 and 3.9 are examples of contour maps of equal vibration intensity. The reference temporal signal was taken from location (3,4). The time instant that the contour map represents is indicated by the end of the thickened line and the vertical cursor. The crossings of the grid represents the locations where the measurements were taken.

To simplify the information contained in the contour maps, one can draw attention to some signal features and study how they vary with time. One possibility is to follow the trajectories of any consistent local maxima and minima in the spatial distribution. Figure 3.10 and 3.11 are time trajectories of various local extremes, represented by their I and J indexes (corresponds to the y and x axes respectively), for the first and second vibrations. Individual trajectories are labelled to allow easy comparison of movements in the x and y directions.

Three main features are noted from these trajectories: (i) there are multiple local extremes occurring at any time; (ii) the trajectories are subject to discontinuity and (iii) the local extremes do not vary appreciably in any common systematic way. These trajectories represent a compact way of isolating some features of the contour maps and the indicated stability of the

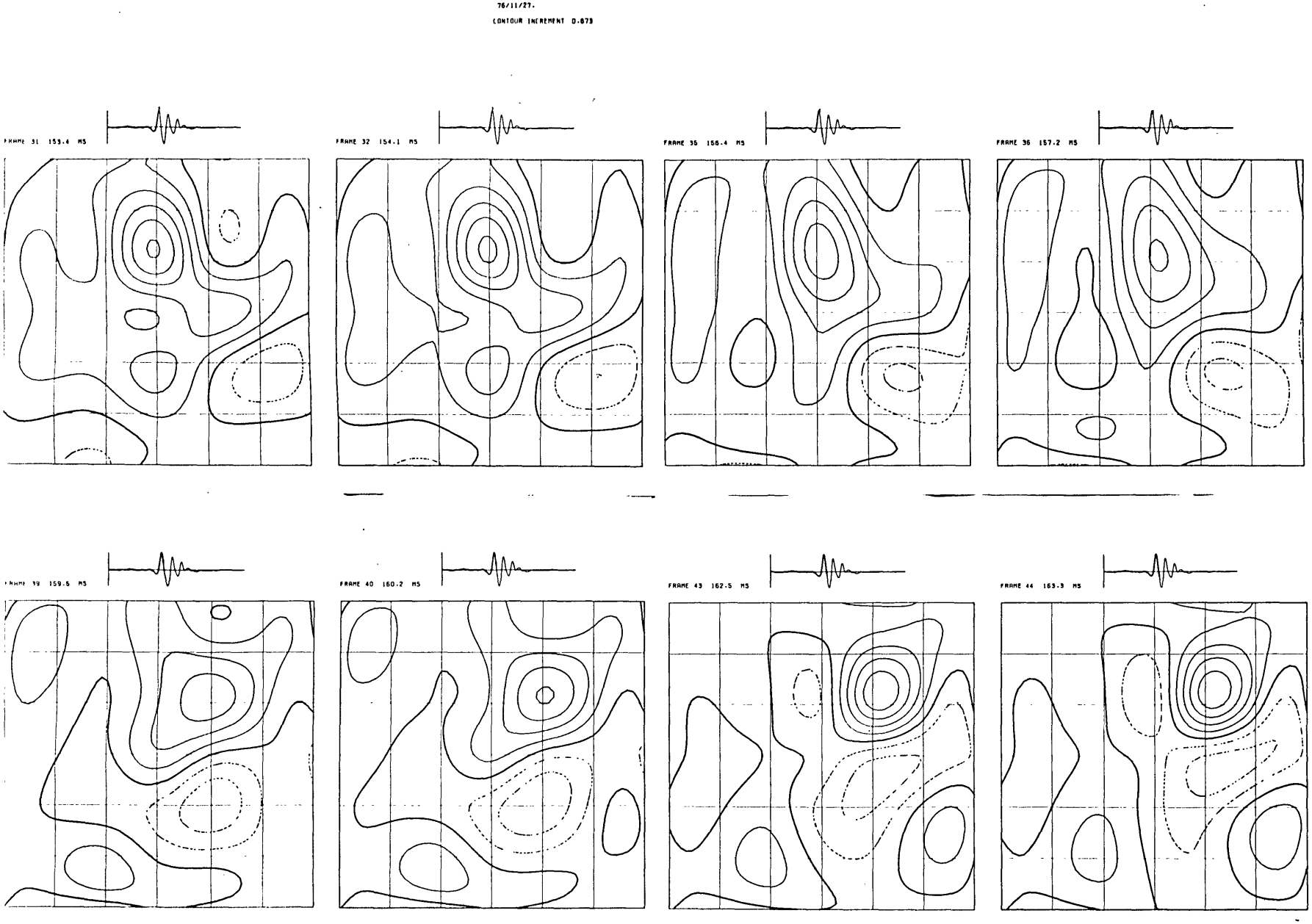

Figure 3.8a Examples of contour maps of the spatial distribution of precordial vibrations at different time frames (broken lines corresponds to negative values). A selected section of the first vibration.

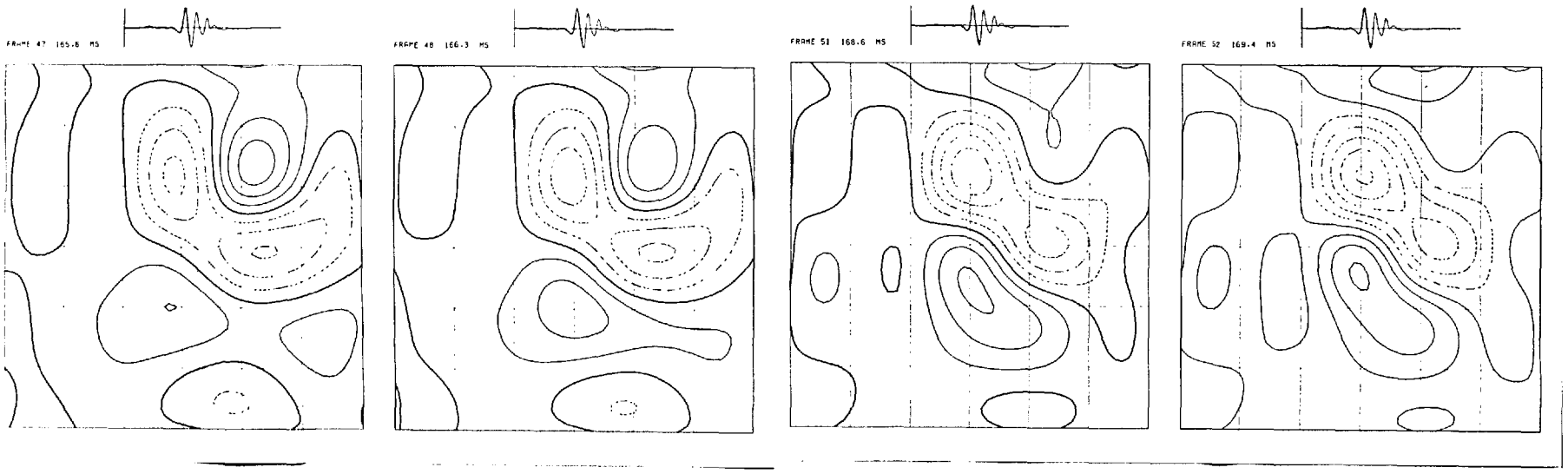

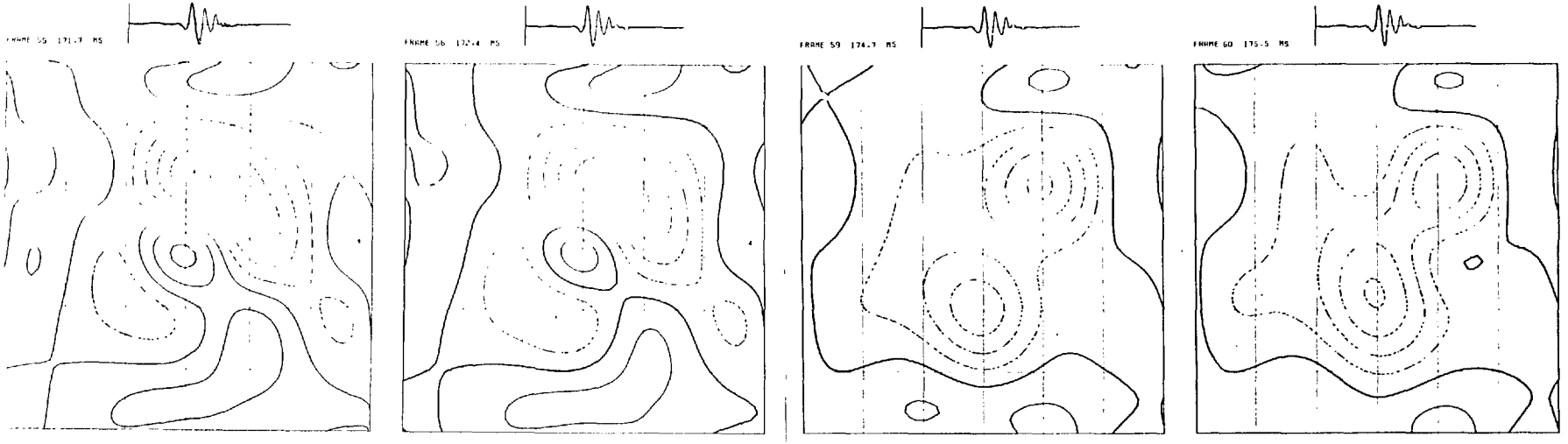

Figure 3.8b (See figure 3.8a)

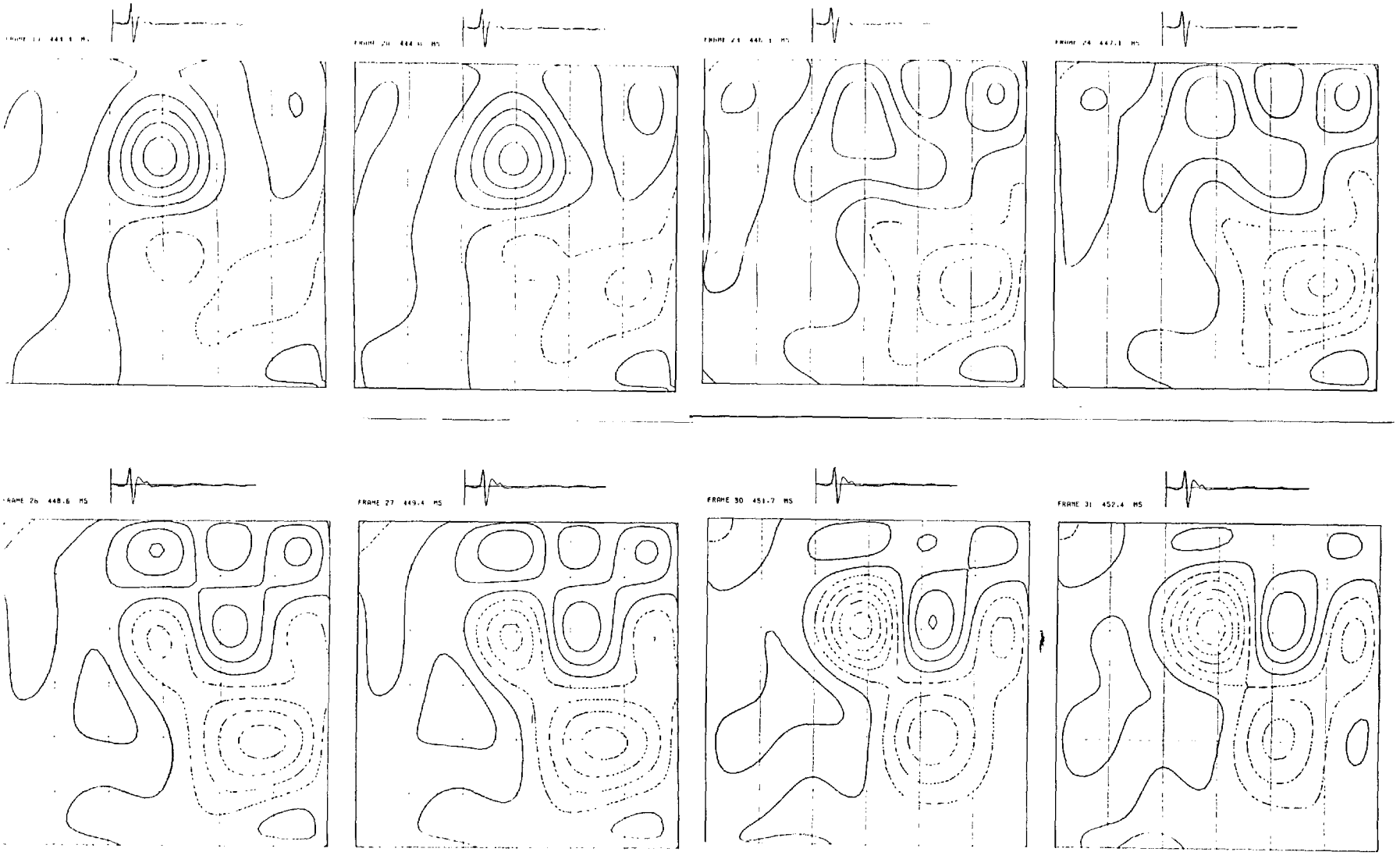

Figure 3.9a Examples of contour maps of the spatial distribution at different time frames.(Selected sections of the second vibration).

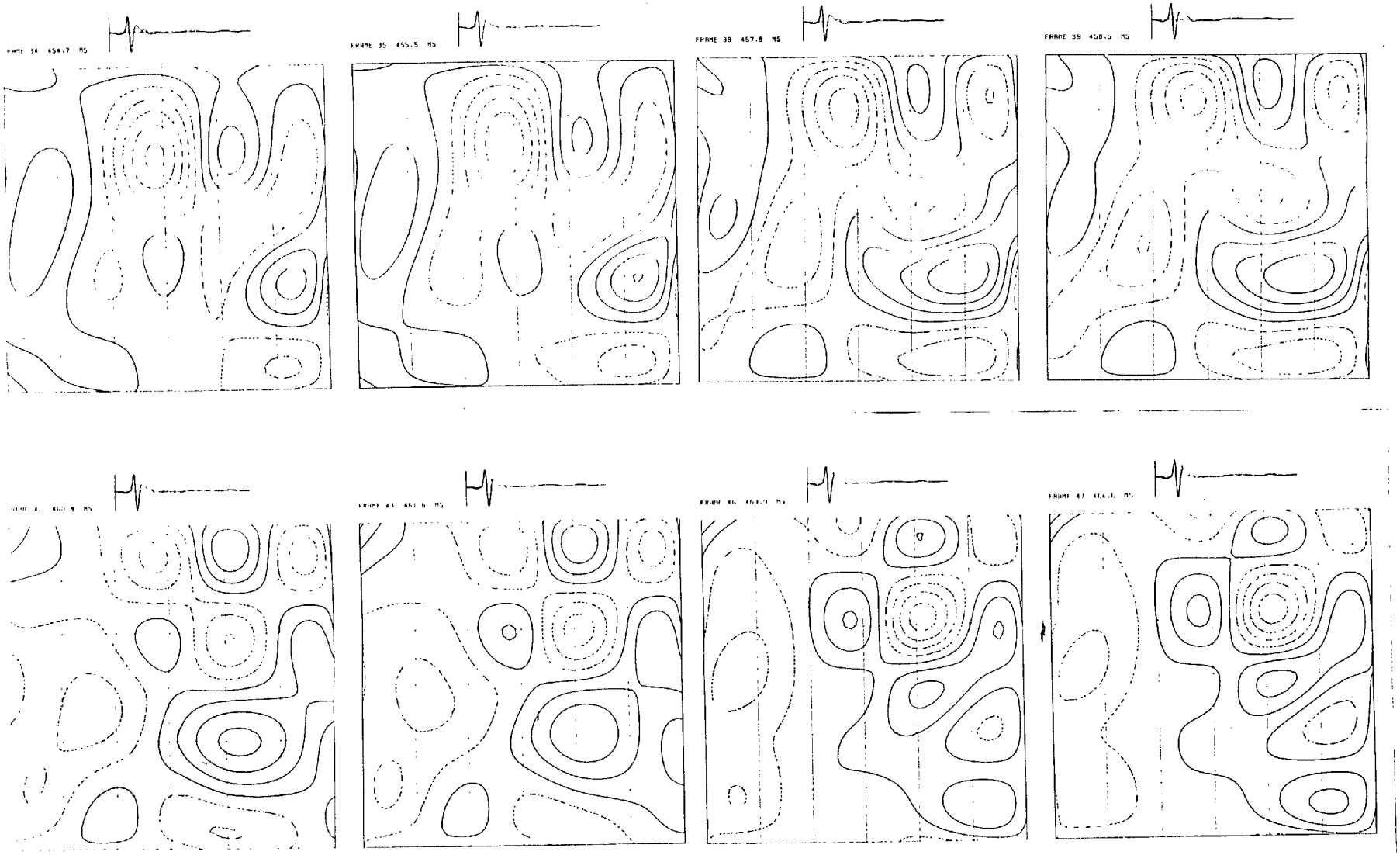

Figure 3.9b (See figure 3.9a)

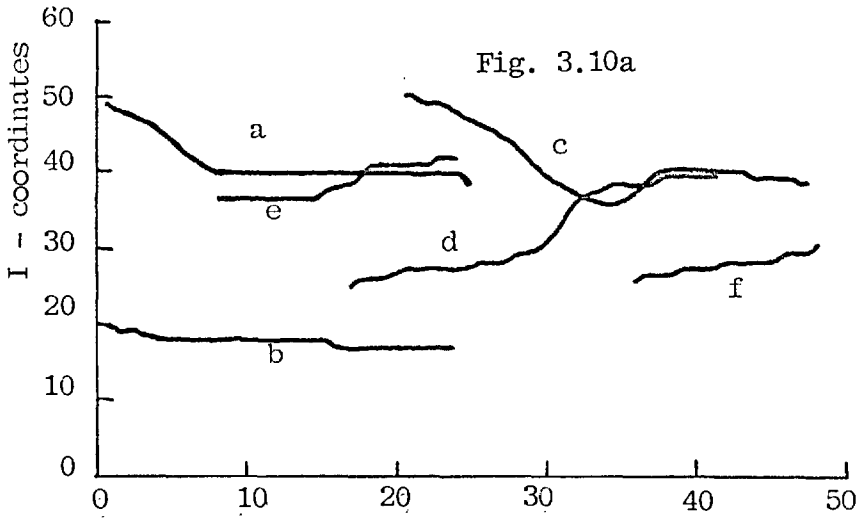

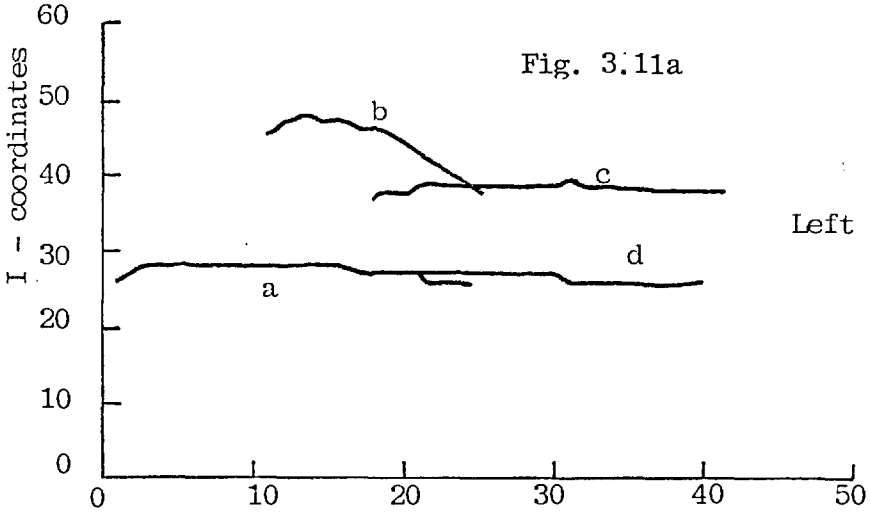

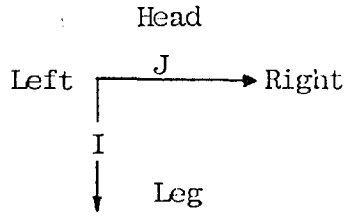

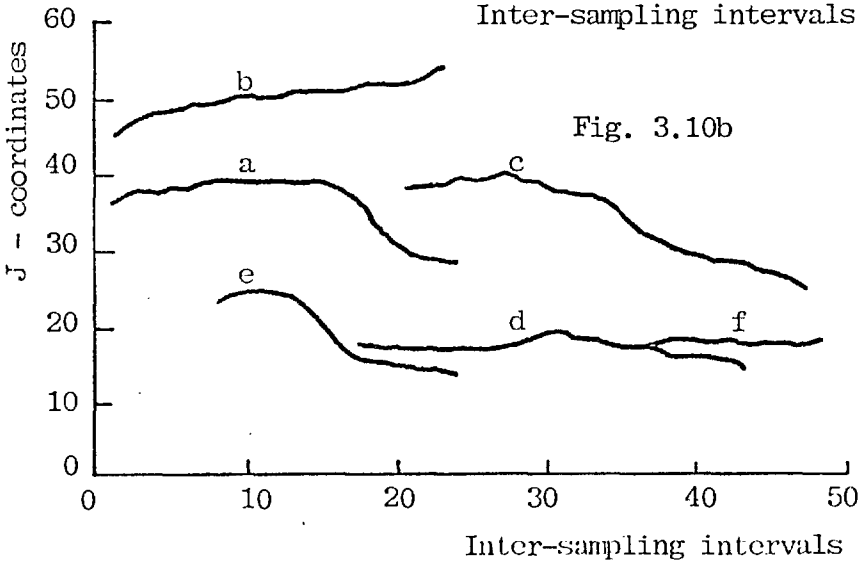

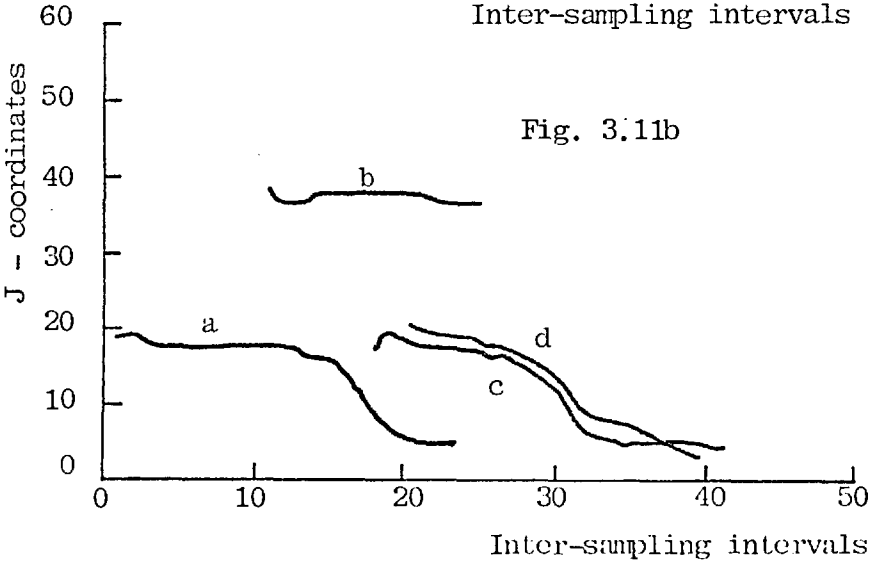

Figure 3.10,3.11 Trajectories of local maxima and minima of selected section of the vibrations.
(Fig. 3.10 - first vibration, Fig. 3.11 - second vibration)

extremes seems to justify spatio-temporal analysis of these signals.

3.5 Spectral Domain Spatial Contouring

One very interesting question to ask concerning the spatial distribution of precordial vibration is whether different frequency components of the vibration spread differently across the chest wall. This is a very relevant area of investigation to our present study because if indeed different frequency harmonics behave differently on the precordium, this could be an indication that analysis in the spatial context can yield information which is not available from the temporal signals at a few chosen sites.

The spread of different frequency components of the signal can be studied by plotting contour maps of the spatial distribution of the amplitude spectra. The amplitude spectra of the first and second vibrations were calculated for each site using FFT. (The duration of the signals were 390 msec and the fundamental frequency of the spectra were therefore 2.56 Hz). The spatial distribution for each harmonic component was plotted as contour maps at 5 dB intervals using the same interpolation procedure as described in the previous section. Since the amplitude values above the 35 harmonics (about 90 Hz) are very small, the spatial distribution for those components are likely to be heavily contaminated by noise. Therefore only the first 35 components were contoured.

Figure 3.12 shows examples of the contour maps of

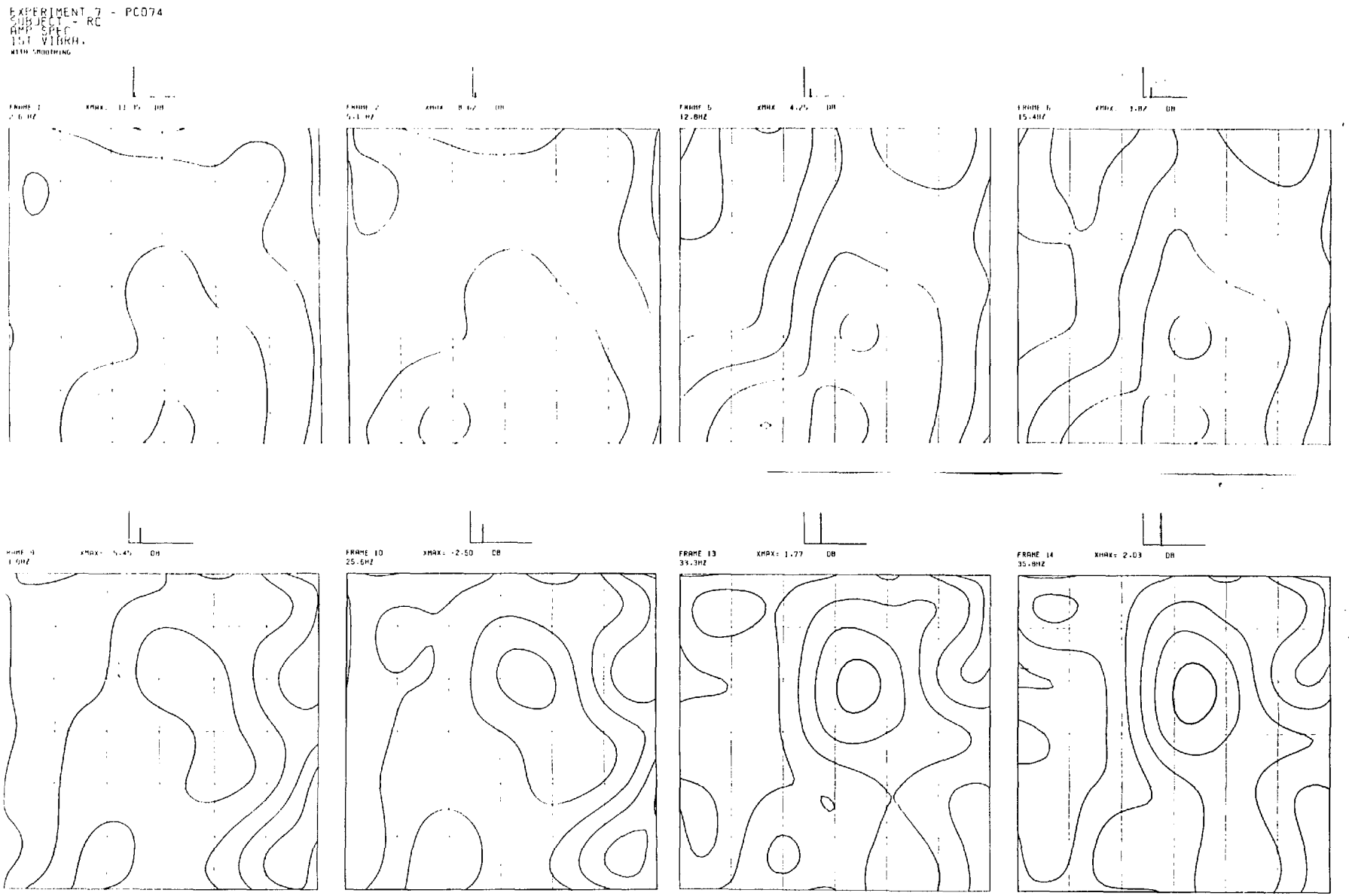

Figure 3.12 Example of contour maps of the spatial distribution of amplitude spectra of first vibration for various harmonics. Contour intervals = 5 dB.

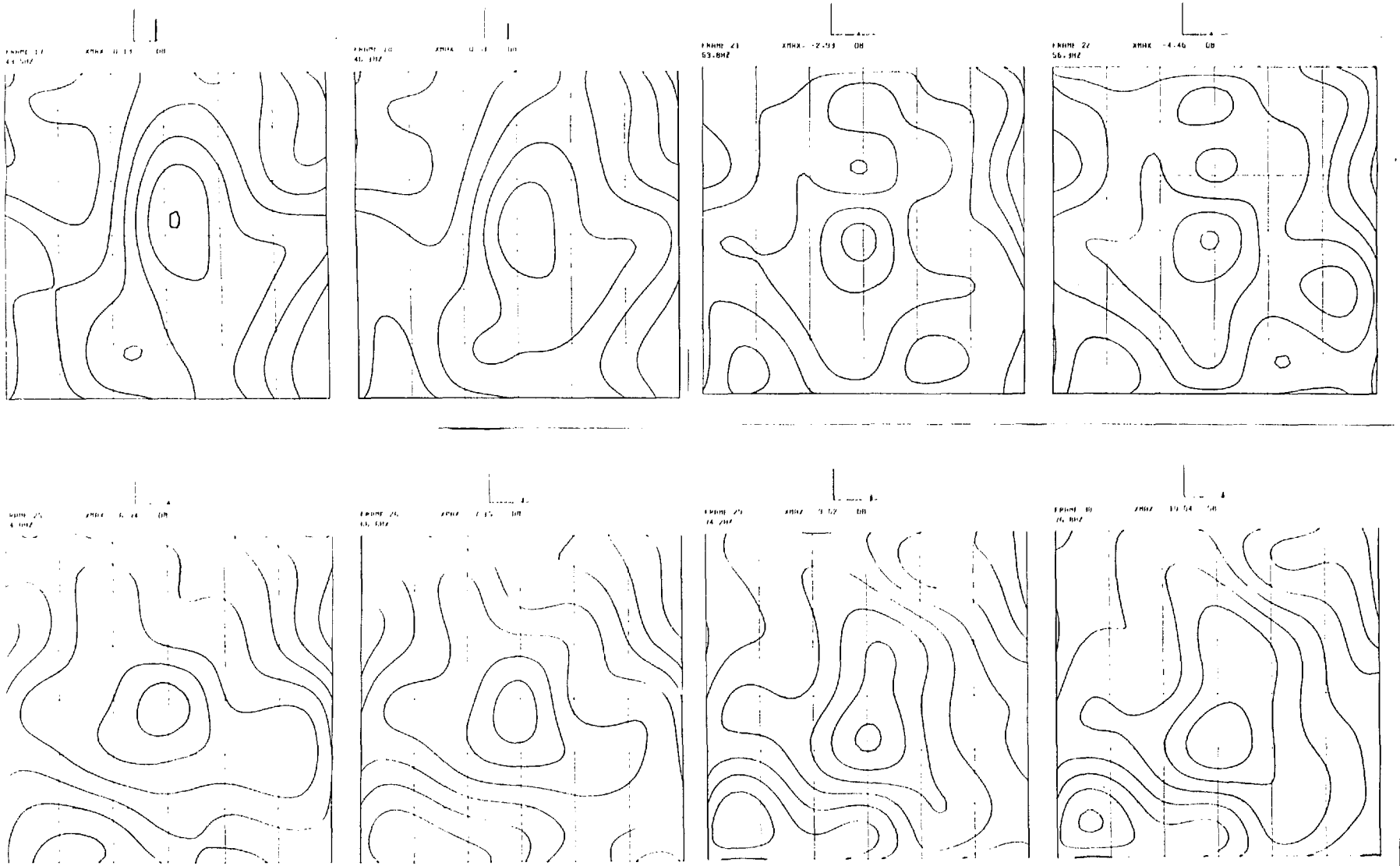

Figure 3.12b (See figure 3.12a)

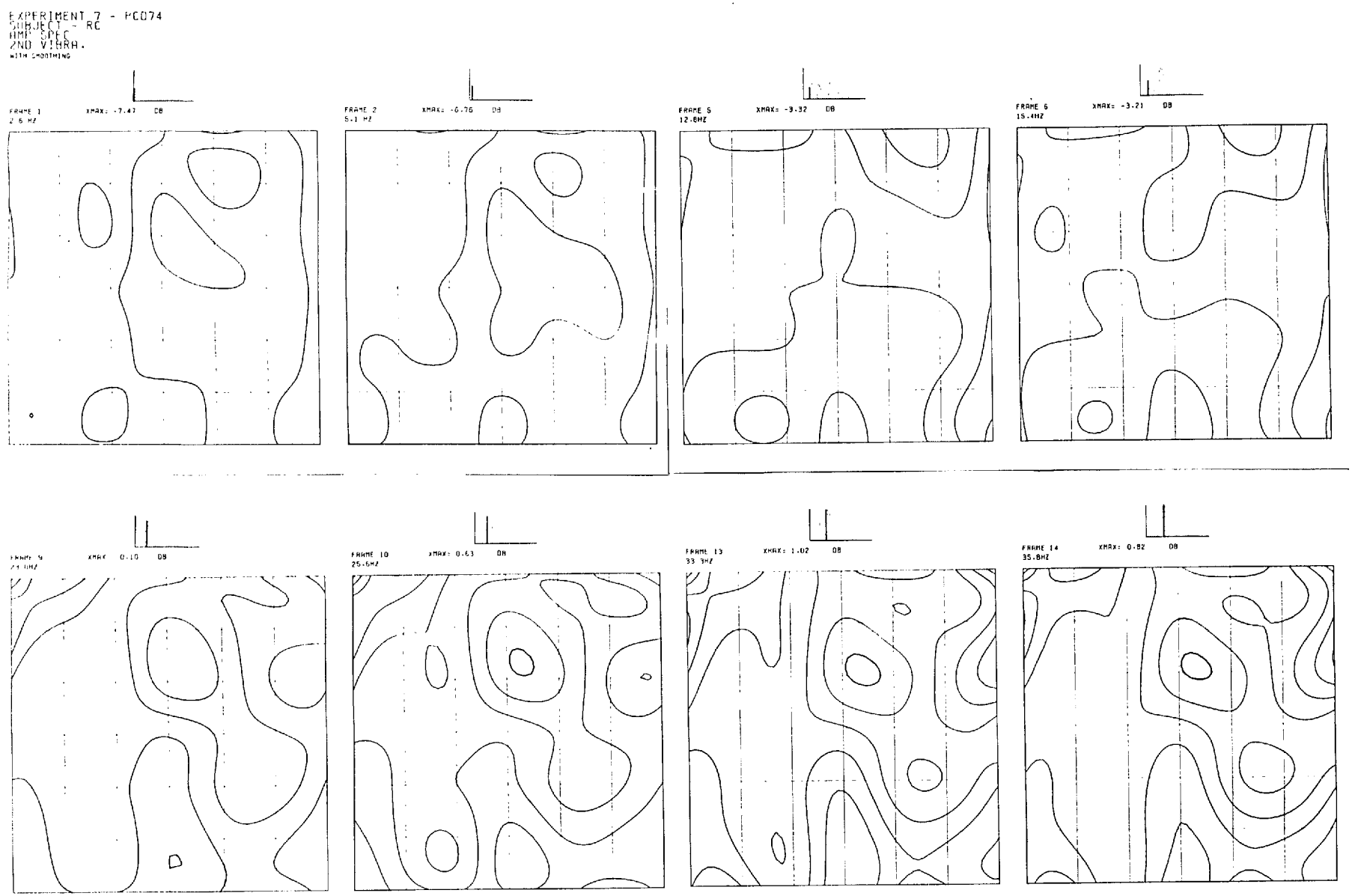

Figure 3.12c Example of contour maps of the spatial distribution of amplitude spectra of the second vibration for various harmonics. Contour intervals = 5 dB.

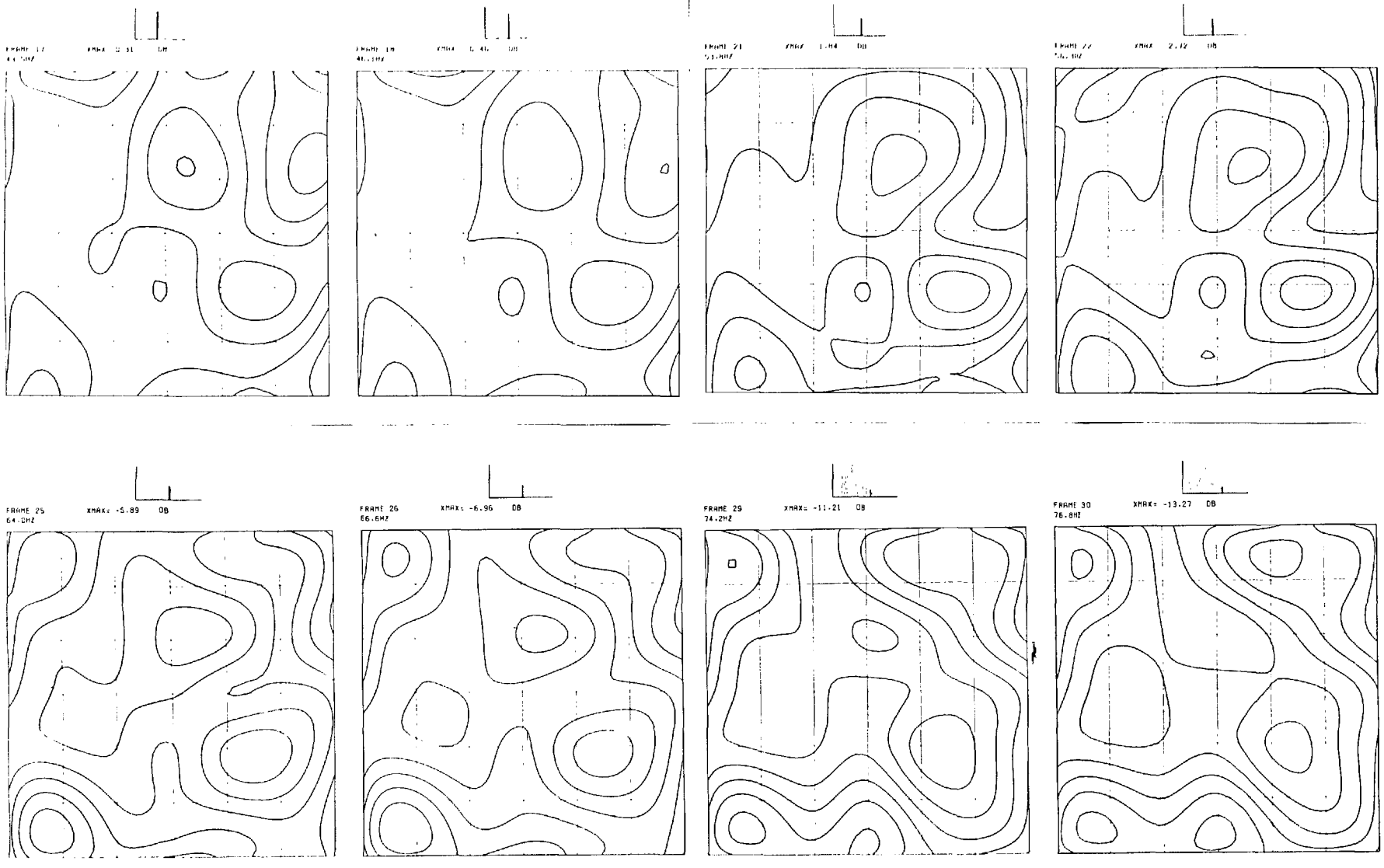

Figure 3.12d (See figure 3.12c)

amplitude spectra for a number of harmonics. The reference spectrum corresponds to that at location (3,4) and the frequency harmonic that the contour map represents is indicated by the thickened component. It is noted that the contour maps that the locations where maximal amplitude values are observed vary with frequency. As a whole, the spatial pictures change appreciably with frequencies. At low frequencies, the maximal activity is found to occur at the area beneath the sternum and move to the left parasternal region at higher frequencies.

The fact that the contours were drawn at 5 dB intervals allowed the amount of spatial damping over the precordial area where the measurements were taken to be estimated; this is simply related to the number of 5 dB lines at each harmonic. Predictions about the spatial damping are available from other worker (FABER, 1963). Figure 3.13 a and b show the number of 5 dB lines at different frequency harmonics for the first and second vibrations. The damping of the first vibration was found to be monotonically increasing with frequency as predicted by Faber. But for the second vibration, maximum damping seemed to occur at about 70 Hz. It was also noted that the damping was not symmetrical about the sites where maximal amplitudes were observed.

3.6 Isochrone Maps

Various workers (FABER, 1962; VERBURG, 1975) have studied the spread of precordial vibrations by plotting

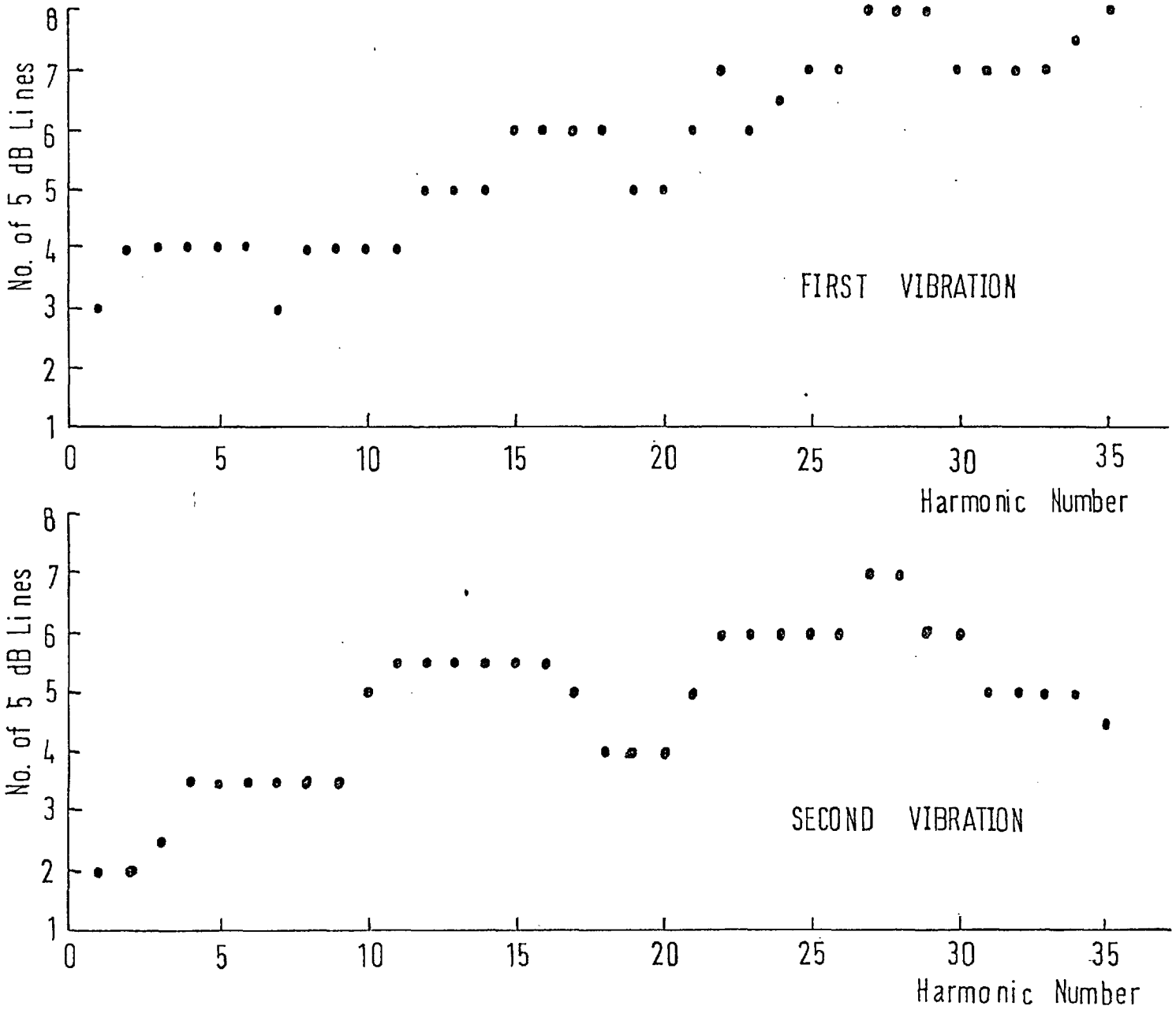

Figure 3.13 The number of 5 dB lines at different frequency harmonics for the first and second vibrations.

isochrone maps - contour maps of equal 'time delay' of activity on the chest wall. The delay measurements were made using some signal feature like the peak of the first large positive excursion of the signal. However, an examination of the spectra of the signal indicates that the spectral shapes vary significantly across the precordium (figures 3.1, 3.2). This variation will manifest itself in the time domain signal which implies that using the peak of the time domain signal as a basis for delay measurement is questionable.

In order to overcome this difficulty, we attempted to estimate the time delays between signals using frequency-domain rather than time-domain measurements. Since it is known that a time shift of a signal causes a linear trend added to its phase spectrum, it is therefore possible to estimate such a shift by measuring the slope of any linear trend in the unwrapped phase spectra of the signal at different locations. If a signal f(t) with a complex spectrum $F(\omega)$ is advanced in time (i.e. occurs earlier) by δt, it can be shown (appendix B) that the spectrum becomes $\exp(j\omega\delta t)F(\omega)$. This is equivalent to adding a ramp with a gradient of t to the phase spectrum of the signal. Since phase angle values are expressed in the principal angle range of $\pm\pi$, the phase ramp will cause discontinuity (or wrapping) in the phase spectrum especially in the higher harmonic terms. One may attempt to unwrap such a spectrum by adding or subtracting multiples of 2π to the phase values

in order to make all the differences of two consecutive phase spectral values less than π. However there can be ambiguity especially when the wrapping is complicated. An alternative method of unwrapping is by spinning the signal. Now, an even function centred symmetrically about zero time will obviously have a zero phase spectrum. For signal with no symmetry, the 'simplest' phase spectrum is obtained if it is positioned such that it approximates as close to an even function as possible. Hence a simple and reliable method of unwrapping the phase spectrum is by spinning the signal round until the simplest phase spectrum is obtained. Figure 3.14a, demonstrates the effect of spinning the signal, in one sample point steps, on the phase spectra of some of our measurements. Once the simplest phase pattern is obtained, the rest of the unwrapping is straight-forward. The spinning can be conveniently implemented by adding a phase ramp, corresponding to one sample shift, to the phase spectrum and recalculate the phase value to the principal angle range.

According to our earlier results as well as from examining the unwrapped phase spectra, we found that it was necessary to divide the spectra into three frequency bands (H 1-7, H 11-19 and H 21-30) so that the phase spectra in each of the band can be adequately represented by a linear trend for majority of the signals. To the phase spectra of each band, a least square line was fitted. The goodness of fit was estimated by the sum of square of error for the

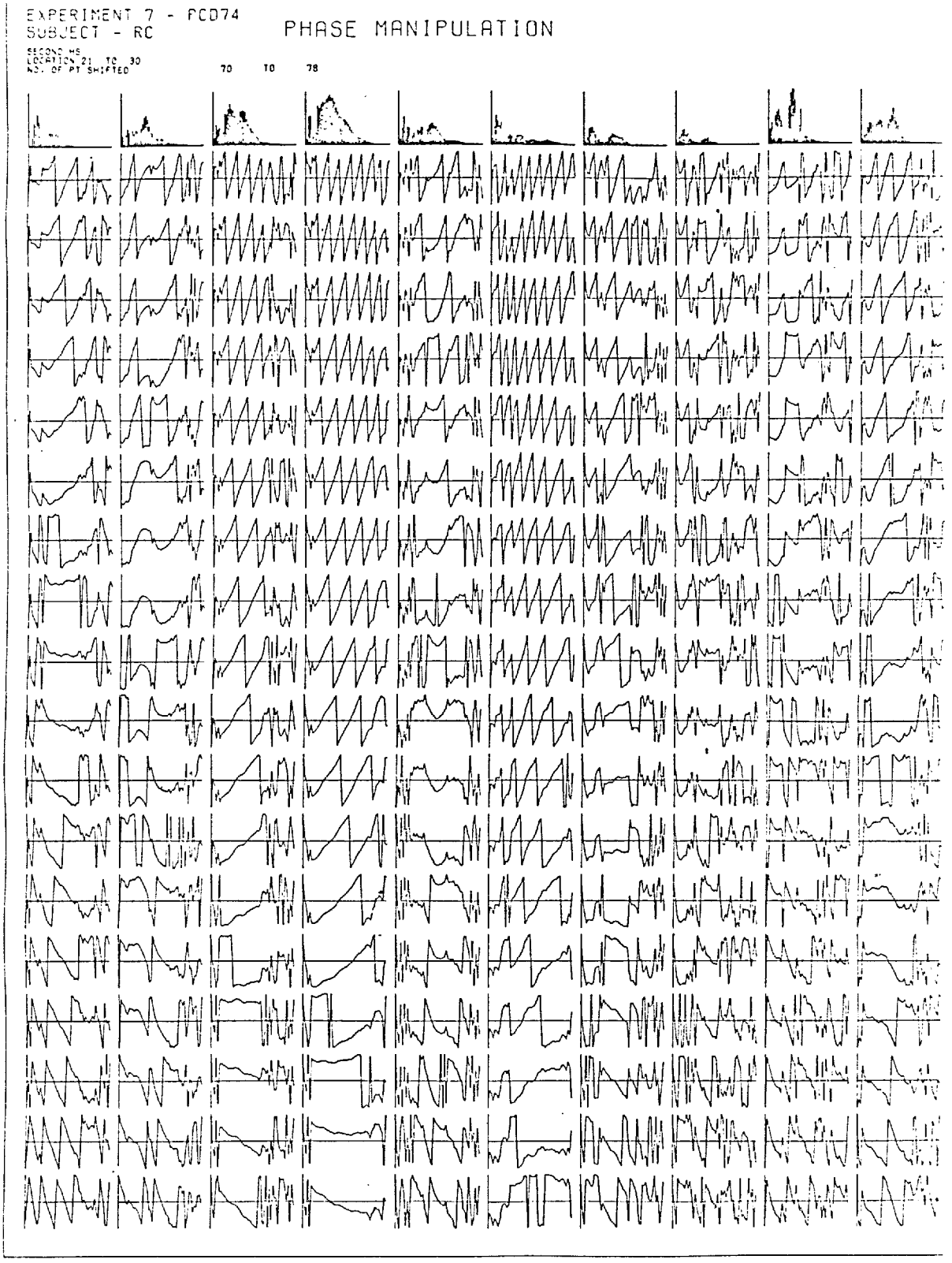

Figure 3.14a Examples of unwrapping phase spectra by spinning the signal one sample point at a time.
(Location laterally; spinning - down the columns)

fitted line. This was repeated over all sites and only those phase spectra which could be reasonably represented by a straight line were considered. (The others can be thought of as having so different a waveshape that it cannot be compared in latency with the other signals). The delays between signals at some of the sites were obtained from the slopes of the least square lines for the three different frequency bands (appendix B). These latency values were then interpolated using bicubic spline surfaces and subsequently contoured. Examples of the isochrone maps are shown in figure 3.14b. The blank areas were areas where the phase spectra could not be represented by a straight line.

The locations where the signal arrived earliest were found to be different in the three bands for both vibrations. Multiple sites of early arrival were also observed. The complicated patterns of the isochrone maps suggested that the notion of 'apparent velocity' was rather difficult to define.

3.7 Spectral Standardisation

Recent research in other areas of biological signals in our laboratory (SAYERS, 1974; SHEPPARD, 1976) have indicated that certain biological signals are better characterised by their phase spectra than their amplitude spectra. It was, therefore, attempted to establish whether the variation of the vibrations observed across the chest wall are amplitude or phase dominant. This can be done by

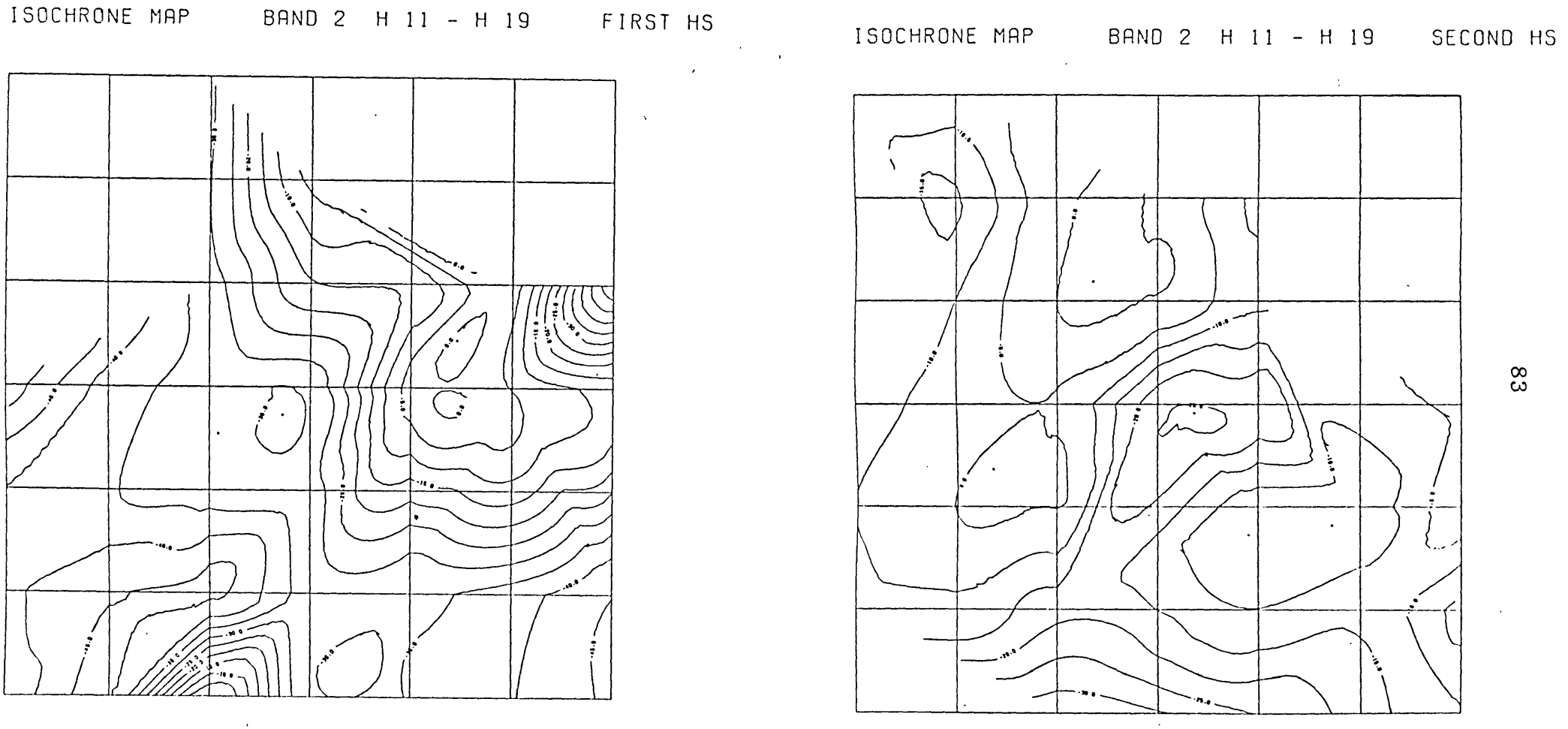

Figure 3.14b Examples of isochrone maps. The contour lines represent equal 'time of arrival' of the signal. Contour intervals = 5 msec.

synthesising the vibrations using standardised amplitude and phase spectra in turn (SAYERS, 1974). The vibration at each site was synthesised from a reference amplitude spectrum and the corresponding phase spectrum of that site. This was repeated with a reference phase spectrum and the individual amplitude spectrum. The two sets of synthesised signals were compared with the actual observations by cross-correlation functions (normalized). Figure 3.15 shows the CCF of the signals synthesised from a reference amplitude spectrum and the observations. Figure 3.16 is that from a reference phase spectrum. The reference spectra were taken from location (3,4) and the example shown is for the first vibration.

A comparison of figures 3.15 and 3.16 with the auto-correlation functions of the observations (figure 2.16) indicates that the signals synthesised from a reference amplitude spectrum are more similar to the observations than that synthesised from a reference phase spectrum.

In order to allow all harmonic components to contribute equally (instead of being dictated by the spectrum of the reference location), the exercise was repeated with a uniform amplitude spectrum and a random phase spectrum (rectangularly distributed between $+\pi$ and $-\pi$) as a reference in turn. Figure 3.17, 3.18, 3.19 and 3.20 are the synthesised signals and their cross-correlation functions with the observation respectively. Table III and IV give the respective maximum values of cross-correlation coeffi-

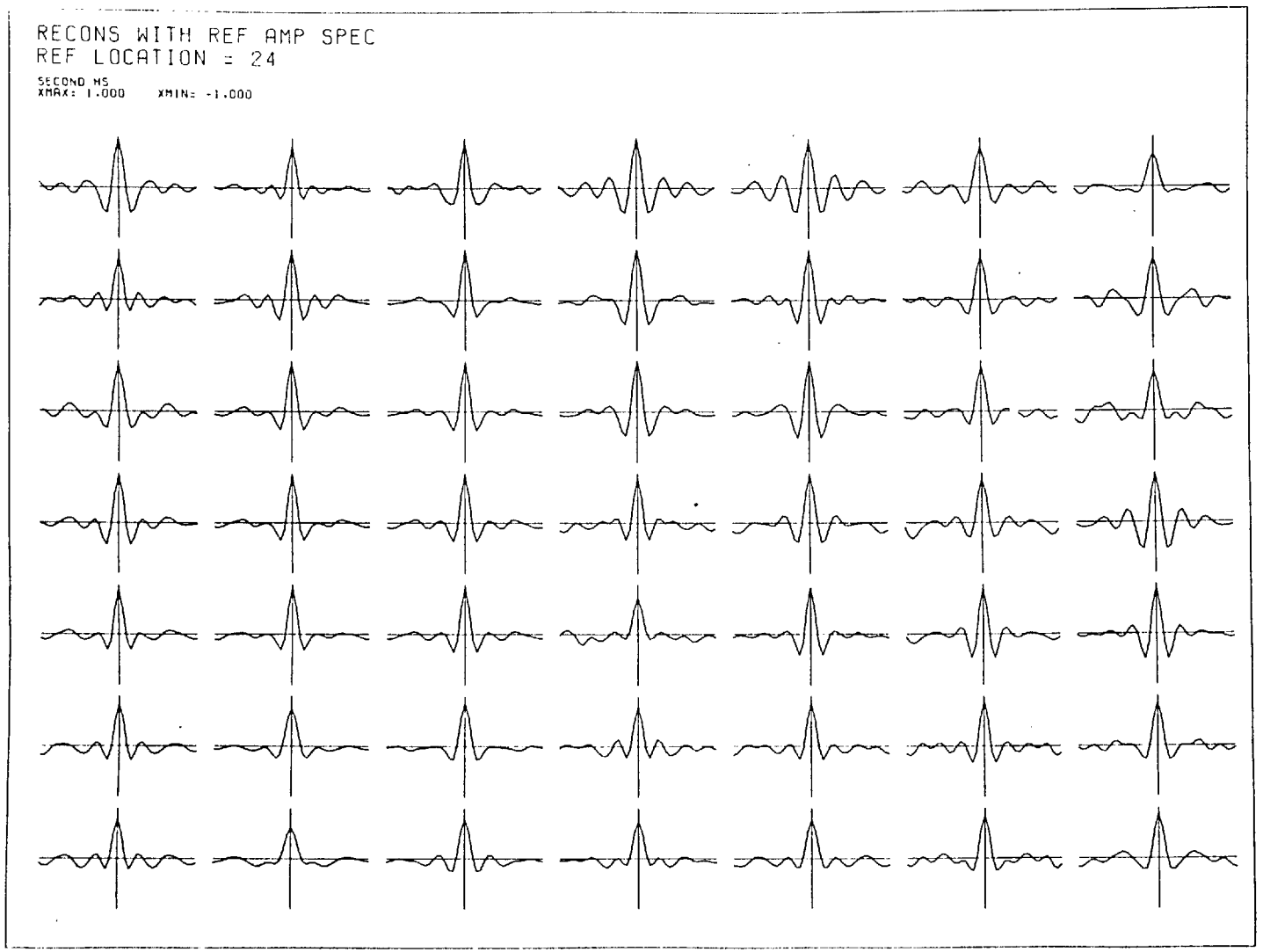

Figure 3.15 The normalized CCF between the observations and signals synthsised from the amplitude spectrum of a reference location (3,4). (compare with figures 1.16 & 3.16)

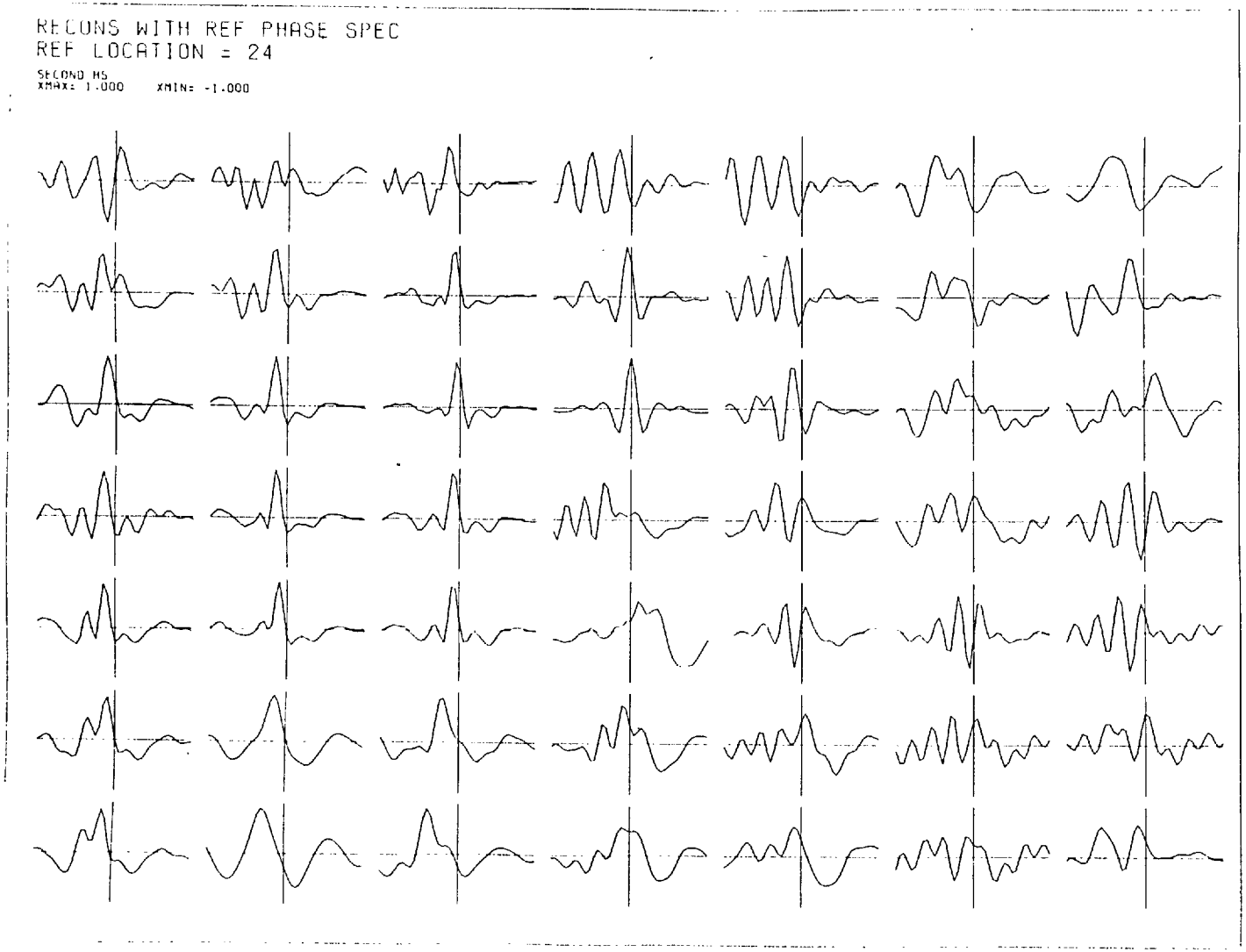

Figure 3.16 The normalized CCF between the observations and signals synthesised from the phase spectrum of a reference location (3,4). (Compare with figures 1.16 & 3.15).

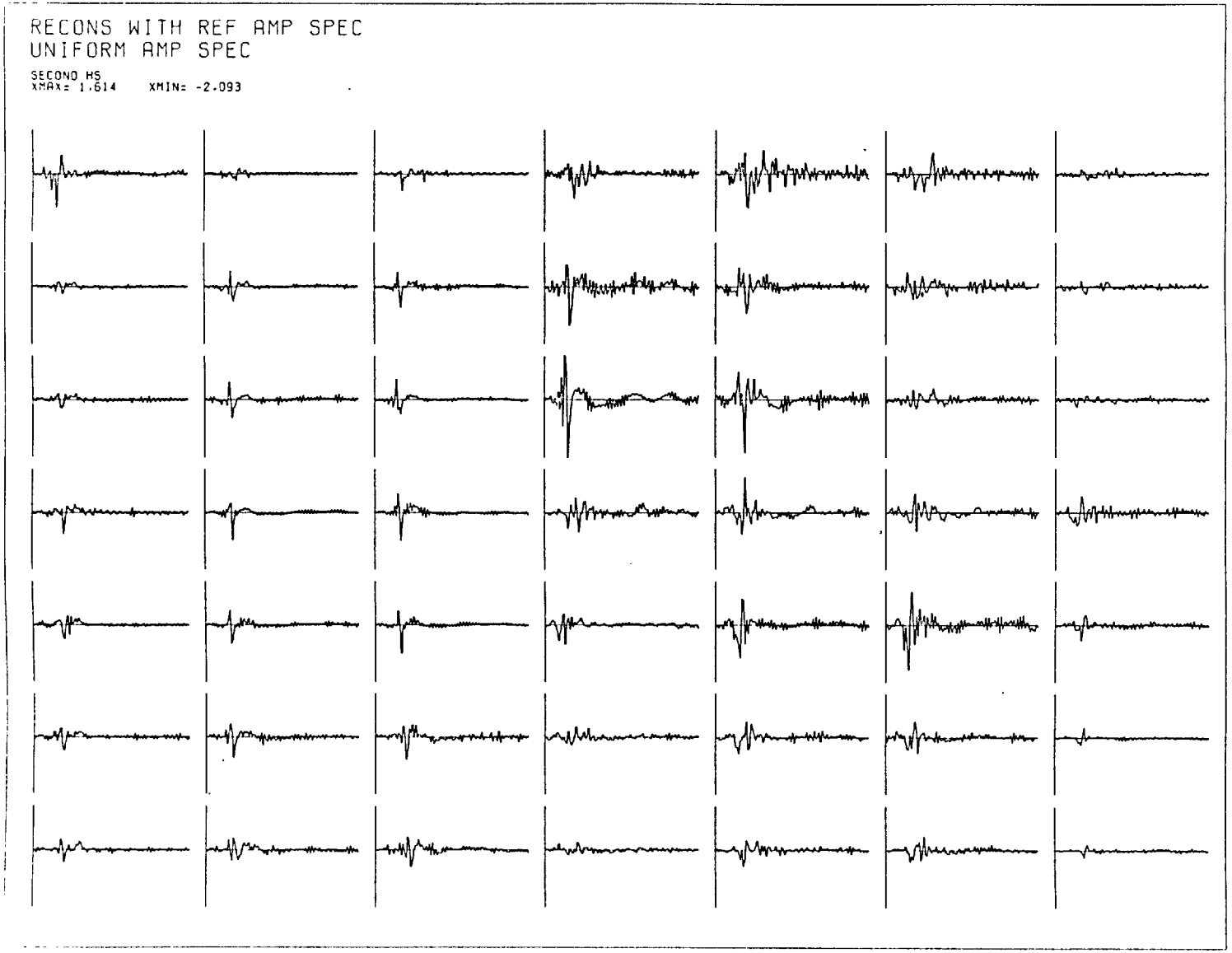

Figure 3.17 Synthesised signals using a uniform amplitude spectrum of each individual observation (compare with figure 1.14 & 3.18).

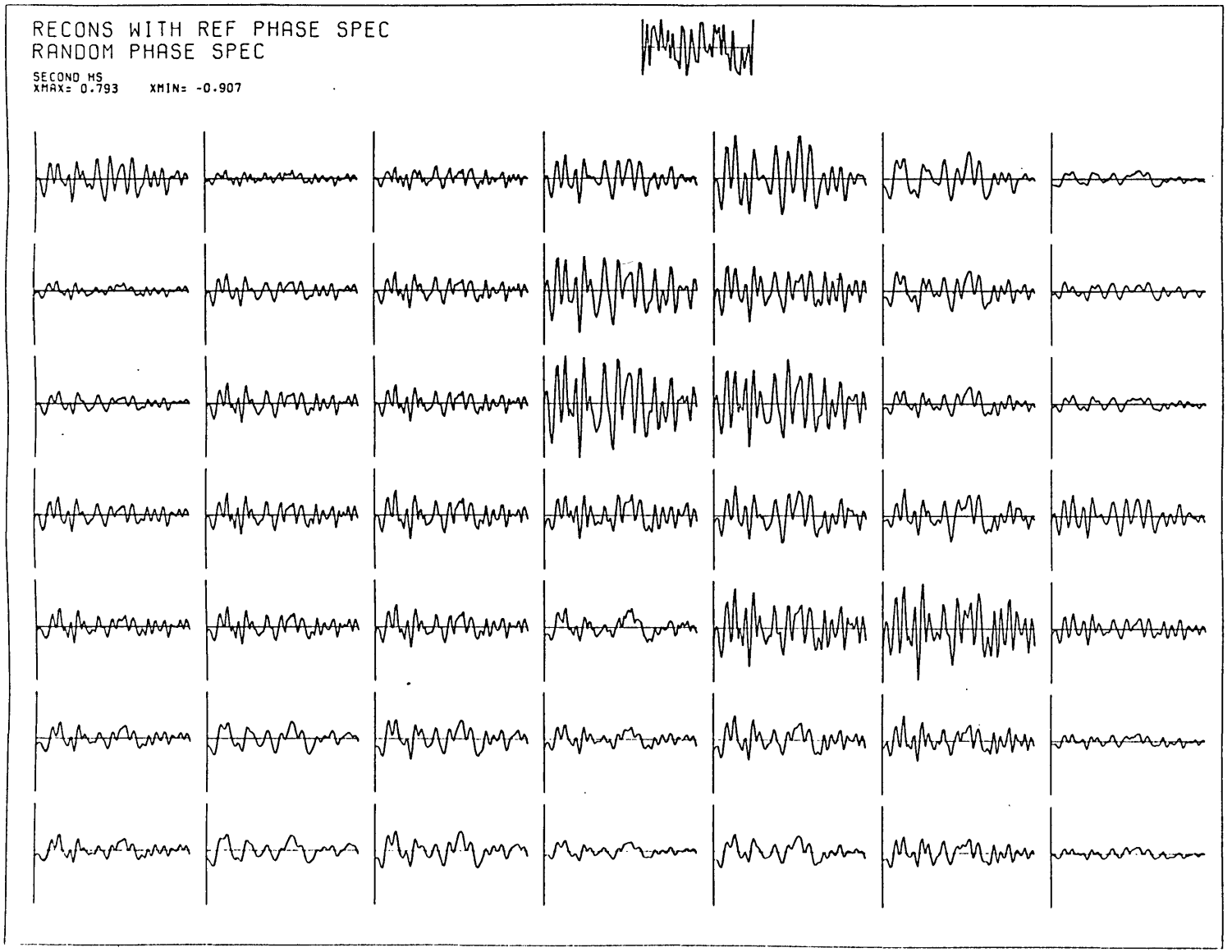

Figure 3.18 Synthesised signals using a random phase spectrum and the amplitude spectrum of each individual observation.

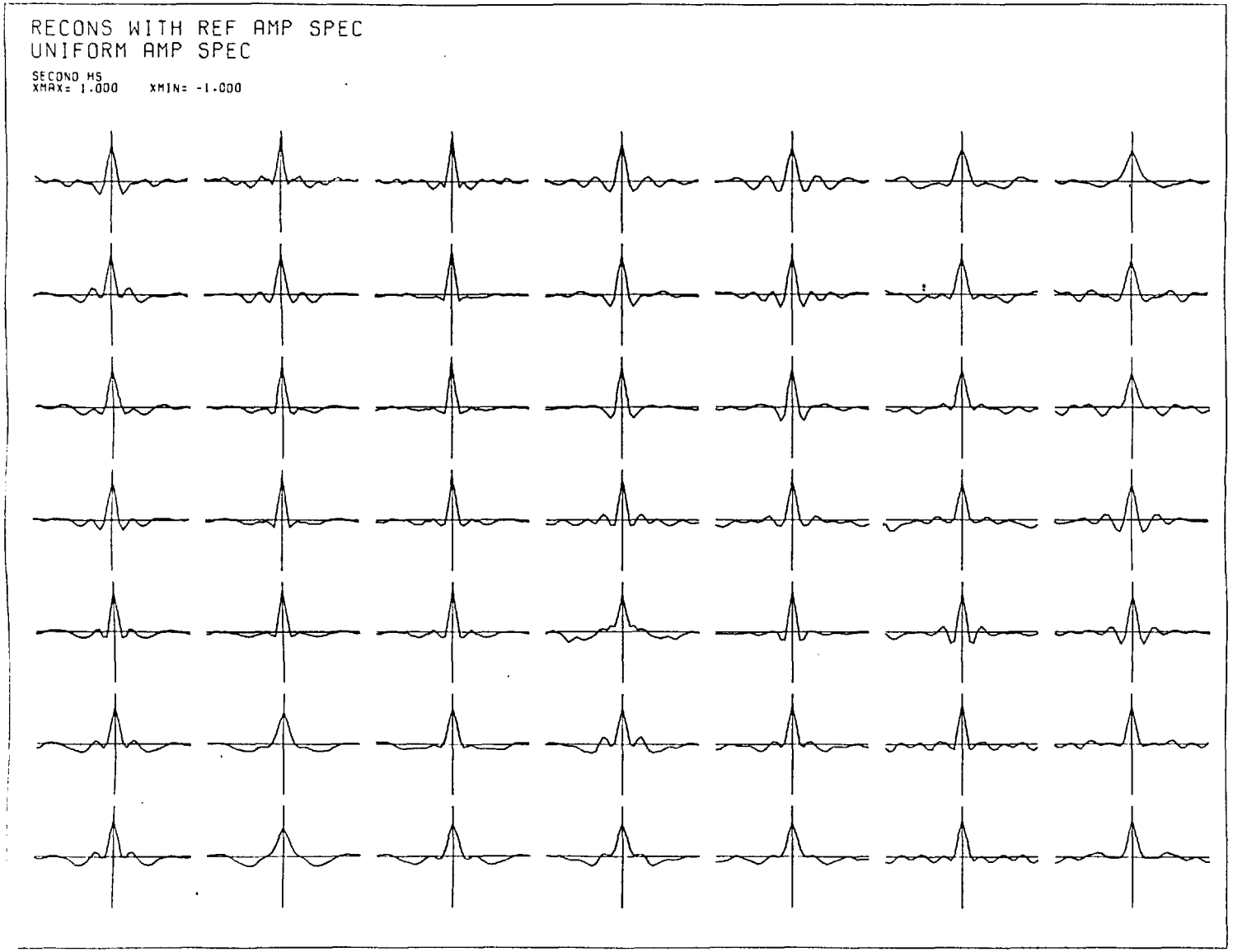

Figure 3.19 The normalized CCF between observations and signals synthesised from a uniform amplitude spectrum.

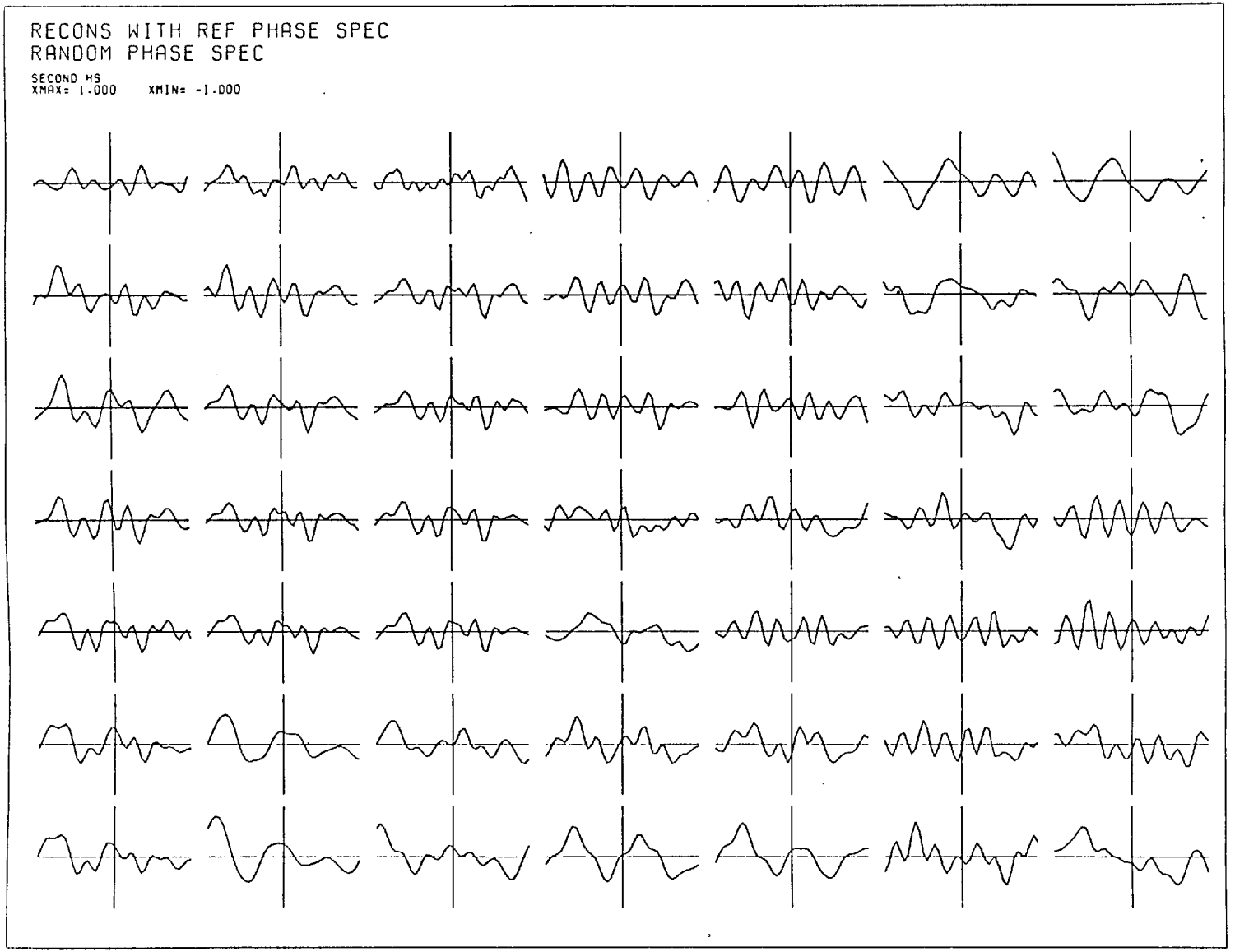

Figure 3.20 The normalized CCF between observations and signals synthesised from a reference random phase spectrum.

	.67	.77	.76	.71	.61	.54	.48
	.69	.72	.78	.68	.65	.62	.55
	.66	.71	.79	.63	.62	.70	.63
TABLE III	.75	.81	.81	.74	.71	.70	.62
	.79	.82	.83	.81	.72	.74	.70
	.71	.61	.67	.72	.68	.72	.73
	.68	.57	.59	.67	.66	.66	.70

	.62	.51	.50	.38	.46	.45	.55
	.67	.49	.49	.54	.50	.47	.54
	.62	.46	.47	.55	.64	.42	.42
TABLE IV	.36	.45	.45	.31	.40	.41	.48
	.38	.44	.43	.37	.27	.29	.55
	.46	.61	.52	.35	.34	.46	.40
	.58	.66	.46	.32	.42	.48	.50

TABLE III,IV Maximum values of correlation between the observations and the signals synthesised from a uniform amplitude spectrum (Table III) and a random phase spectrum (Table IV) at various measurement sites.

cients at each site, normalised to $\pm$ 1.

The phase spectra evidently dominate the pattern of the signal. The vibrations are still recognisable at most locations with the amplitude spectra disregarded while randomising the phase spectra destroys the signal pattern completely.

3.8 Transient Simulation

A careful examination of the unwrapped phase spectra (figure 3.21) of the first vibration reveals two features for which explanations are needed. Some phase spectra (e.g. location (3,4))exhibit sudden discontinuities which amount to about 180^{o} and therefore cannot be caused by the 'wrapping effect' of phases. Other phase spectra (e.g. location (4,3)) show an 'oscillatory' phenomenon. Our evidences so far suggested a possibility of vibrations from more than one source being transmitted through different pathways and summated at the surface. If this model were indeed applicable, the phenomena observed in the phase spectra could possibly be accounted for by the interaction of two transients, perhaps of different basic frequencies and at a certain time delay one to another.

The amplitude and phase spectra of a simulated summation of two transient oscillation signals $f_1(t) + f_2(t)$ were calculated where;

$$f_1(t) = \exp(-\beta(t-t_0)) \sin \omega_1(t-t_0)$$

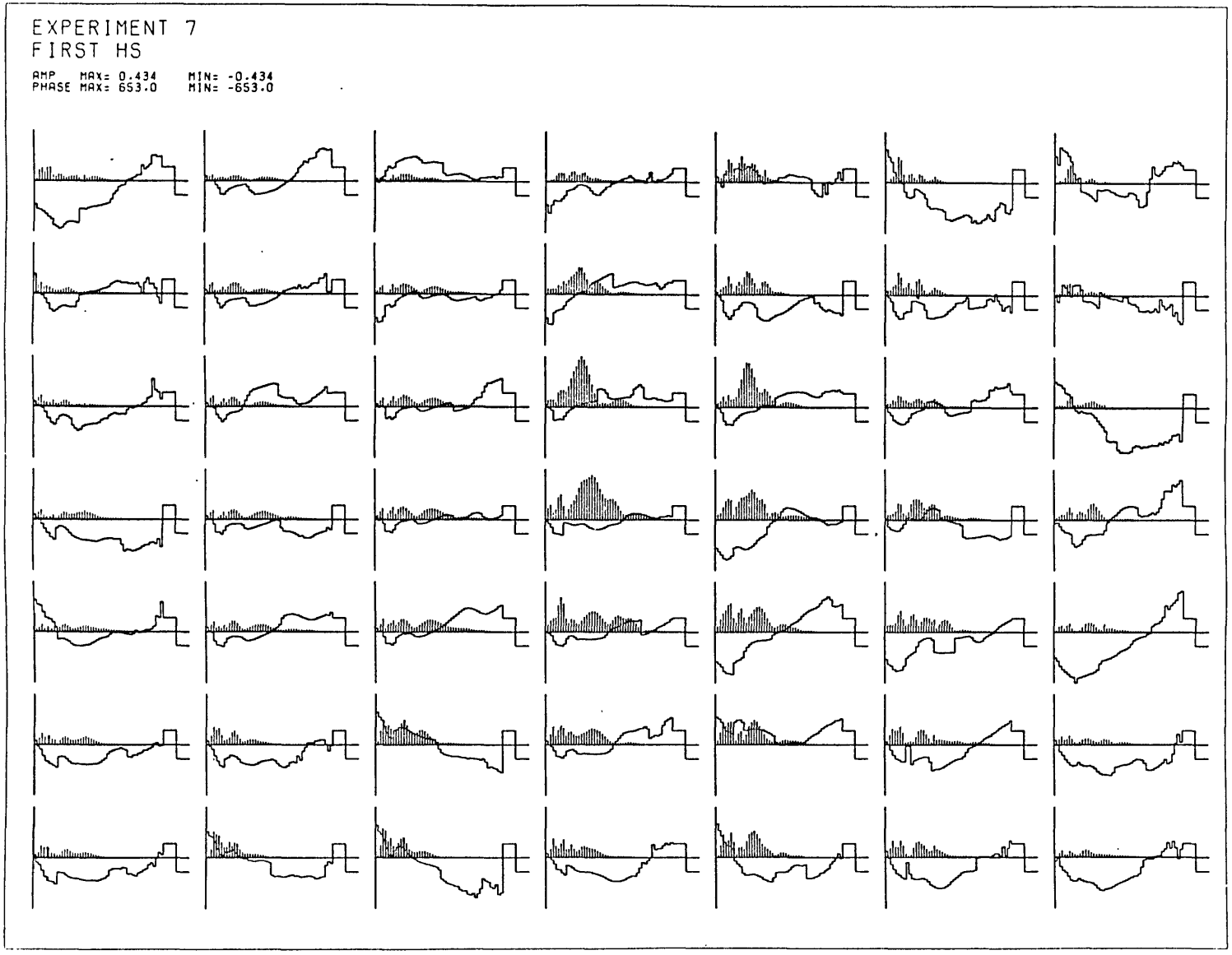

Figure 3.21 The unwrapped phase spectra of measurements at various sites plotted with their amplitude spectra. The last 10 phase values are $\pm 180^0$ reference. Note the sudden phase discontinuities and the oscillatory phase patterns.

$$f_2(t) = \exp(-\beta (t-t_0-t_d)) \sin \omega_2(t-t_0-t_d)$$

.....(3.5)

The fundamental frequency ω_2 and the time delay t_d were allowed to change gradually in turn in order to observe the corresponding variations in the amplitude and phase spectra of the summated signal.

Figures 3.22 and 3.23 are examples of the spectra where the fundamental frequency of f_1 was fixed at 28 Hz and the time delay t_d at 30 msec respectively while $f_2$was allowed to increase gradually from 28 Hz at 1.5 Hz increments.

Both the phase discontinuity and the oscillatory phenomenon of the phase spectra were reproduced. Some of the phase spectra of the simulated signals are not too dissimilar to that of the observations.

3.9 Deconvolution Study

One possible method of studying the relationship between related signals is by enquiring what network is required to produce one signal from another. In our case of precordial vibrations, the signal at one site can be thought of as a 'source' and one enquires whether the characteristics of the hypothetical networks which connect this reference signal to all other signals exhibit any consistent feature across the chest wall. The procedure is effectively a deconvolution type of operation and is summarised in the following steps:

1. The signal $f_0(t)$ which had the broadest frequency

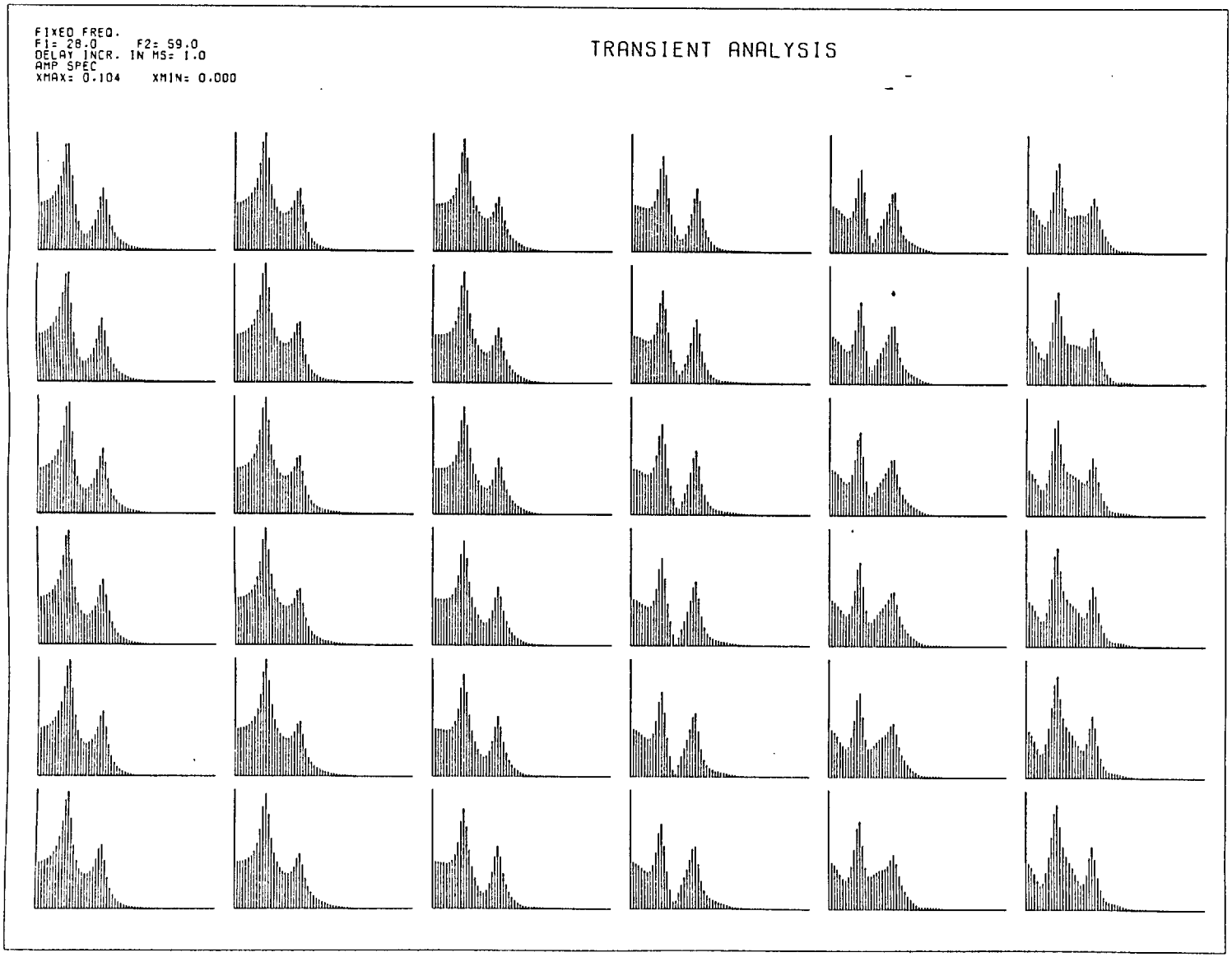

Figure 3.22 The amplitude spectra of the simulated transient oscillations of two sources.

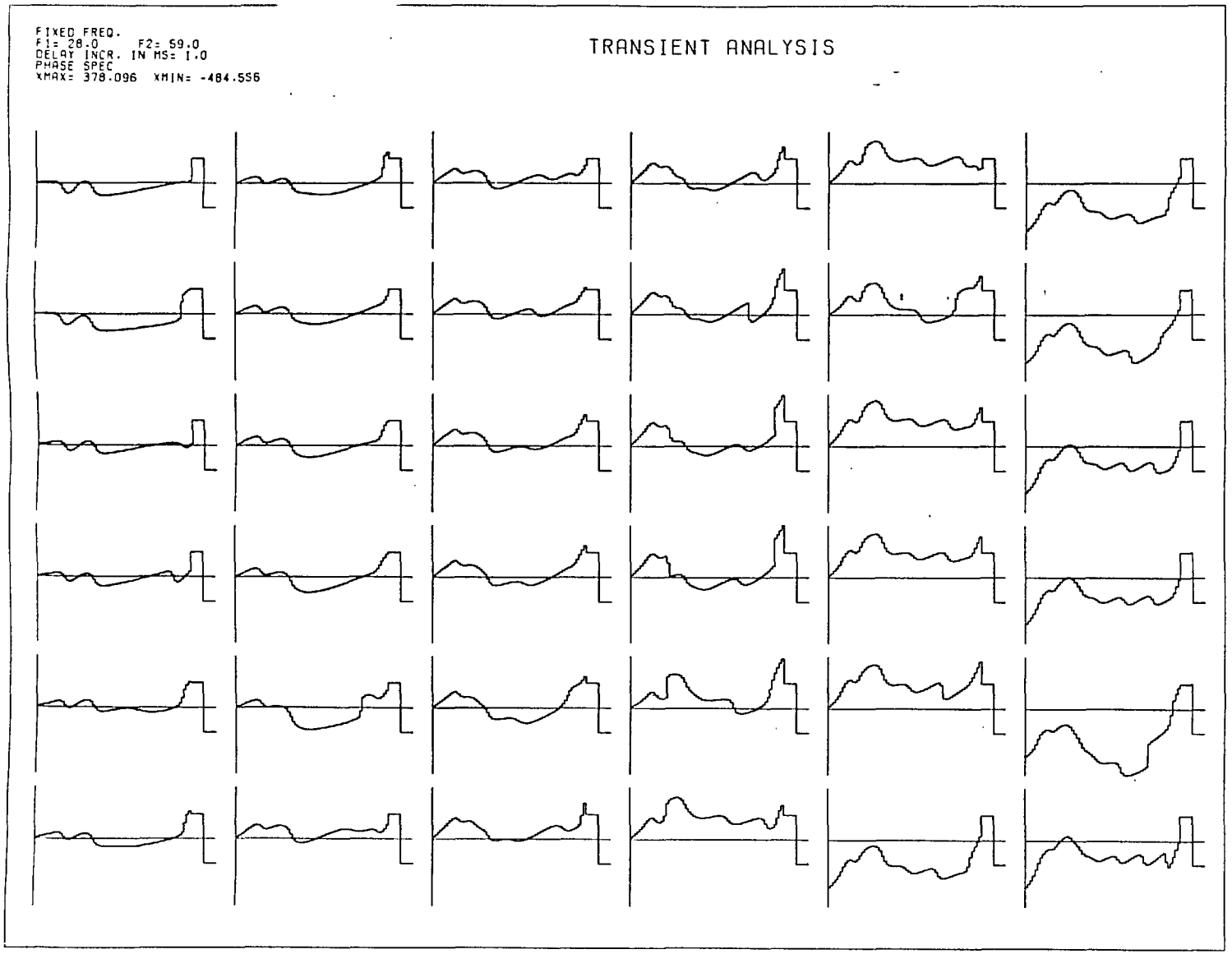

Figure 3.23 The unwrapped phase spectra of the simulated transient oscillations of two sources.

spectrum was chosen as reference (location (5,4) for the first vibration and (3,4) for the second).

2. The complex spectra $F_0(\omega)$ of this reference signal and that of all other signals $F_i(\omega)$ at location i were calculated by FFT.

3. The complex transfer functions $T_i(\omega)$ were computed using the relationship

$T_i(\omega) = F_i(\omega) / F_0(\omega)$ provided $F_0(\omega)$ for the given is greater than 10% of the maximum of all $F_0(\omega)$.

$T_i(\omega) = 0$ otherwise.

4. From $T_i(\omega)$ the amplitude and phase characteristics were calculated.

Figures 3,24 and 3.25 show the amplitude and phase characteristics of such a set of networks for the first vibration taking location (5,4) as reference. No obvious relationship between the responses at different sites were observed except the regional similarity at the sternum and the long delay of the signals below the sternum characterised by the negative phase slope.

3.10 Discussion

One of the main difficulties in the study of any spatio-temporal signals is tha vast amount of data that must be measured, analysed and displayed. With the present day advances in digital computers, this is no longer a limiting factor. The fore-going exercise demonstrates how such

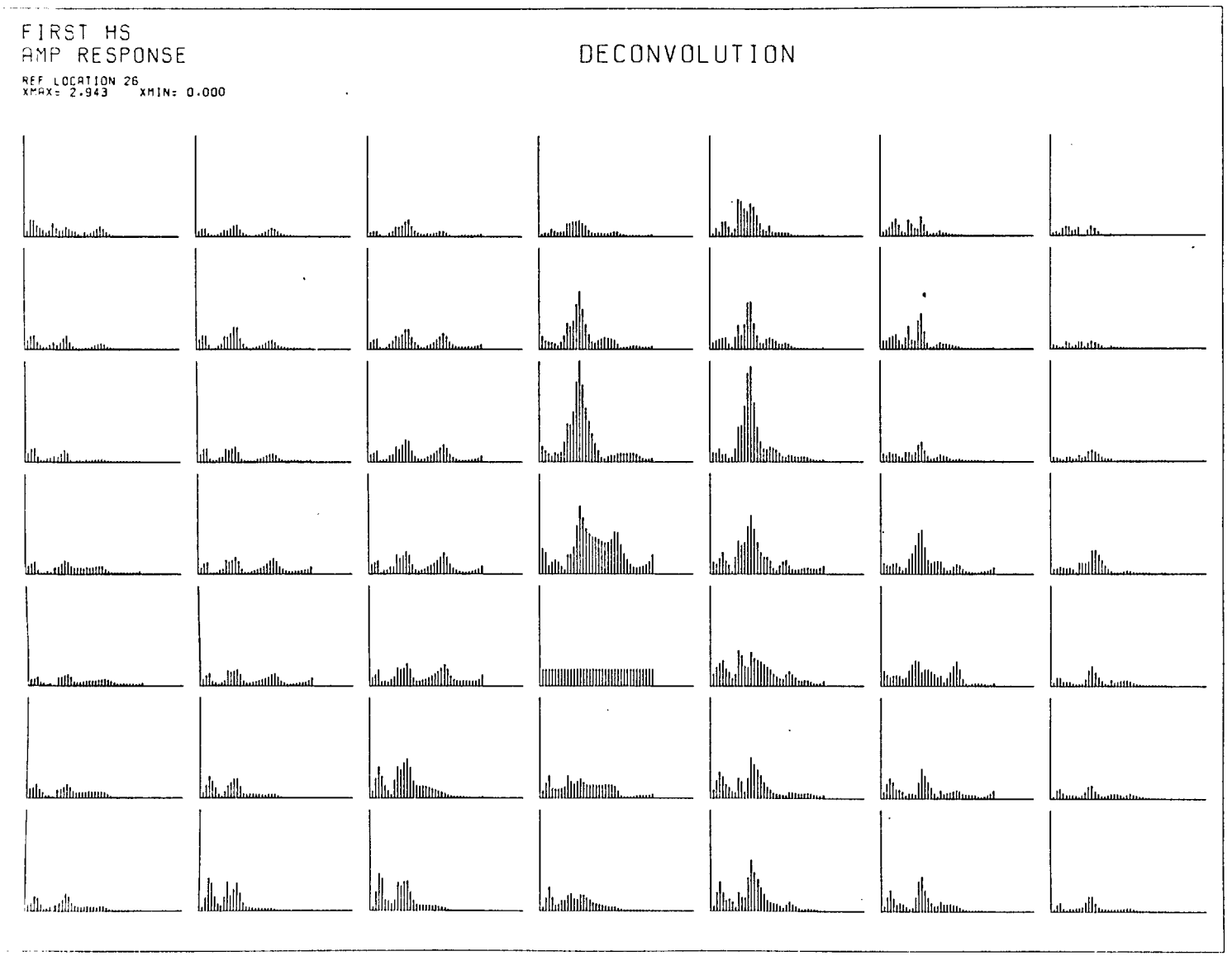

Figure 3.24 The amplitude response of the simulated 'networks' in the deconvolutions study. (First vibration, reference location (5,4)).

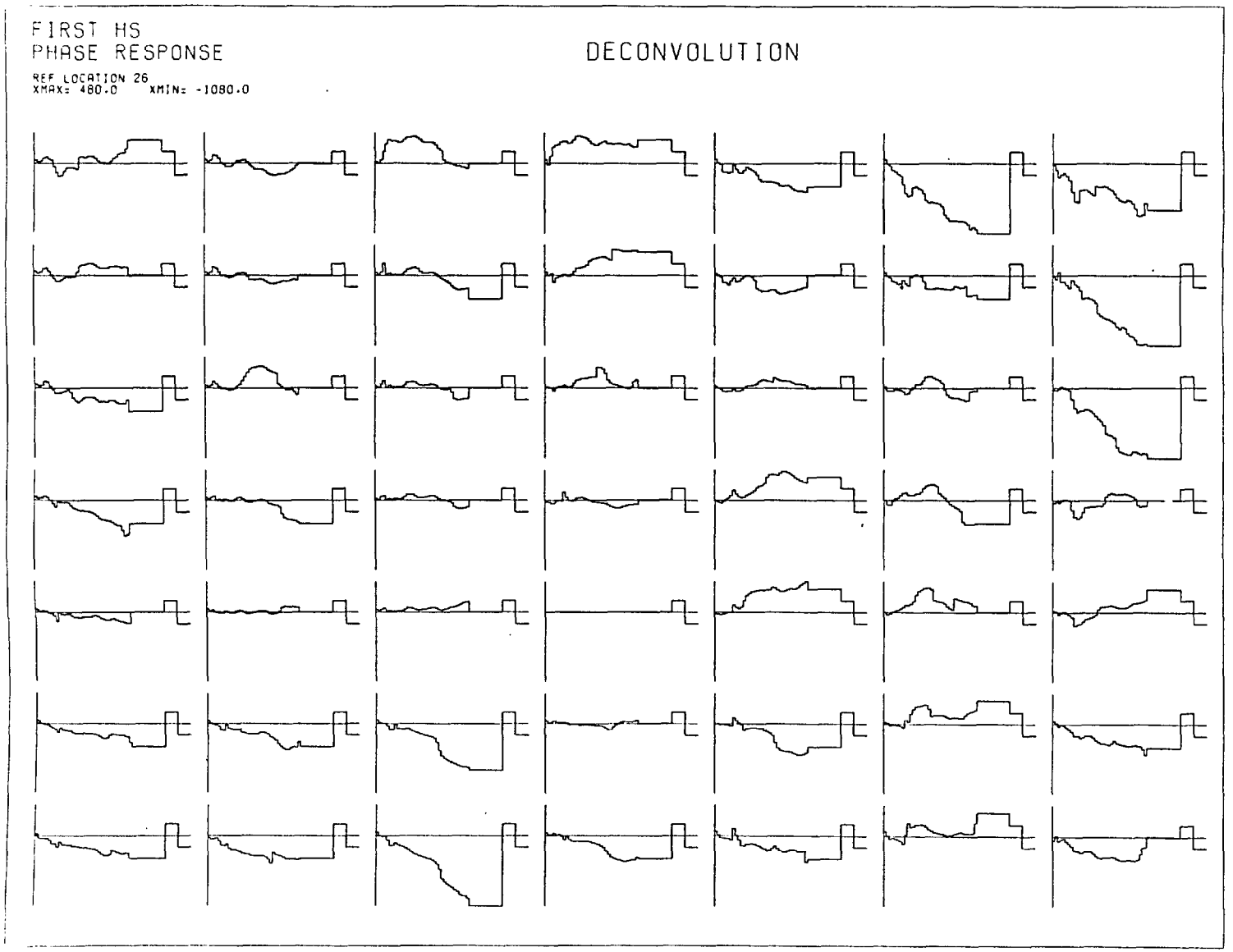

Figure 3.25 The phase responses of the simulated 'networks' in the deconvolution study. (First vibration, reference location (5,4)).

signals can be handled. The time varying signals can be displayed in their appropriate spatial positions clearly (and cheaply on microfilms) to give an overall impression of the spatio-temporal signals. The availability of a representative set of vibration patterns over a large area of the precordium allowed us to observe the double reversal of phase in the second vibration. Verburg (1974) suggested that such reversal of phase is produced by a vibrating source which can be represented by a mechanical dipole model. The double phase reversals observed by us suggest that two or more such sources are needed to represent the genesis of the vibration.

Spatio-temporal analyses of the signal support the speculation that multiple sources transmitted through multiple pathways are responsible for the genesis of the cardiac vibrations detected on the chest wall. The simultaneous multiple local maxima and minima in the spatial contour maps of the vibration signal could possibly be caused by vibrations generated by one or more sources, transmitted through pathways of different characteristics and interferred with one another on the chest surface. The discontinuity of the trajectories of the extremes could also be caused by change of such interferrence pattern as vibrations from a later pathway arrive at the surface.

The shifts of the local extremes in the contour maps of the amplitude spectra can also be explained by the multiple pathway model. Since the chest wall is a complicated

structure of tissues with very different mechanical properties, the transmission pathways from the source to different sites on the precordium can have very different frequency characteristics and causes frequency groups to spread differently.

The complicated isochrone maps we obtained made it difficult to calculate the apparent velocity of spread of the vibrations on the chest wall. The spread, however, is different in a complicated way for different directions which makes the 'apparent velocity' difficult to be defined. The multiple sites of early appearance of signal are in agreement with our other findings.

The reconstruction of signals using standard references for the amplitude and phase spectra demonstrates very well the importance of phase spectra in the pattern of any structured signals. This supports the need for the development of methods and techniques for handling phase spectra which have been so far very much neglected, perhaps because of wrap-around effects. The phase spectral averaging technique and the methods of computing and displaying the statistics of phase spectra developed for this work may therefore prove to be valuable in this and other signals.

The transient simulation of the chest wall vibration was found to be helpful in explaining various features which appeared in the unwrapped phase spectra of the signal. This reinforces our speculation that the precordial vibrations can only be adequately represented by a model of multiple

sources through multiple pathways.

The deconvolution study was not found to be particularly fruitful. This is probably because the interactions of vibrations from different sources and pathways were too complicated to be represented by a series of network from a 'secondary source' to other sites on the precordium.

CHAPTER 4

THE INVERSE PROBLEM

4.1 Introduction

The work reported in earlier sections is entirely based on the analysis of observations. An alternative approach that should be investigated is the theoretical analysis that may further help to explain the findings and describe the nature of the signal. This section therefore considers mathematical modelling, and solving the inverse problem for the inferred sources of the precordial vibrations. In view of the fact that a comprehensive set of measurements of precordial vibrations was available to us, there are at least two reasons which merit such an investigation. Firstly, solving the inverse problem (i.e. source inversion) may serve as a data reduction procedure which combines the information from many measurement sites into signals representing the sources which are generally much smaller in number. Secondly, the ultimate purpose of measuring the precordial vibration is to make inferences about the condition of the sources from these measurements. Any method which brings us 'nearer' to the sources may be advantageous.

There are two general steps in solving any kind of inverse problem. The first is to simulate the system between the source and the measurement by some model from

which the transfer function or coefficients can be calculated. The second step is to calculate the possible source (or sources) which will give rise to the measurements after passing through the simulated system.

A mathematical model for the precordial vibrations was implemented on a digital computer in order to calculate the transfer coefficients. The formulation of the model and its implementation are presented below. The problem of using the conventional least square method for the inversion is demonstrated and a modified constrained least square method used for the inversion is discussed in the light of its application and limitation.

4.2 A Mathematical Statement of the Inversion Problem

Any linear system can be expressed by the following matrix equation

$$\underline{y} = A\ \underline{x} \qquad \text{.....(4.1)}$$

where $\underline{x}$ is a (n x 1) column vector representing n sources after passing through the system represented by the (m x n) matrix A produces m observations represented by the (m x 1) column vector $\underline{y}$. Theoretically if $\underline{y}$ can be measured with infinite accuracy and A is exactly known, only m observations are needed to calculate m sources and the source vector is given by

$$\underline{x} = A^{-1}\ \underline{y} \qquad \text{.....(4.2)}$$

In practise, A is usually only a simulation and the observations are contaminated by noise. This causes large errors

in the calculation of $\underline{x}$. Redundancy is usually introduced by making the number of measurements greater than that of the source and solve the linear system by the least square method.

$$\underline{x} = (A^T A)^{-1} A^T \underline{y} \qquad \text{.....(4.3)}$$

with $m > n$

4.3 The Model

The modelling of the chest for the purpose of calculating the transfer from the vibration sources to the measurement sites can be approached in two parts: (i) a mathematical model which represents the nature of the generators, the mode of transmission of the vibration and the behaviour of the transmission pathways; (ii) a geometric model simulating the geometry of the chest.

Mathematical model

The mechanism of wave propagation in a viscoelastic medium like body tissues had been well studied by Frank (1951), von Gierke (1952) and Oestreicher (1951) and applied to the modelling of precordial vibration by Verburg (1974). The mechanical properties of such media are described by its density ρ and the Lame's constants:

$$\lambda = \lambda_1 + i\omega\lambda_2$$

$$\mu = \mu_1 + i\omega\mu_2$$

where μ_1 = coefficient of shear elasticity,

μ_2 = coefficient of shear viscosity,

λ_1 = coefficient of volume compressibility,

λ_2 = coefficient of volume viscosity.

A discussion of the general properties of a viscoelastic medium is given in appendix D.

Our model was implemented basing on the following assumptions:

(1) The chest is an infinite, homogenous, isotropic, incompressible, viscoelastic medium.

(2) The sources of vibration are small spheres situated in the heart and are permitted to oscillate in any direction about their quiescent positions.

(3) The medium is linear. The vibration at the sources can be decomposed into its harmonic components and the vibration measured at any point in the medium is a summation of these components with their appropriate attenuation and phase shift.

(4) Assuming the centre of the source sphere of radius, a, situated at the origin and vibrating the x-axis in any Cartesian frame of reference with an amplitude S_0, the x, y and z-components of the vibration at any point in the medium are given by:

$$A_x = S_0 \, e^{j\omega t} \left[A_1 \left(\frac{x^2}{r^2} h_2(kr) - \frac{h_1(kr)}{kr} \right) + B_1 \left(2h_0(hr) - \left(1 - 3\frac{x^2}{r^2}\right) h_2(hr) \right) \right]$$

$$A_y = S_0 \, e^{j\omega t} \left[\frac{xy}{r^2} A_1 h_2(kr) + 3B_1 h_2(hr) \right]$$

and $A_z = A_y$ with y replaced by z due to symmetry about the x-axis. ..... (4.4)

where $h = (\rho\omega^2/\mu)^{\frac{1}{2}}$ = wave number for the compressive wave.

$k = (\rho\omega^2 (2\mu+\lambda))^{\frac{1}{2}}$ = wave number for the shear wave.

$h_n(z)$ = spherical Hankel function of order n.

$r = (x^2+y^2+z^2)^{\frac{1}{2}}$ = distance from the centre of the sphere.

A_1 and B_1 are constants defined by the boundary condition that at the surface of the source sphere, r = x = a and $S_x = S_0$ and $S_y = S_z = 0$. It can be shown that,

$$A_1 = \frac{3Ka\ h_2(ha)}{ka\ h_2(ka)\ h_2(ha) - 3\ h_1(ka)\ h_2(ha) - 2ka\ h_2(ka)\ h_0(ha)}$$

$$B_1 = -\frac{A_1}{3}\ \frac{h_2(ka)}{h_2(ha)} \qquad \ldots\ldots\ldots\ (4.5)$$

(For the derivation and the implementation of the field equation, see appendix E).

(5) Spatially the vibration of the source S can be decomposed into three orthorgonal vectors: S_x = back to front, S_y = left to right and S_z = head to feet, the front, left and head being the positive direction of the vectors. Hence for each frequency ,

$$\underline{S}(\omega) = S_x(\omega)\ \underline{i} + S_y(\omega)\ \underline{j} + S_z(\omega)\ \underline{k}$$

(6) The principle of superposition holds for multiple sources. Therefore the vibration measured at any point in the visoelastic medium will be the vector sum of the contributions of all the sources at that point.

(7) The first vibration is generated by two sources, one in each ventricle. The second vibration is generated by three sources, one in the aorta above the aortic valve, one in the pulmonary artery above the pulmonary valve and one in the left ventricle.

Geometric Model

Three sets of information are needed for the geometric model : the spatial coordinates of each measurement site, the direction ratios of the normal through these points and the coordinates of the sources of vibration.

The coordinates of the measurement sites were obtained by tracing out carefully the contour of the chest wall of the subject at each horizontal level (constant z) using an adjustable curve. The position of the sites were marked on the curve and later transferred to graph paper. The intersection of the sternum (R4 in figure4.2) and the horizontal section through the third row of the measurements in the first experiment was taken as the origin. Figure 4.1 and 4.2 show the horizontal and vertical contours of the chest surface of the subject. By visual inspection it

can be seen that the error introduced by assuming a constant z value for each row was not very large.

The direction ratio (l,m,n) of the normal to the body surface at each point P was estimated by the fact that it was normal to both the partial gradients $\frac{\partial x}{\partial y}\Big|_{z=\text{const}}$ in the x-y plane and $\frac{\partial x}{\partial z}\Big|_{y=\text{const}}$ in the x-z plane. The partial gradients were estimated using cubic spline fit to the measurements. The short lines in figures 4.1 and 4.2 are the partial normals to the surface at the measurement sites. The normalized direction ratio of the normal to the surface at any point P(x,y,z) is given by,

$$l = \frac{1}{(1 + m_1^2 + m_2^2)^{\frac{1}{2}}} \quad ;$$

$$m = \frac{-m_1}{(1 + m_1^2 + m_2^2)^{\frac{1}{2}}} \quad ;$$

$$n = \frac{-m_2}{(1 + m_1^2 + m_2^2)^{\frac{1}{2}}} \quad ;$$

where $m_1 = \frac{\partial x}{\partial y}\Big|_{z=\text{constant}}$ & $m_2 = \frac{\partial x}{\partial z}\Big|_{y=\text{constant}}$

Note that in order to minimize error due to end-effect in the calculation of the direction ratios, two rows and one additional column of contour were traced from the subject. The measuring sites were bounded between S2 to S8 and R2

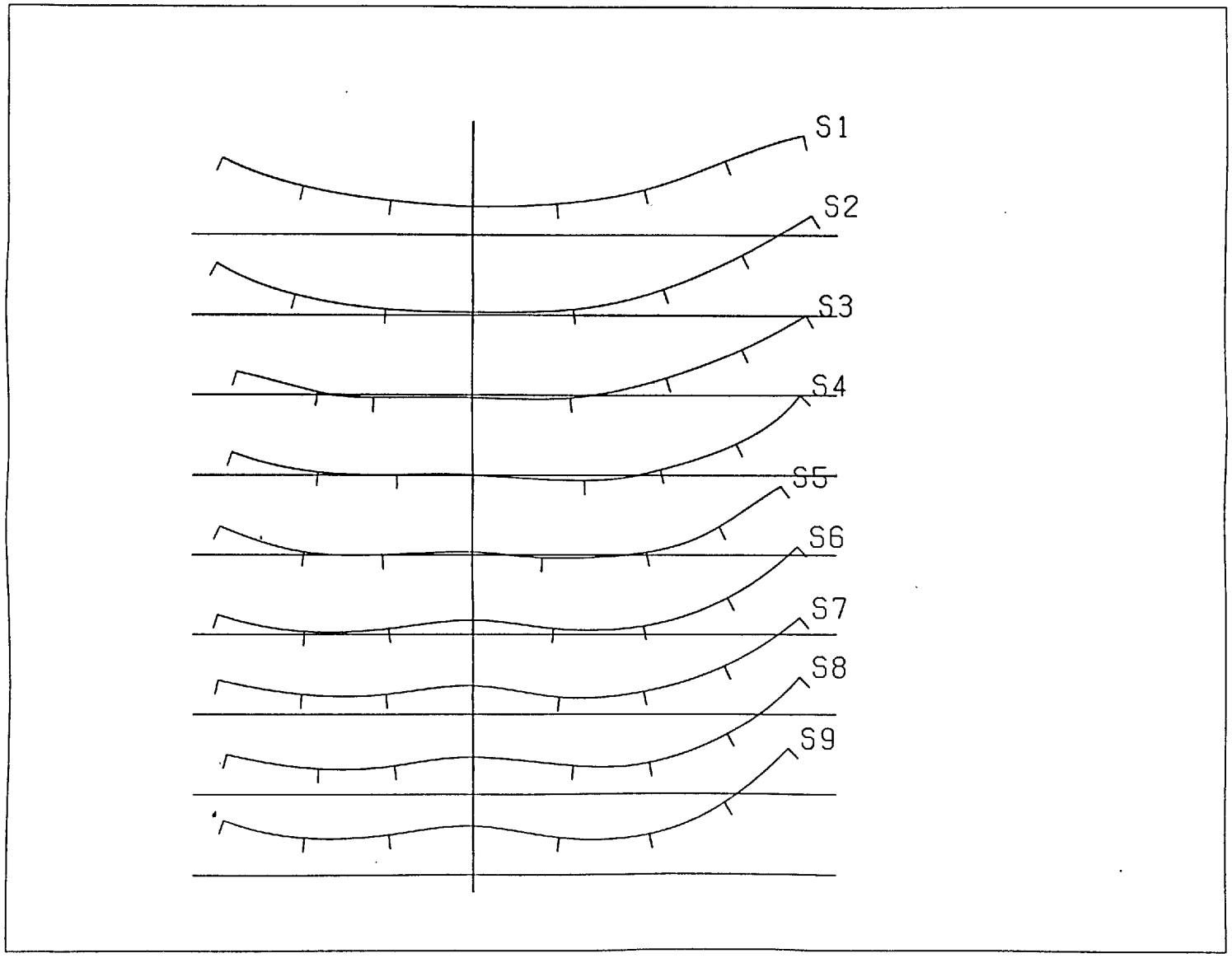

Figure 4.1 The horizontal contours of the chest wall showing the partial normals to the chest surface at the measurement sites.

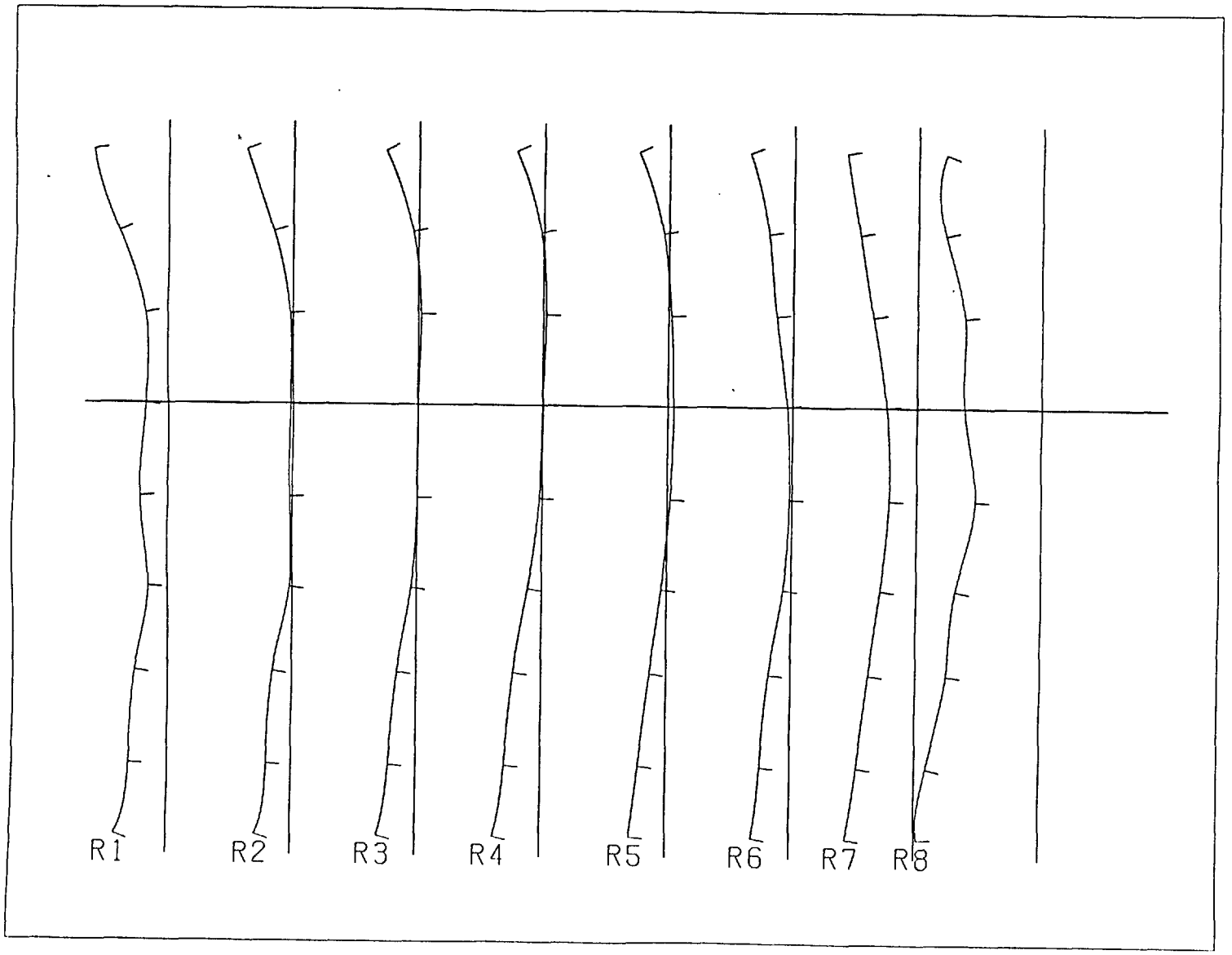

Figure 4.2 The vertical contours of the chest wall showing the partial normals to the chest surface at the measurement sites.

to R8 in the figures.

The positions of the sources were estimated from the cross-sectional anatomy given by Eycleshymer and Schoemaker (1938). The third row of our measurements corresponds approximately to section 26 on the anatomical atlas. The two sources for the first vibration were assumed to be in the two ventricles near the mitral and tricuspid valves respectively. They simulated the vibrations caused by the acceleration and deceleration of the blood mass in the haemodynamic system during the onset of ventricular systole. Two of the sources for the second vibrations were placed in the aorta and the pulmonary artery just above the two semilunar vales (section 25) and the third source was placed somewhere in the left ventricle (between section 26 and 27). They simulated the vibration caused by the acceleration and deceleration of the blood mass in the vessels and in the left ventricle at the beginning of diastole. Table V shows the coordinates of the centres of the sources taking the intersection of the vertical through the sternum and the third row as the origin. The axes are defined as shown in the diagram.

4.4. Discussion on the Assumption of the Model

By assuming the chest as a infinite medium, one implies no reflection from the chest wall. Although there is no direct evidence that this is the case, Verburg (1975) has pointed out that the reflection from the chest surface is unlikely since the vibration diminishes rather rapidly along

SITES	X	Y	Z
Mitral	-7.50	2.25	-2.80
Tricuspid	-4.75	-0.25	-3.50
Aortic	-5.25	-0.75	4.00
Pulmonary	-5.62	1.00	3.00
Ventricular	-5.50	5.00	-2.00

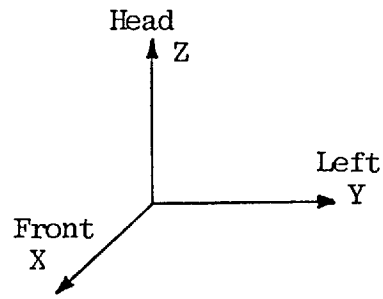

TABLE V The coordinates of the sources (cm)

its path through the tissues. Introduction of a finite boundary to the medium will make the equation of motion unsolvable analytically. In reality, the thorax is obviously inhomogeneous. This will, in theory, cause surface Rayleigh waves to propagate along the interface of the media and the general theory of wave propagation in viscoelastic medium provided by Oestreicher will not be applicable. For simplicity, homogeneity was assumed. The assumption of incompressibility implies $\lambda_1 \rightarrow \infty$ and $\lambda_2 = 0$. This is applicable for infinitesimal deformation. According to von Gierke (1952), in the frequency range up to 20 kHz, λ_2 is unlikely to have any influence on the mechanical impedance of the body tissues.

The oscillating sphere model is actually different from the mechanical dipole concept used by Verburg (1975). In his model, the oscillating sphere is confined to move within one orientation and hence is analogous to the 'dipole' in electromagnetic field theory. This is the case if the

vibrations are attributed to the valvular movements alone as suggested in the cited work. There are, however, evidences that acceleration and deceleration of the haemodynamic system, including the ventricles, aorta and blood mass, are also important sources of heart sounds (LUISADA, 1971; RUSHMER, 1970). Therefore we adopt a more flexible model by allowing the sphere to oscillate in any orientation about its quiescent position. In this way each source is described by three independent orthorgonal spatial components and the actual vibration of the source is the vectorial summation (or the resultant) of these three spatial components (S_x,S_y,S_z).

The linear property (that is, a sinusoidal source of frequency ω will produce vibrations of frequency ω only no matter where in the medium the vibrations are detected) is inherent of a viscoelastic medium. The superposition assumption implies that the generating sources are independent of each other. In view of the fact that no information is available about the interaction between 'generators' of cardiac vibrations, this seems to be a reasonable assumption.

The choices of the sources and their locations, though containing elements of arbitrariness, are based on plausible physiological evidence. Luisada (1971) has demonstrated the 'valve closure' and 'valve tension' can at most be a minor contributing factor to the genesis of the first heart sound. The major contribution actually

comes from the accelerations and decelerations of the left ventricle and its blood mass. Therefore a generating source in the left ventricle near the mitral valve appears to be a reasonable choice. Although it was shown that the right ventricle had little contribution to the genesis of the first heart sound (LUISADA, 1971), a similar source is placed in the right ventricle because at low frequency, the right ventricle is likely to contribute somewhat to the vibration. Experimental evidence (MacCANNON, 1964; MORI, 1964) has shown that the aortic and 'pulmonary' components of the second sound follow the closure of the aortic and pulmonary valves. They are caused by "the vibrations of the closed valve, infundibulum and vessel wall at the time of the incisura. The latter is caused by rebound of the last part of the stroke mass over the already closed semilunar valves producing a second rise in pressure. Thus, there is acceleration followed by deceleration, which manifest itself as sound". Therefore the best locations of the sources seemed to be in the aorta and the pulmonary artery just above the semilunar valves. The phase reversal observed between location (3,4) and (5,5) (figure 2.14) seems to suggest that the sudden check of the blood mass in the ventricles caused by the closure of the semilunar valves also causes some vibration. Therefore a'ventricular' source somewhere in the centre of the left ventricle was placed.

4.5 Transfer Matrix Calculation

The mechanical properties of the chest tissues were

not readily available. The values used by Verburg (1975) appeared to be reasonable and were therefore adopted as the following:-

$$\lambda_1 = 1.25 \times 10^8 \ \text{N.m}^{-2} , \ \lambda_2 = 0$$

$$\mu_1 = 300 \ \text{N.m}^{-2} , \ \mu_2 = 50 \ \text{N.s.m}^{-2}$$

$$\rho = 300 \ \text{kg.m}^{-3} , \ a = 3 \ \text{cm}$$

For each source there are three orthogonal components x,y and zwhich can be taken as independent sources. Therefore there are six effective source components for the first vibration and nine for the second. Each of these components has a transfer coefficient to each measuring site given by the dot product $\underline{\alpha}.\underline{d}$ where $\underline{\alpha}$ is the complex attenuation vector given by equation (4.4) and $\underline{d}$ is the direction ratio of the normal to the body surface at that site on the precordium. From the geometic model the coordinates of the site with respect to the source and the direction ratio $\underline{d}$ can be calculated by simple geometic transformations. By implementing equation (4.4) on the digital computer the transfer from each component of each source to the measuring sites were obtained for each harmonic frequency. The harmonic frequencies, ω, were defined by the fundamental frequency and its harmonics of the measurements. Since 100 samples were taken for each vibration at a sampling rate of 256 samples per second, $f_0 = 2.56$Hz. In this way, a complex transfer matrix of m rows and n columns was obtained for each

ω where m is the number of measurement sites on the precordium and n is the number of sources x 3. The magnitude and phase of the complex transfer coefficients correspond to the attenuation and phase shift of the pathways for that particular frequency.

Finally, the transfer matrices $A(\omega)$ for solving the inverse problem were obtained by multiplying the transfer elements from the sources to each site by a weighing factor w_i, where

$$w_i = \left(\frac{p_i}{\sum_{i=1}^{n} p_i} \right)^{\frac{1}{2}}$$

i = site number

p_i = the total power of the signal at site i

This weighing factor was included to simulate the effect of inhomogeneity. Since the variation of the signal strength across the chest wall was at least partly caused by the differences of mechanical properties of the body tissues along the various pathways, a weighing factor which is a function of such variation seems to be reasonable. The square root power was an arbitrary choice. Hence the final transfer matrices $A(\omega)$ were given by

$$A(\omega) = W\, A'(\omega)$$

where

$$W = \begin{bmatrix} w_1 & 0 & 0 & 0 & . & . & . \\ 0 & w_2 & 0 & 0 & . & . & . \\ 0 & 0 & w_3 & 0 & . & . & . \\ . & . & . & . & . & . & 0 \\ . & . & . & . & . & . & 0 \\ . & . & . & . & 0 & 0 & w_n \end{bmatrix}$$

4.6 Inversion by Least Square Method

In general, an over-determined system, where the number of equations is larger than the number of unknowns, cannot be satisfied exactly. The least square method is the most commonly used procedure to solve such a system. It effectively finds the set of solutions $\underline{x}'$ for the system $A\underline{x} = \underline{b}$ by minimizing $(Ax' - b)\,(Ax - b)^T$. In other words, it finds the sources which, after transformed by the given system A, give the closest match to the observations. Mathematically it is equivalent to solving,

$$\underline{x}' = (A^T A)^{-1} A^T \underline{b} \qquad \text{.....(4.6)}$$

In order to reduce the factor of over-determination, not all measurements were used for the inversion. A 5x5 grid (row and column 2 to 6) and a 6x6 grid (row and column 1 to 6) were used for the first and second vibrations respectively. The grids were chosen to include signals of appreciable strength. This gave a factor of over-determination equal to four for both vibrations. The vector $\underline{b}$ was computed from the spectral averaged signals (100 points at 256 sample per second for each vibration) by FFT. The source solution was computed from equation (4.6) for each frequency component. The vibration pattern of the source could then be reconstructed from the inverse harmonic components by inverse FFT. Figure 4.3 is an example of the inverse source solutions of the first vibration. Figure 4.4 shows the calculated observations at the measuring sites using the inversed sources and the transfer coefficients

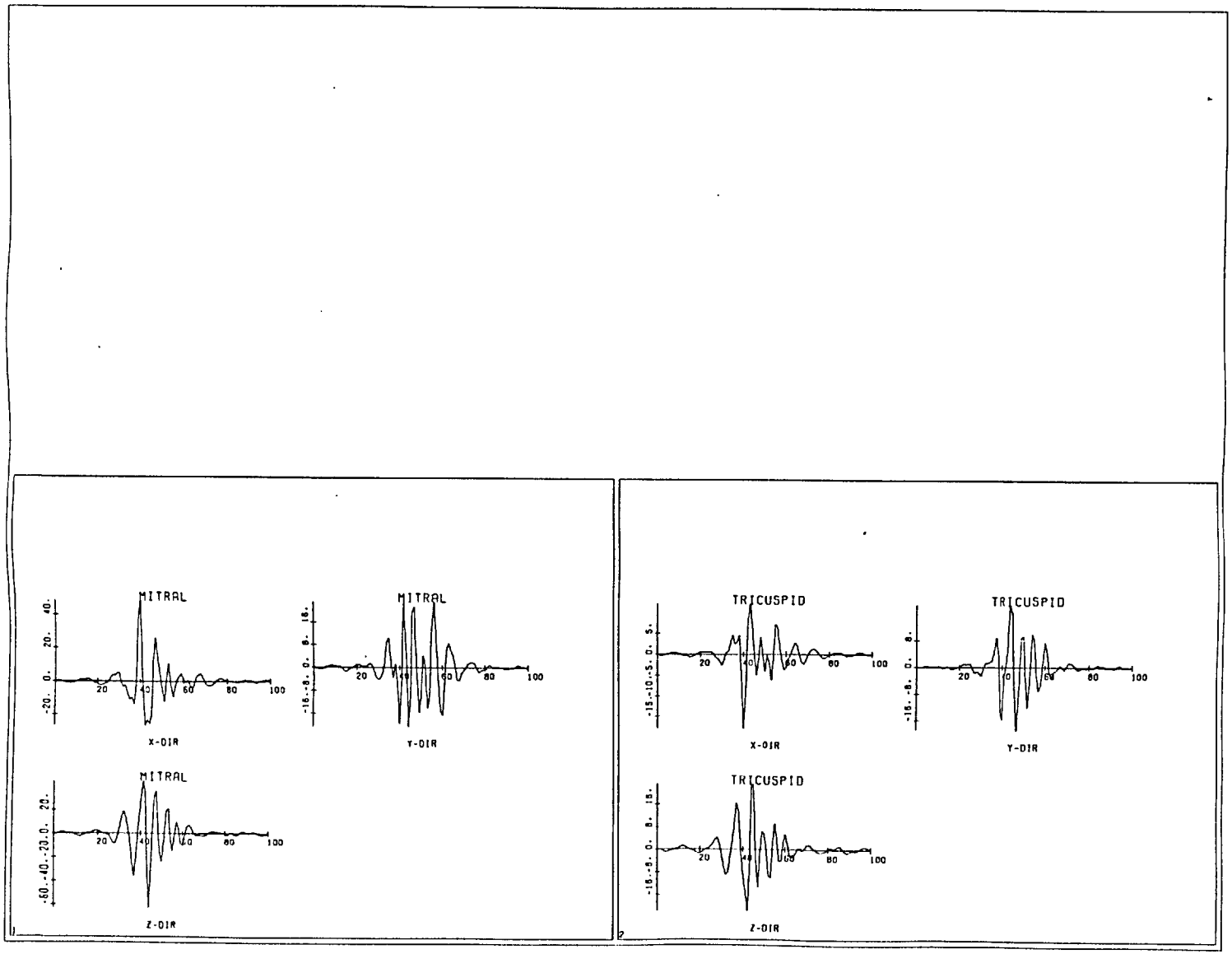

Figure 4.3 The inversed source vibration pattern for the first vibration obtained using the conventional least square method.

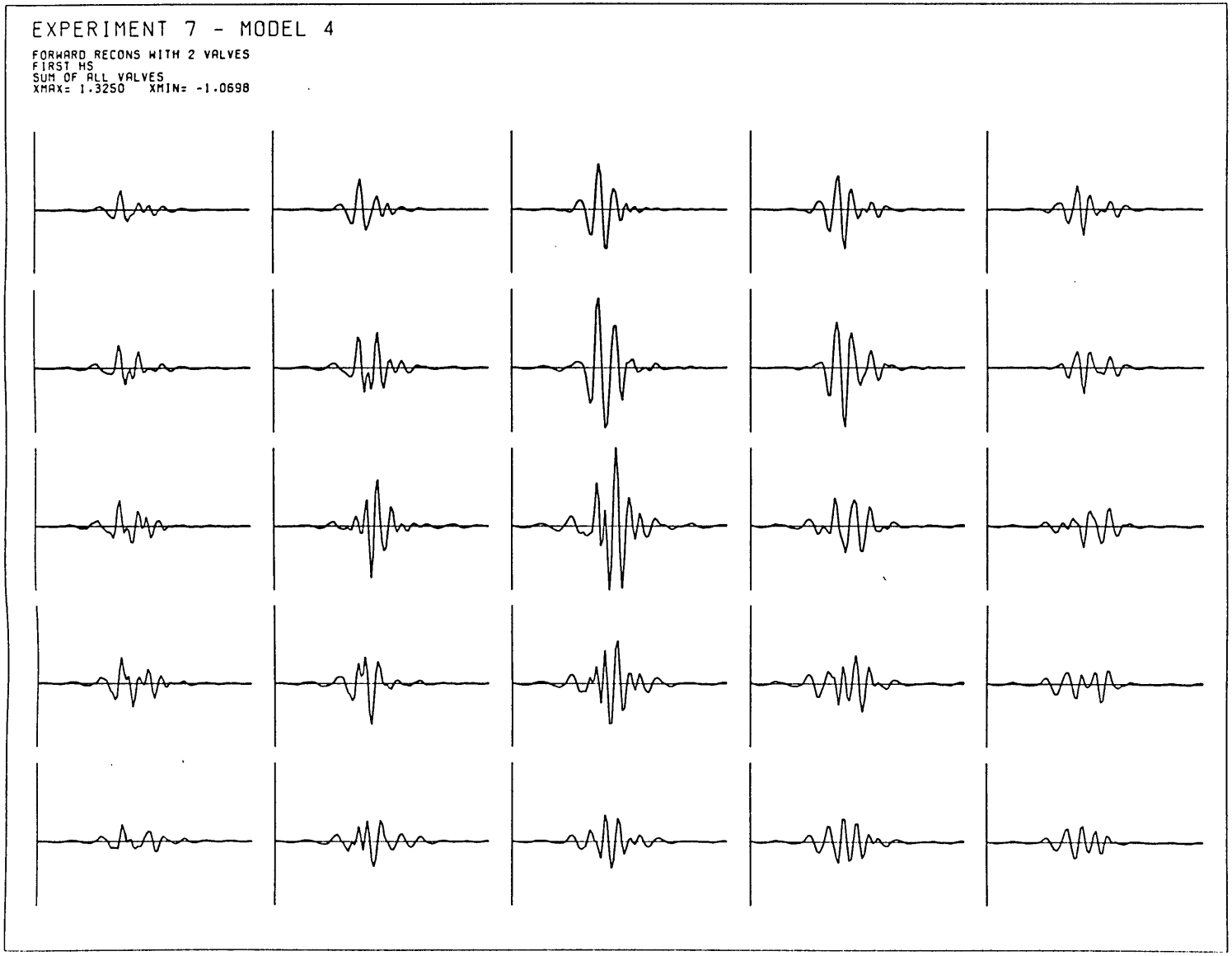

Figure 4.4 The forward reconstruction of 'observations' produced by the inversed sources in figure 4.3. Note their similarity with the actual observations in figure 2.14. (See also fig. 4.5 & 4.6)

of the model. Although the forward reconstruction of the observations resemble very closely the experimental observations in most of the sites, this however does not necessarily imply closeness of the inversed source solutions to the actual vibration mechanism in the heart, even if the model is a good representation of the mechanism. Separating the calculated observations into the individual source contributions reveals why this is so (figure 4.5 and 4.6). The contributions from the two vibration sources (for the first vibration) cancel one another to produce the closeness of match to the exprimental observations. This could not have been due to a genuine out-of-phase interaction of the sources (caused by the asynchronous nature of the two ventricles) for two reasons. First, the asynchrony of the two ventricles should cause delay of the on-set of vibrations, which was not found in our case. Secondly, if the small amplitude signal is actually a summation of two large signals of comparable magnitude but 180^{o} out of phase, the variability of the signal should be very much larger than actually observed.

4.7 Constrained Least Square Method

A similar problem has been investigated and discussed by Twomey (1965) under the general heading of 'indirect sensing' measurements - inference of a function f(x) from physical measurements of some other function g(y) where there is no simple one-to-one relationship between x and y. He showed rigorously that for a linear system $\underline{Ax} = \underline{b}$, using

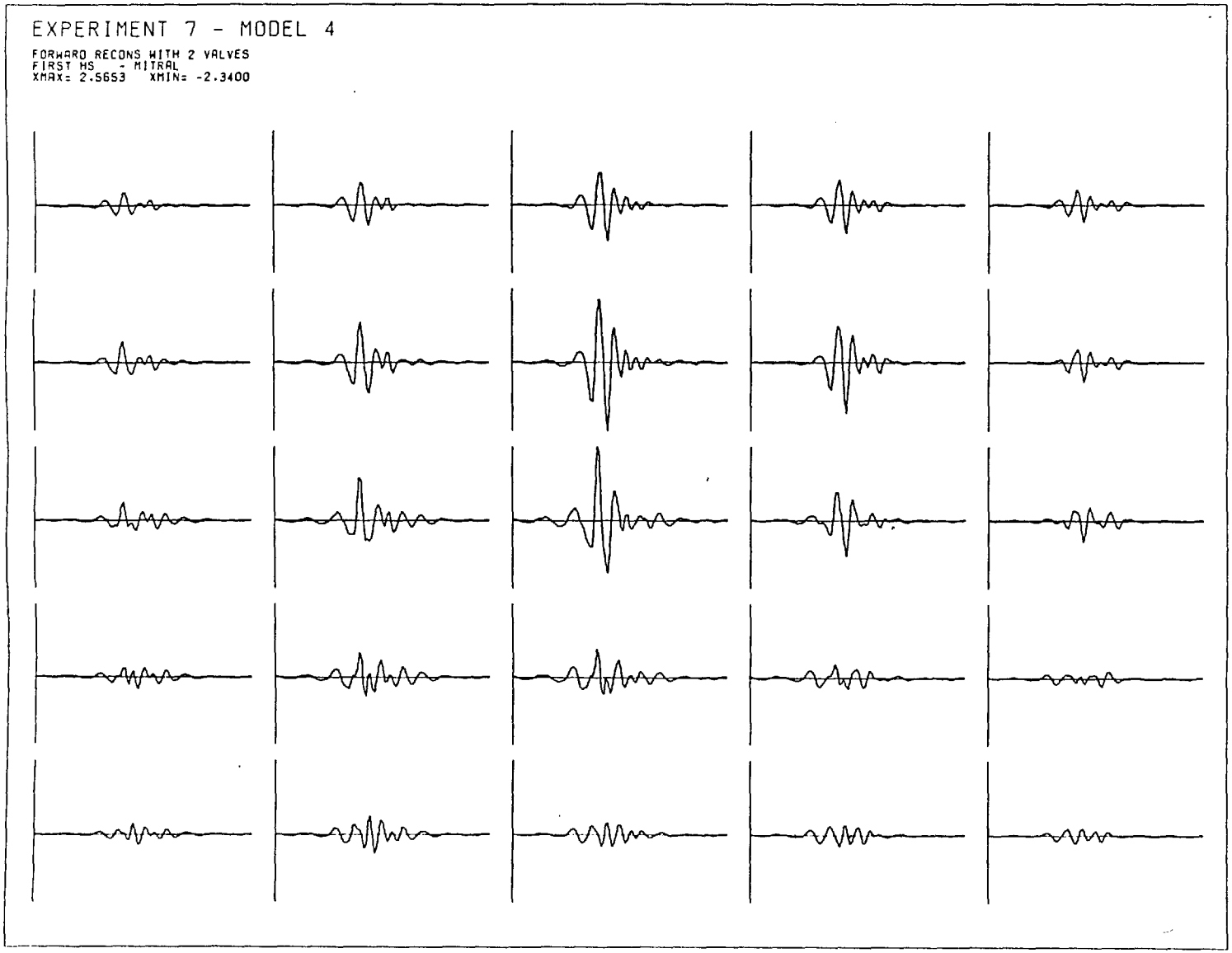

Figure 4.5 The 'mitral' component of the forward reonstructions in figure 4.4.
(100 data points over 0.39 sec)

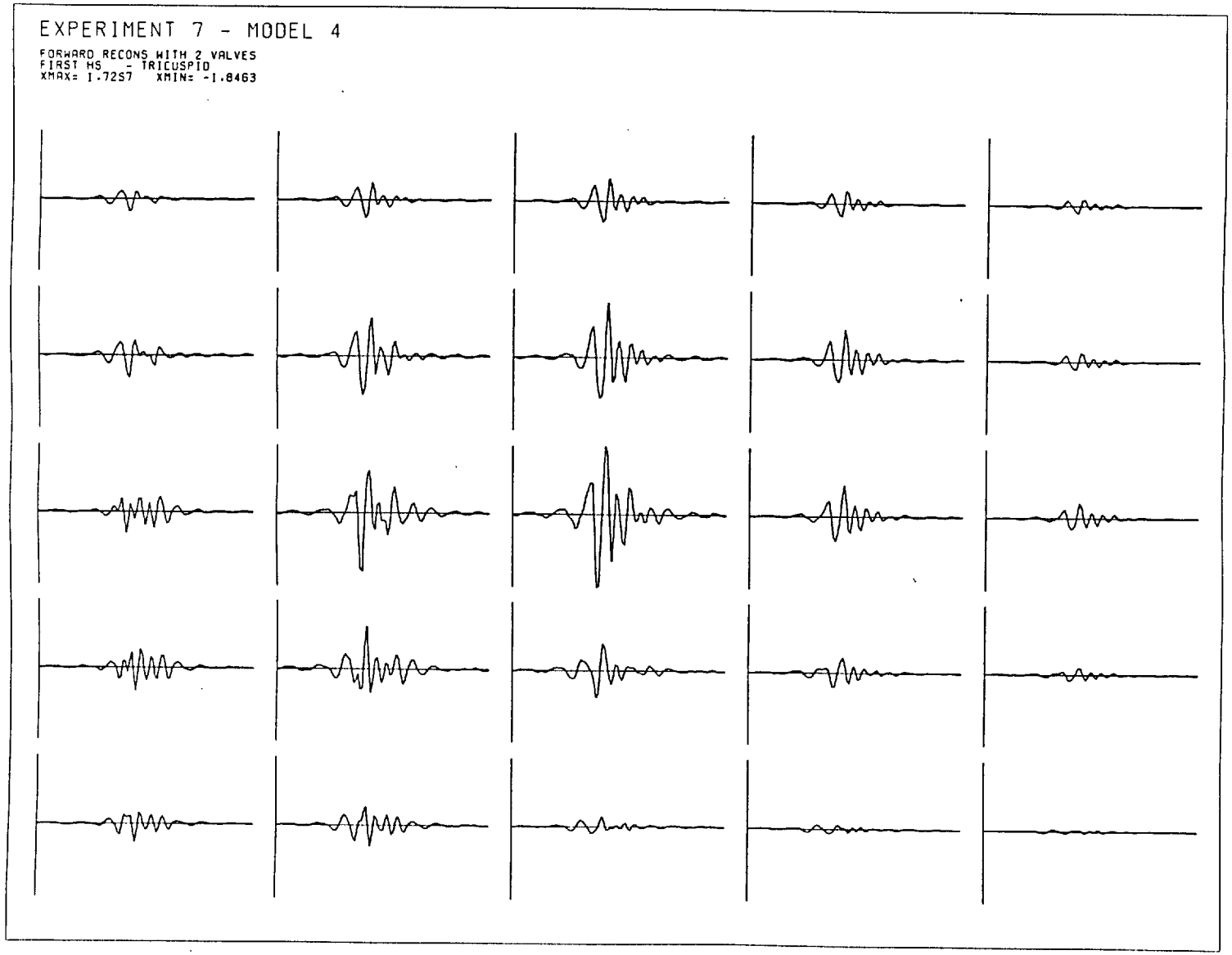

Figure 4.6 The 'tricuspid' component of the forward reconstructions in figure 4.4.

the nearness of the transfrom $\underline{b}'$ and $\underline{b}$ to gauge the nearness of the 'inverse transform' $\underline{x}'$ and $\underline{x}$ is based on an incorrect premise if the observation $\underline{b}$ is subject to error (due either directly to measurement inaccuracy or indiectly to errors in transfer matrix estimation from the model).

A method based on the application of constraints to the solution was proposed. It effectively selects a stable unique solution from the infinite sets of possible solutions which possess forward transforms lying within a prescribed norm of the observed $\underline{b}$ according to some plausible criterion imposed on the solution $\underline{x}$.

Mathematically the application of a constraint can be expressed as follows:

$$\text{given that } A\underline{x} = \underline{b} + \underline{\epsilon} \quad ; \quad \text{with } \sum_{i=1}^{n} \epsilon_i^2 \leq e^2 \qquad \ldots\ldots\ldots\ldots \quad (4.7)$$

The aim is to solve the equation by varying $\underline{\epsilon}$ within the permissible limit (instead of minimizing it) so as to minimize a quantitative criterion on $\underline{x}$. In our case, it is desired to constrain the sources such that the contributions from the sources are within a certain relative phase angle limit (i.e. they are vectorially enhancing instead of cancelling). This effectively constrains the orientations of vibrations of the sources.

The constraints were implemented in two steps. First, a first estimate of the source solution, $\underline{y}$, was calculated

for each source taking in turn that source as the only source of vibration in the system. Secondly, equation (4.7) was solved with the constraint that minimizes $(x_i - y_i)^2$. It can be shown that the problem can be expressed in the following equation (see appendix F),

$$(A^T A + \gamma I)(\underline{x} - \underline{y}) = A^T (\underline{b} - A\underline{y}) \quad \ldots\ldots\ldots (4.8)$$

where γ is a Lagrangian multiplier which determines the 'degree' of constraint applied. Instead of setting limits to the error $\underline{\epsilon}$, limits for a parameter α, called the norm ratio, which effectively measures the amount of cancellation between contributions from the different sources, was used. (See appendix G for the formulation of the 'norm ratio'). The norm ratio was found to be a slowly deceasing function of γ. The equation (4.8) was solved for a number of value of iteratively until α reached the defined limit.

The following example demonstrates the improvement of the constraint method over the conventional least square method. The forward tranforms of a hypothetical set of source complex spectra were calculated using the transfer coefficients for one frequency component (14th harmonic of the first vibration). The source spectra used were :

M_x = (2.0, 0.0); M_y = (2.0, 0.0); M_z= (-2.0, 0.0)

T_x = (1.0, 0.0); T_y = (1.0, 0.0); T_z= (-1.0. 0.0)

The signal $\underline{c}$ thus obtained on the surface were perturbed with noise such that $\underline{b} = \underline{c} + \underline{n}$. (The noise components were complex numbers z_i of random phase angle rectangularly

distributed between $\pm$ 180° with its norm square, $|z_i|^2$, equal to 30% of the power of the signal at site i.)
The inverse solutions were then calculated from the contaminated observations with different values of γ. The procedure is summaried in the block diagram in figure 4.7.

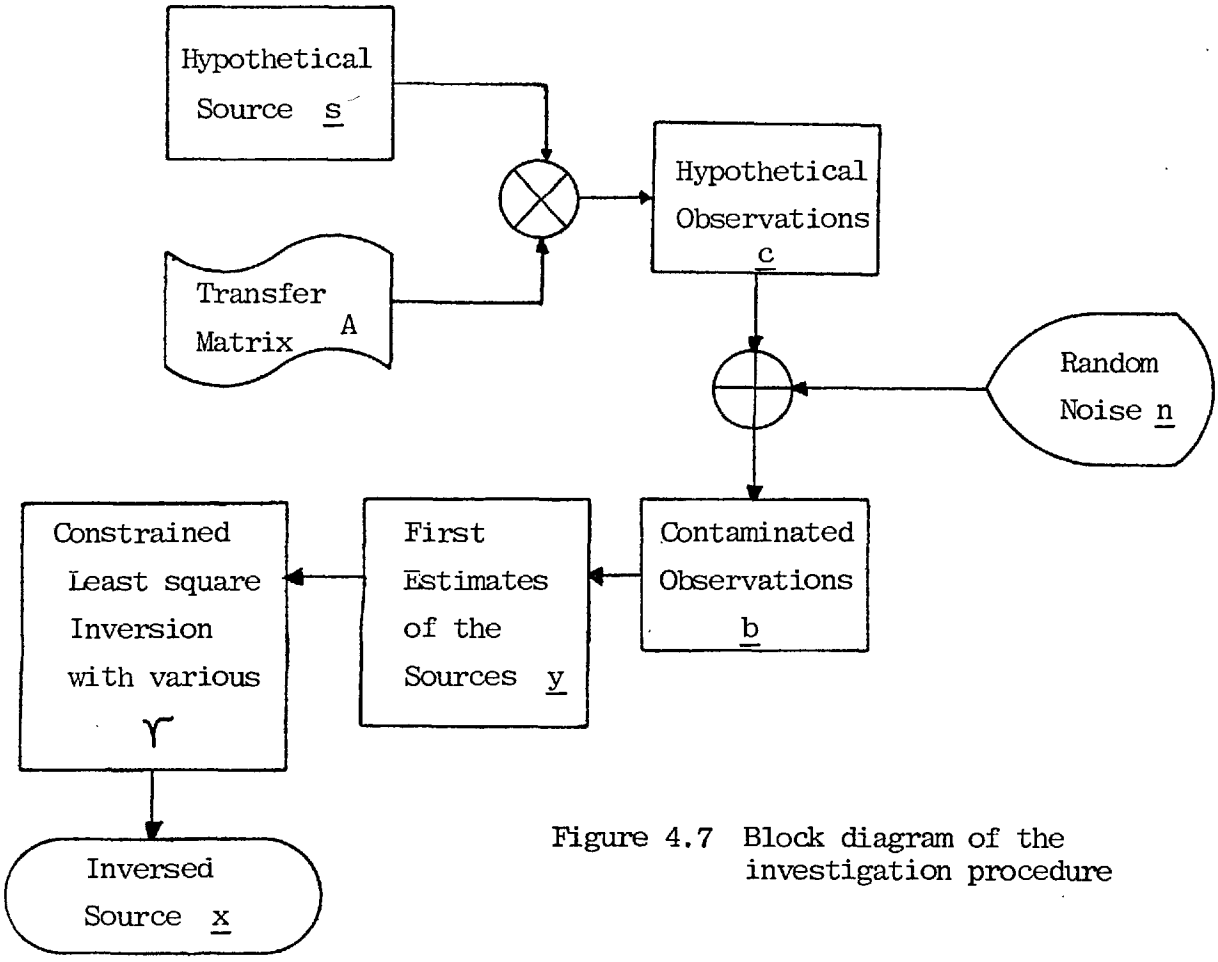

Figure 4.7 Block diagram of the investigation procedure

Figure 4.8 show the polar plot of the solutions for the various value of γ. Figure 4.9 show the variations of the norm ratio, α, the mean phase angle between the mitral and tricuspid components at the measuring sites and the percentage increase of residue caused by the constraint with γ. γ = 0 corresponds to no constraint (i.e. conven-

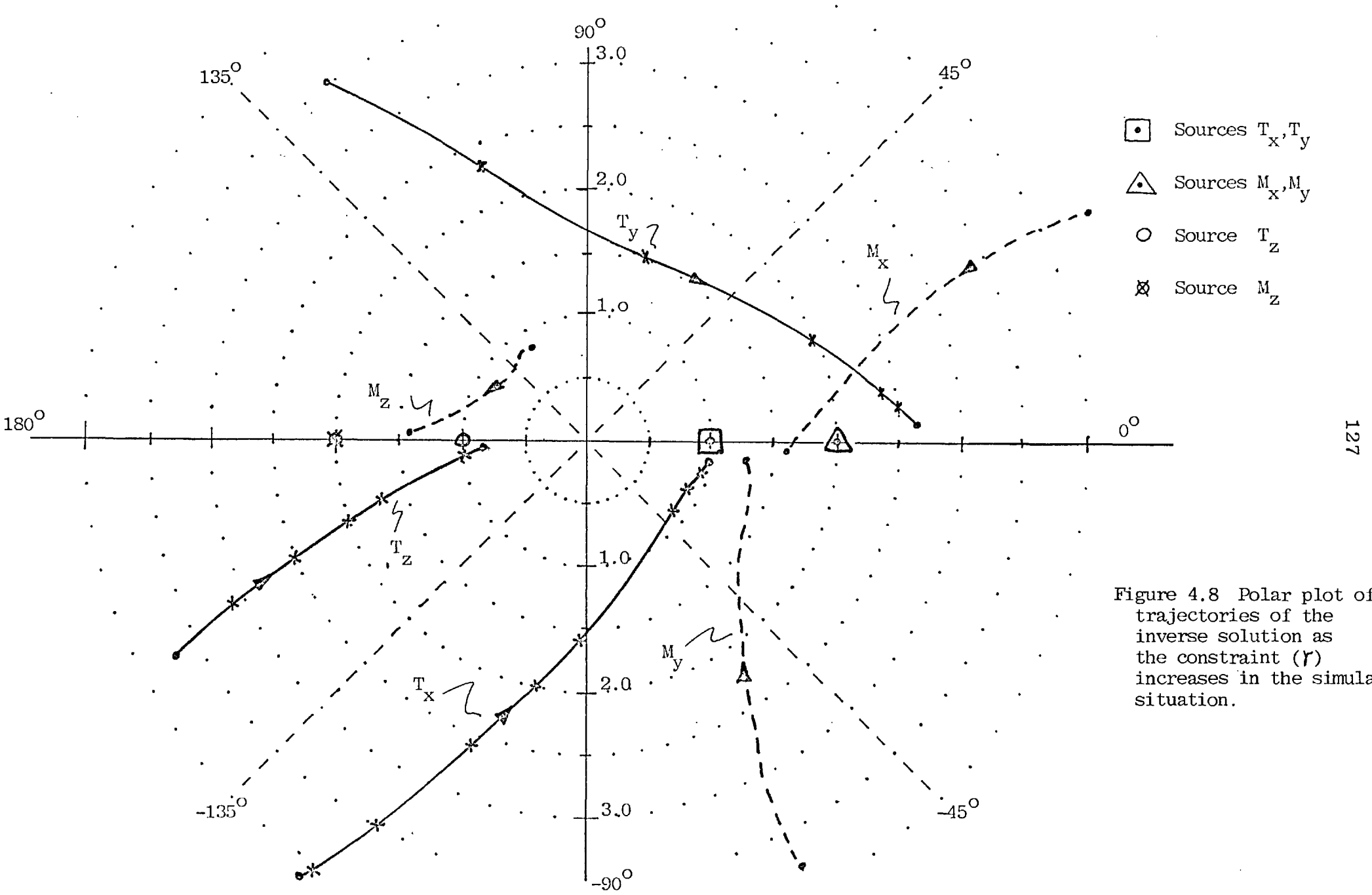

Figure 4.8 Polar plot of trajectories of the inverse solution as the constraint (γ) increases in the simulated situation.

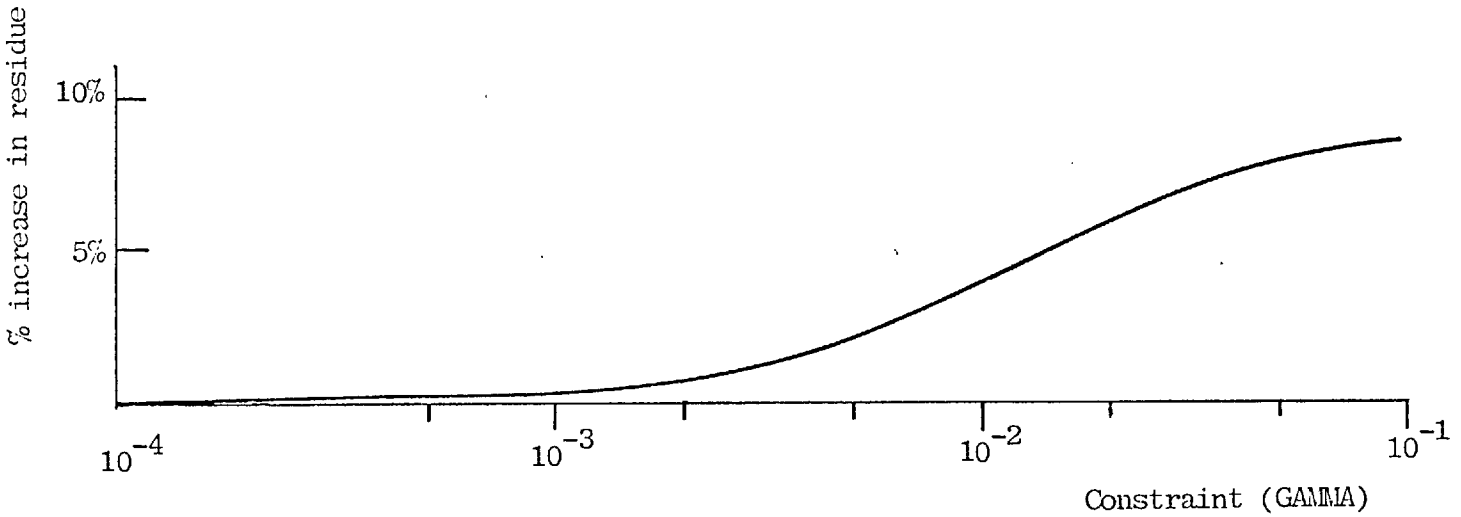

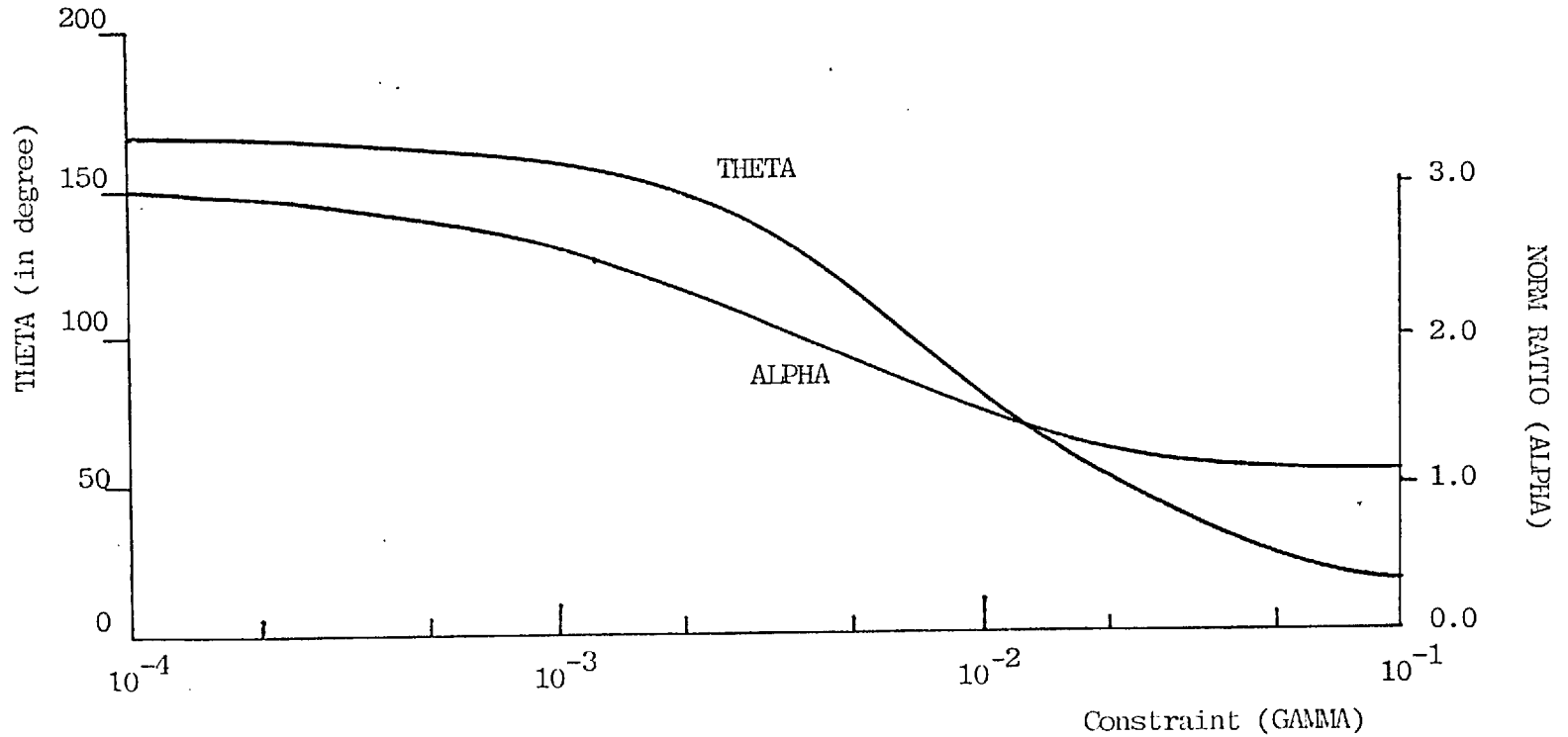

Figure 4.9 The percentage increase in residue, the changes of angle between the two source components (THETA), and the norm ratio (ALPHA) with different constraint (GAMMA).

tional least square) and the amount of constraint increases with γ. Note that at $\gamma = 0$, although the residue is nearly zero, the inverse solutions are far off from the true solutions. As γ increases the inverse solutions approach the true solutions although the residue also increases. A few trial runs showed that a value of α between 0.3 to 0.4 for the first vibration (with 2 sources) and 1.4 to 1.5 for the second vibration (with 3 sources) appeared to be optimal without 'over-constraining' the solutions.

4.8 Inversion by Constrained Least Square

The implementation of the constrained least square method on the actual measurements presented a number of obvious problems. For the first vibration, if the 'first estimate' of the sources, $\underline{y}$, were calculated by taking in turn the 'mitral' and the 'triscuspid' sources as the only source of vibration in the system, this inherently implies an equal contribution from both ventricles. As discussed in earlier section, there are experimental evidences that majority of the contribution to the first heart sound comes from the left ventricle. Therefore the first estimation of the sources were actually weighed by a factor of 2/3 and 1/3 for the 'mitral' and'tricuspid' sources respectively.

For the second vibration, the complication came from the fact that the sources were rather far apart and it was obvious that the first estimates could not be calculated from the entire 64 observations. (The 'aortic' source could

not be significantly responsible for the vibrations at, for example, location (6,6)). Therefore the first estimates, $\underline{y}$, were calculated from the observations confined only to areas that were near to the sources concerned as shown in figure 4.10

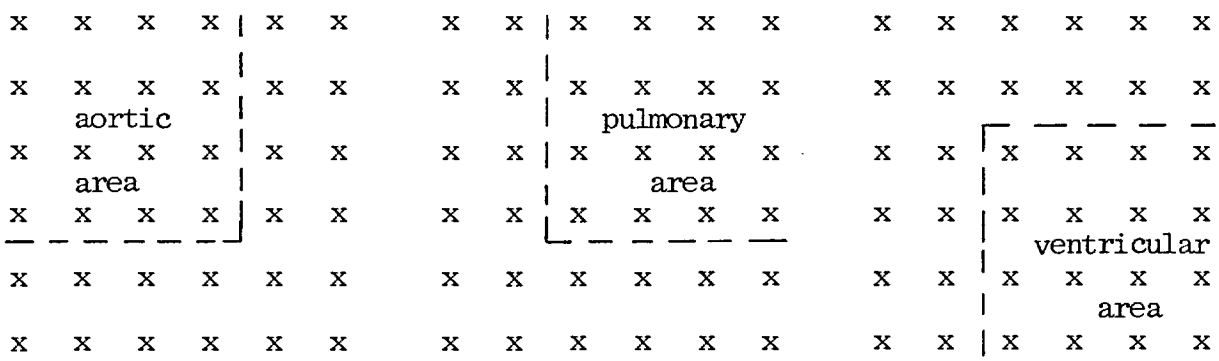

Figure 4.10 Areas used for the first estimates of the inverse solution for the second vibration.

The inverse solutions for the first and second vibrations, calculated using the constraint method, and their amplitude spectra are shown in figures 4.11 - 4.14. Figures 4.15 - 4.17 show the forward reconstruction of the vibrations from each inverse source and the summation of these sources for the first vibration. The forward reconstruction resembles the observations at many locations. Figure 4.18 and 4.19 show the normalised CCF between the forward reconstructed signals and the observations. The ACF of the observations are also shown for comparison (figures 4.20 and 4.21).

It can be seen that the cross-correlation functions

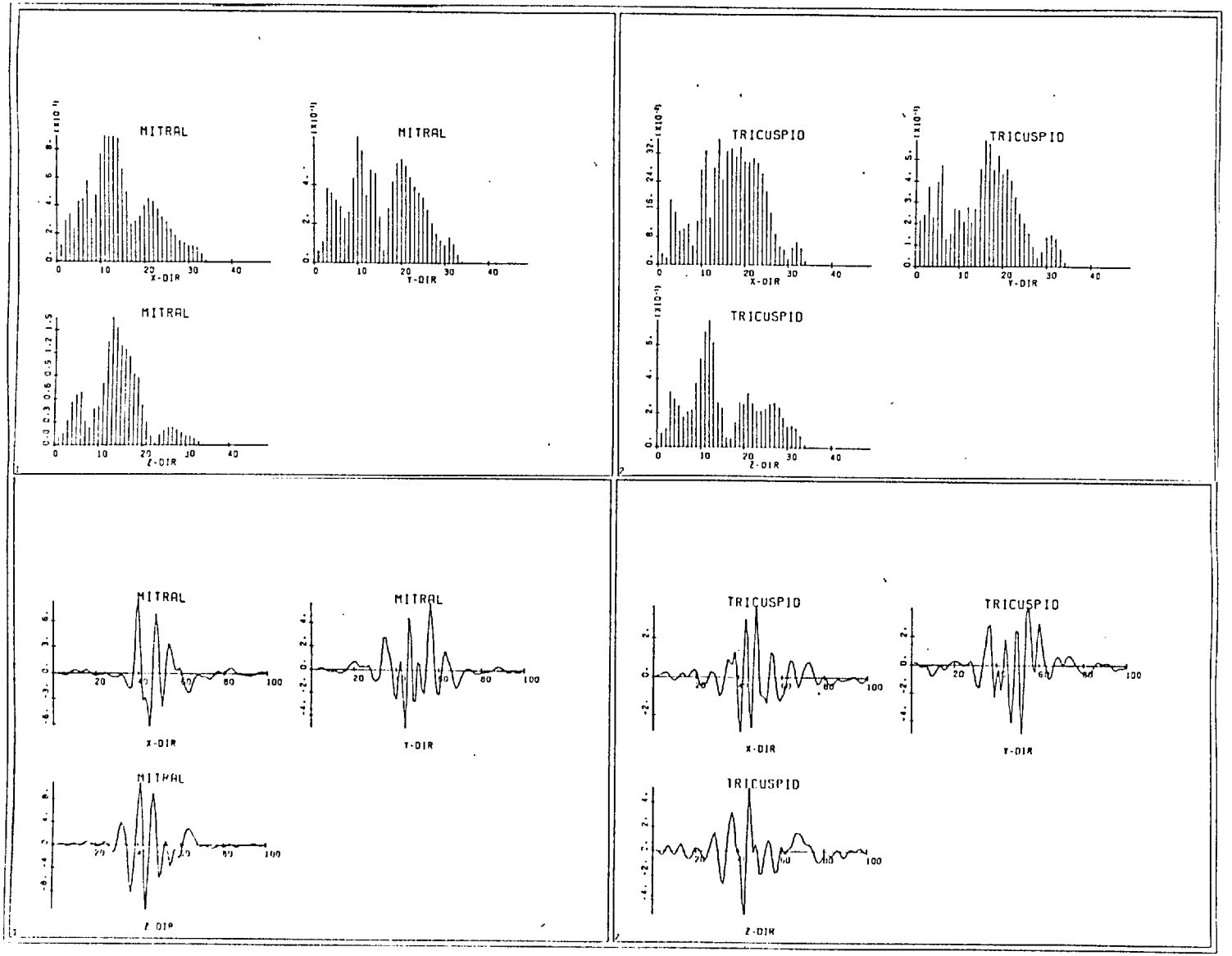

Figure 4.12 The amplitude spectra of the inverse sources in figure 4.11. (H1 ≡ 2.56 Hz)

Figure 4.11 The inverse source vibration patterns obtained using the constrained least square method (First vibration).

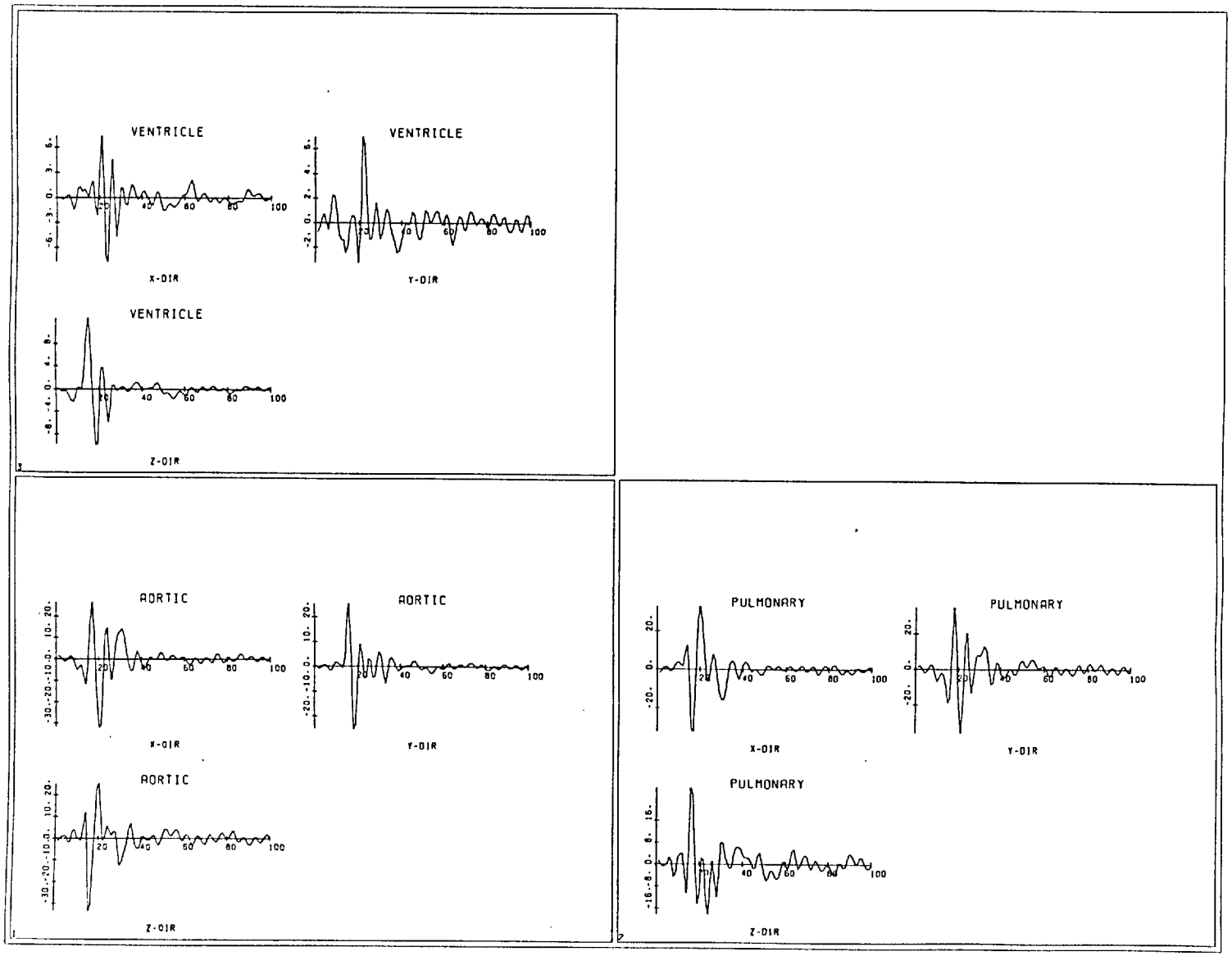

Figure 4.13 The inverse source vibration patterns obtained using the constrained least square method (Second vibration).

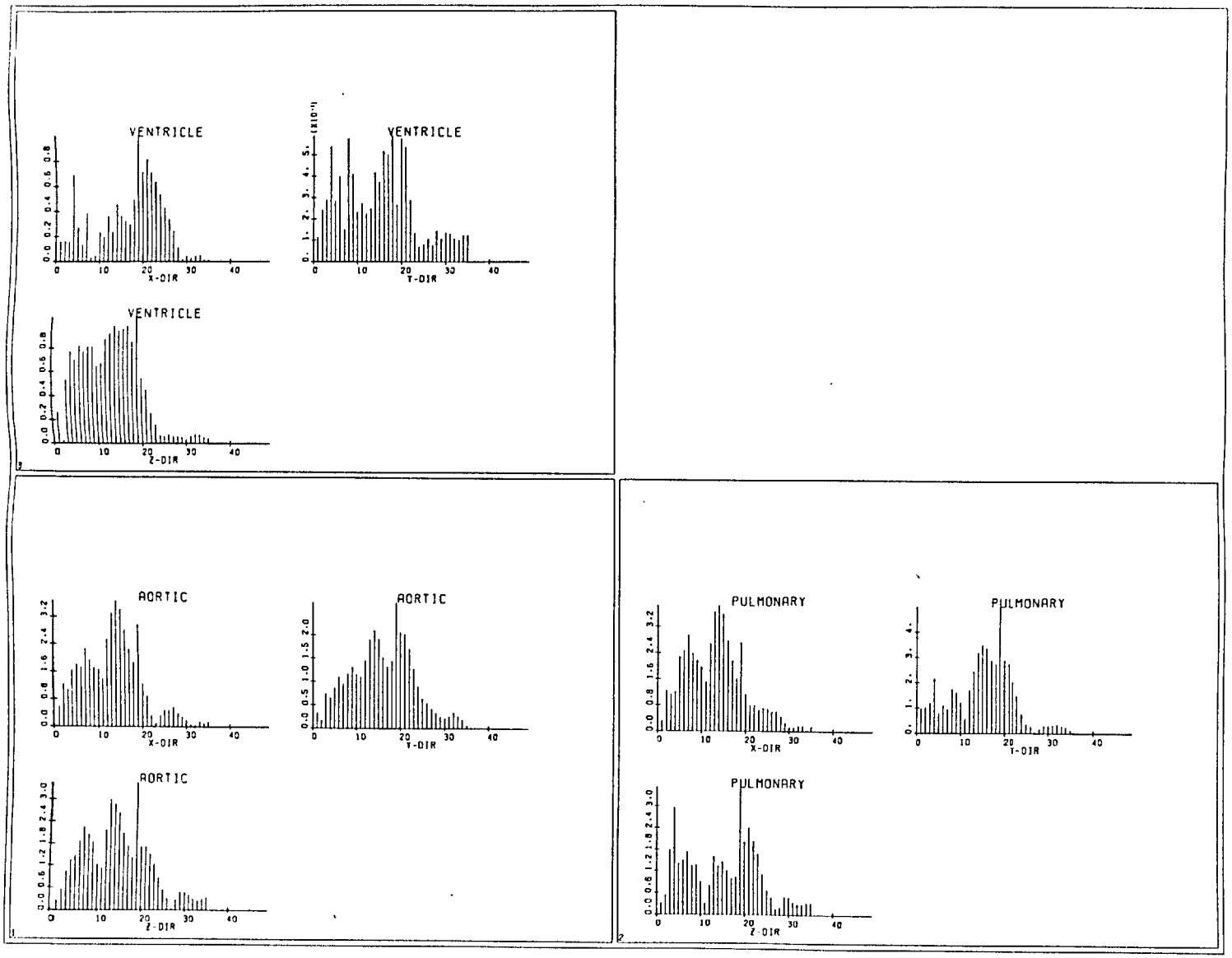

Figure 4.14 The amplitude spectra of the inverse sources in figure 4.13. (H1 ≡ 2.56 Hz)

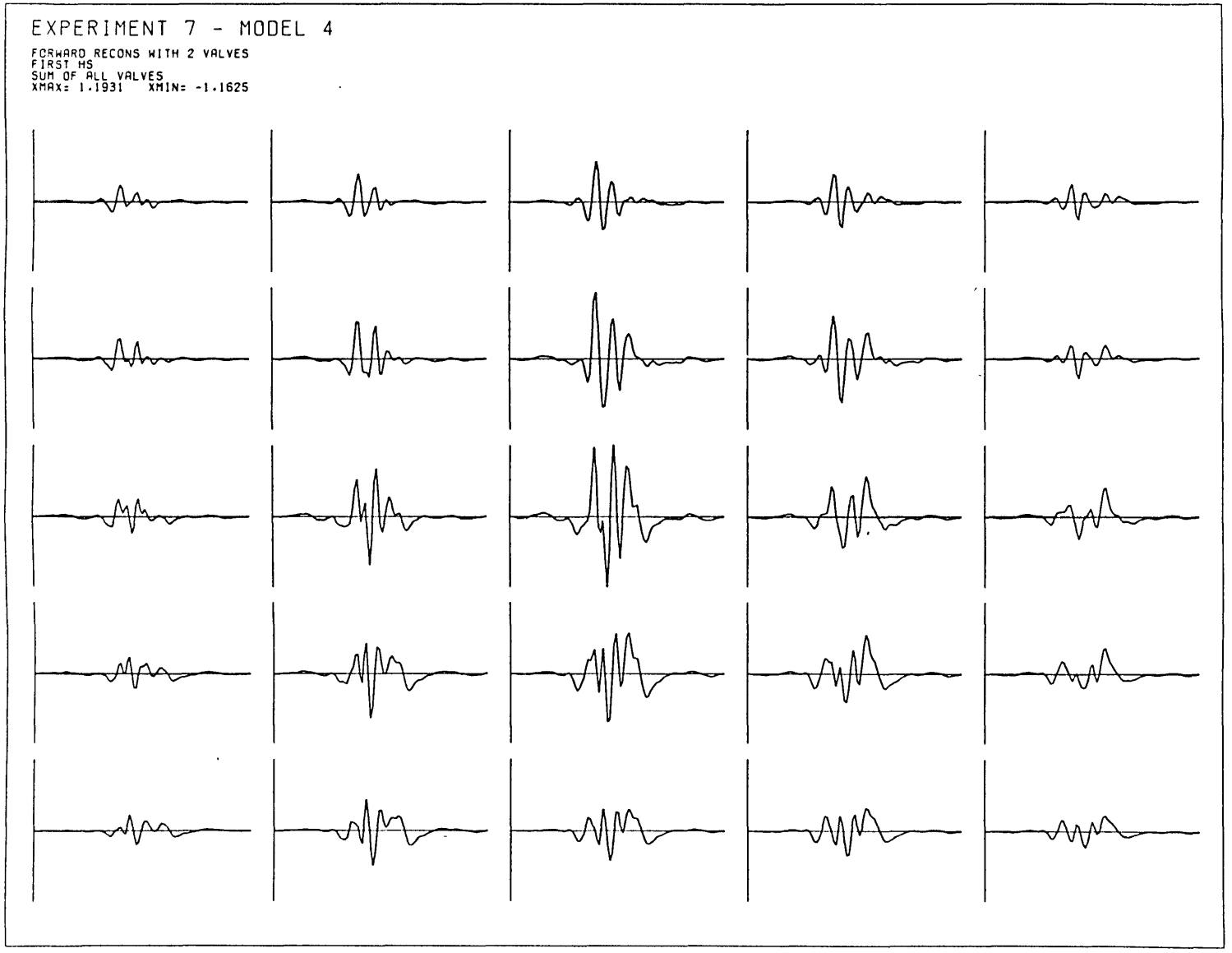

Figure 4.15 The forward reconstruction of the 'observations' produced by the inverse sources shown in figure 4.11.

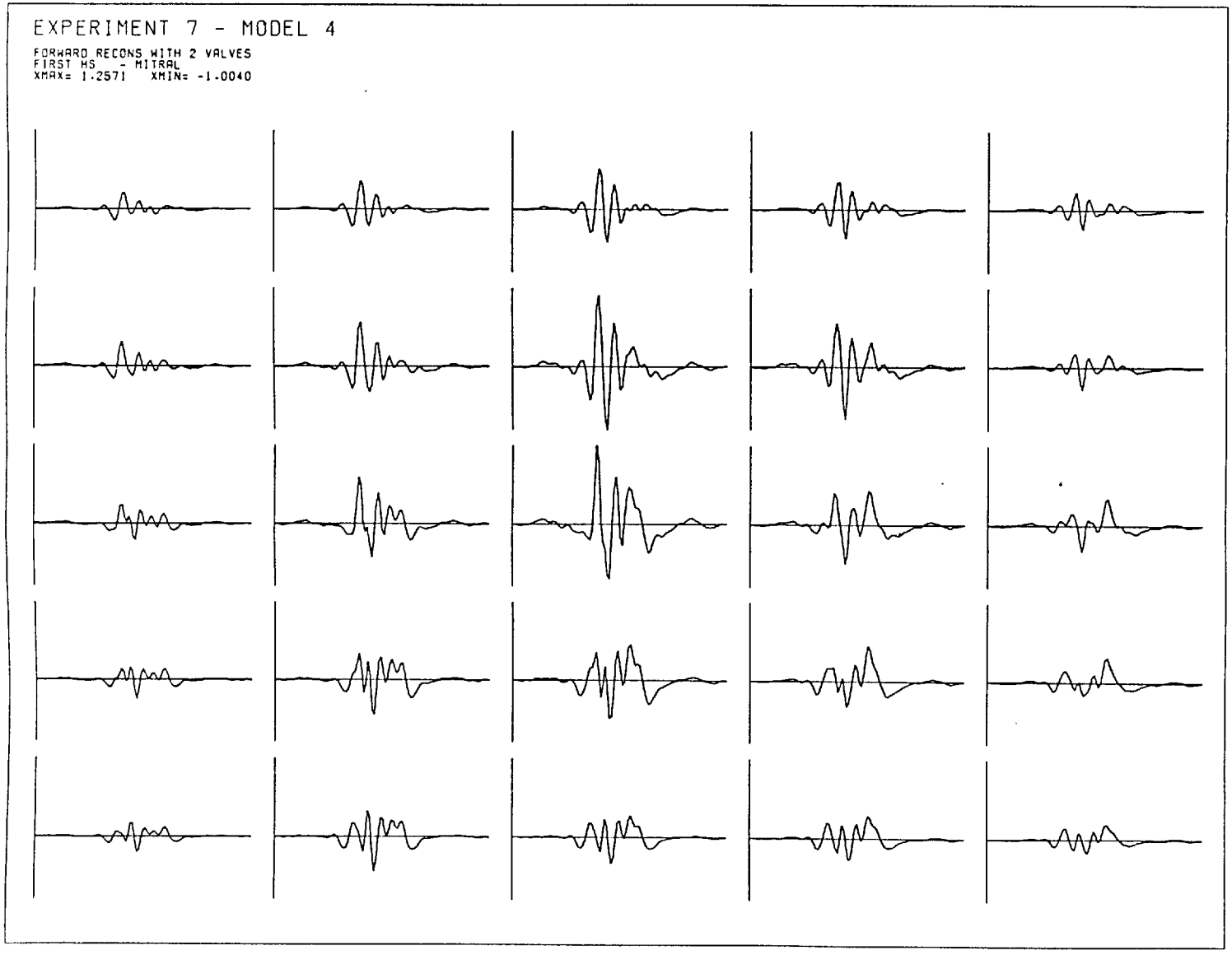

Figure 4.16 The 'mitral' component of the forward reconstructions shown in figure 4.15.

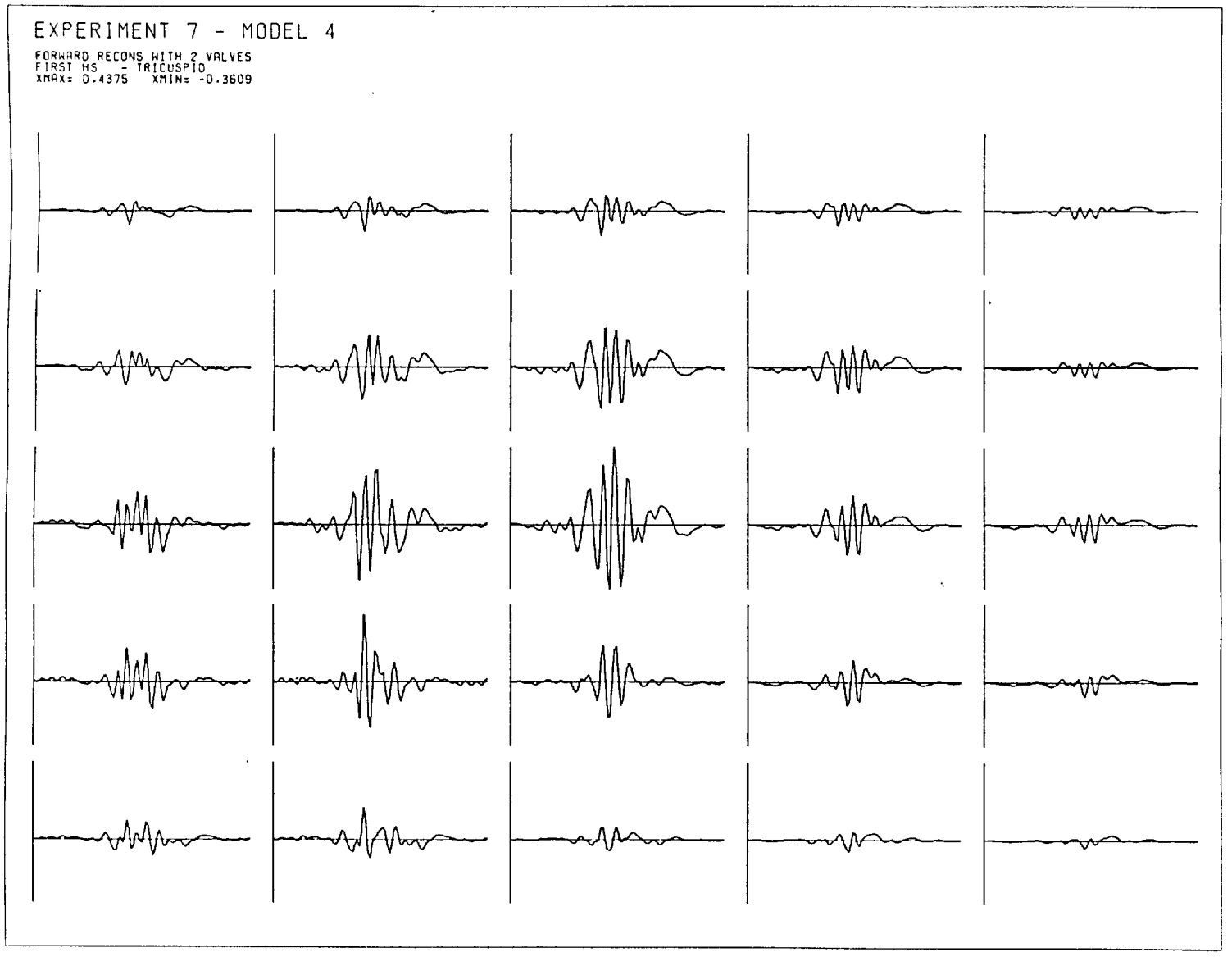

Figure 4.17 The 'tricuspid' component of the forward reconstructions shown in figure 4.15. Compare with figures 4.3 - 4.6.

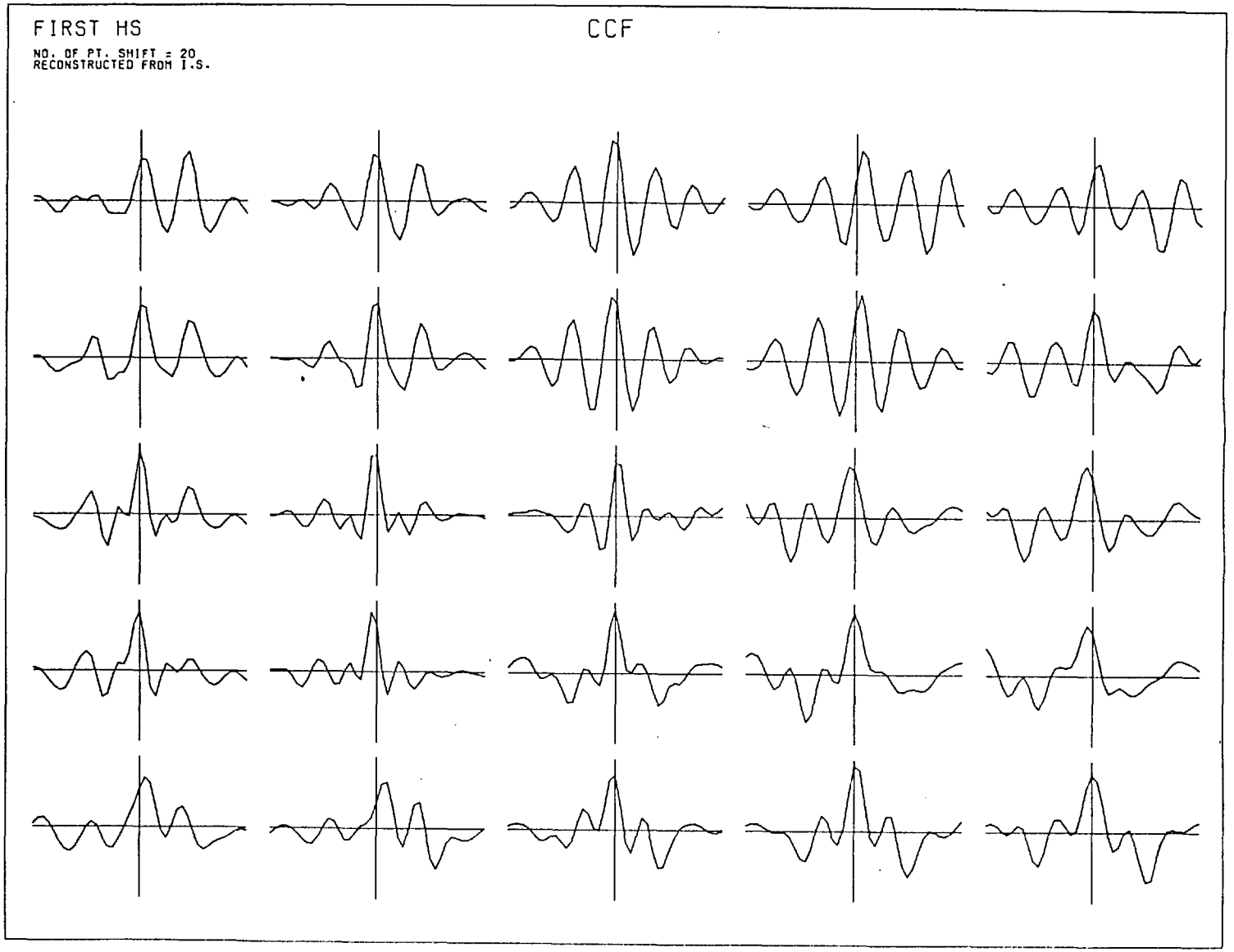

Figure 4.18 The normalised CCF between the observations and the forward reconstructed vibration patterns from the inverse sources for the first vibration (compare with figure 4.20).

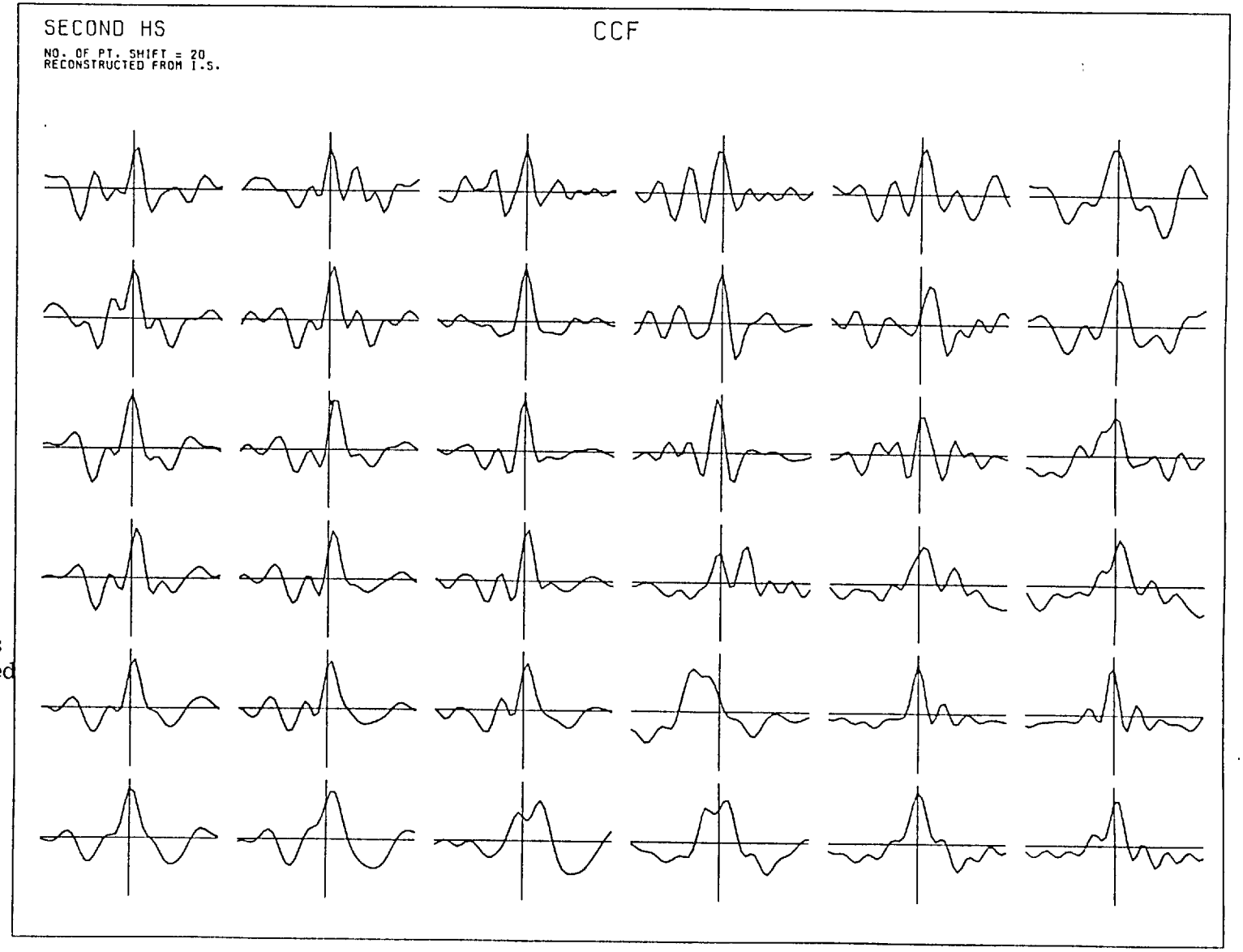

Figure 4.19 The normalised CCF between the observations and the forward reconstructed vibration patterns from the inverse sources for the second vibration (compare with figure 4.21).

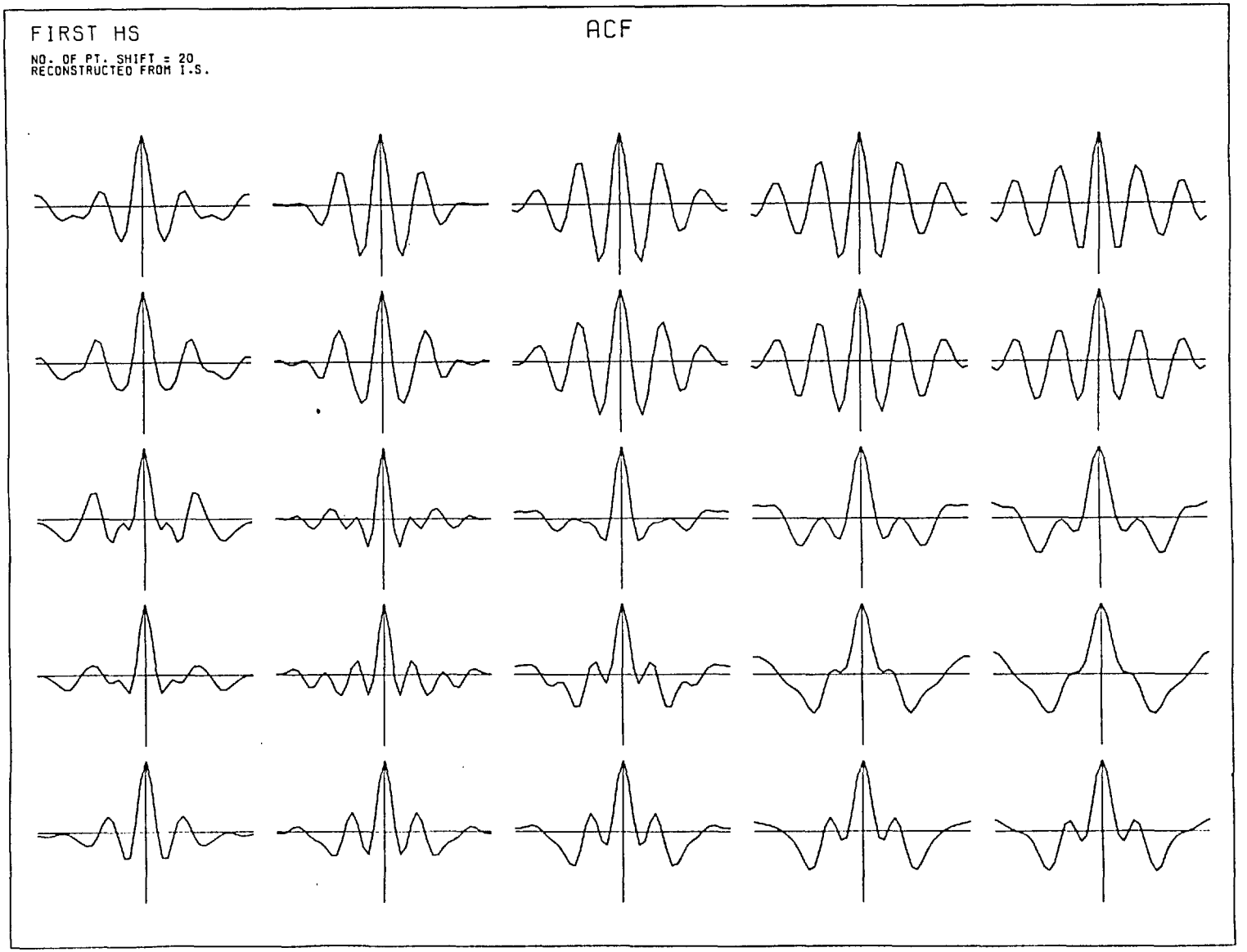

Figure 4.20 The normalised ACF of the observations at various sites for the first vibration.

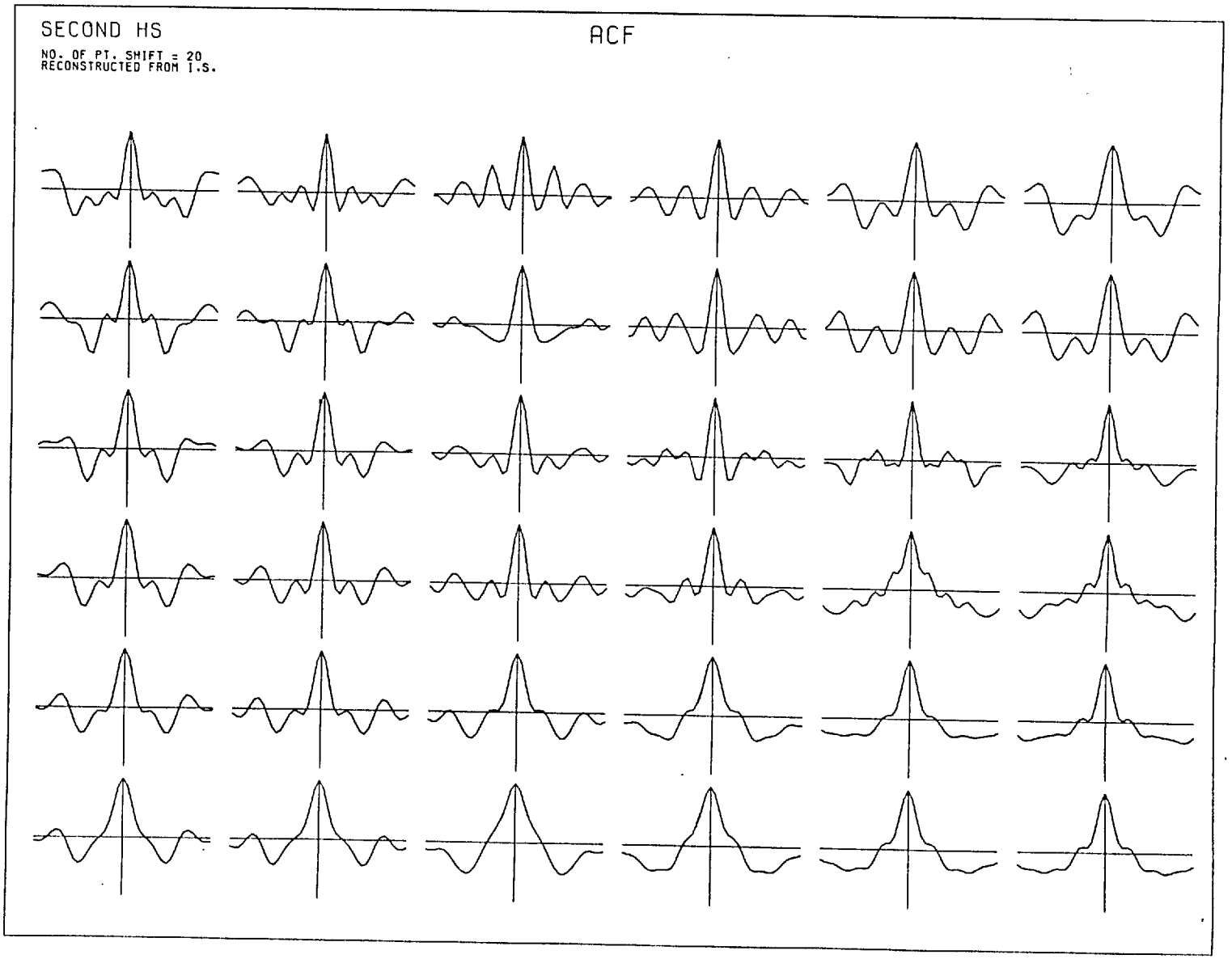

Figure 4.21 The normalised ACF of the observations at various measurement sites for the second vibration.

(CCF) are very similar to the ACF at most sites indicating that the forward reconstructed signals are close to the observations. Hence the system is still a self-consistent one although the error term in equation 4.7 is allowed to vary instead of being minimised. It has been pointed out in earlier section that this self-consistency is a necessary but not sufficient condition for the inversed solutions to be physiologically meaningful. However, with the introduction of constraint, we have eliminated the "oscillation" of the solutions caused by experimental errors (similar to the random noise component in figure 4.7). The forward reconstructed signals (Figure 60-62) do not cancel each other as in the case when the conventional least square method (without constraint) is used (figure 4.4 - 4.6).

4.9 Discussion

The fore-going work constitutes a first attempt to solve the inverse problem in precordial cardiac vibrations. It has successfully demonstrated : (i) how the inverse problem can be formulated using the free vibrating sphere model, (ii) the difficulties in such an inversion, (iii) that a 'self-consistent' system does not necessarily imply a meaningful inverse solution and (iv) the use of a constrained least square method.

However, it must be pointed out that there are a number of limitations. The model is an over-simplified one. The assumptions of isotropicity, homogeneity and an infinite boundary were necessitated by the otherwise unmanageable

mathematics. The choices of various viscoelastic properties of the tissues were limited by our present lack of information. Our choices of the locations of the sources, though bases on plausible physiological criteria, were somewhat arbitrary because the oscillating spheres were only hypothetical representations of the vibration generators. It is also very difficult to assess how well the inverse solution represents the actual sources of vibration. Further, the value of such an inverse solution procedure as a means of data reduction has yet to be assessed by detailed studies into the inter-subject variabilities and the normal-pathological differences of the inverse solutions.

CHAPTER 5

DISCUSSION AND CONCLUSION

This work is set out to investigate the feasibility of spatio-temporal analysis of precordial vibrations. This task includes, first, the development of a procedure, together with the necessary data processing techniques, for measuring the vibration patterns over many precordial sites and second, the study of the spatio-temporal measurements using various methods of analysis in order to assess the likely value of 2-dimensional spatial measurement of cardiac vibrations. In so doing, it was also our aim to develop signal processing methods that can be used not only in this and other spatio-temporal studies, but in processing other kinds of biological signal to which they are relevant.

We believe that these objectives have been achieved. The measurement procedure and the preprocessing techniques developed allows the acquisition of averaged, synchronised, and reproducible signals over a large number of sites on the precordium. Various spatio-temporal analyses of the measurements indicated that signals at different locations could carry very different information and so merit further investigation in such spatio-temporal measurements. In attempting to solve the inverse problem of cardiac precordial vibrations, a way of formulating the problem has

been devised. The implementation of a variable orientation oscillating sphere model and a constrained least square method were also demonstrated. However, there is currently no objective method of establishing that the sources inferred in this way are really representative of the true sources. Indeed the study reported here has been presented as a demonstration of how the matter can be approached and as identifying the kinds of difficulty likely to be met in obtaining a meaningful inverse solution. It must be thus pointed out that the work was carried out as a feasibility study and so emphasis has been put on the methodological and technical aspects of processing and analysis of the precordial vibrations. No attempt is made to draw any definite clinical or physiological conclusions from our results.

Special attention should be drawn to the development of the spectral averaging method. This allows serially-measured signals to be effectively synchronized and the variability of the signals to be reduced. This simple but original method of averaging has been shown to be very useful in synchronising and averaging signals that have no fixed time reference and so is likely to have very wide applicability. The main feature of the method hinges on the understanding of the nature of phase spectra and on the availability of a simple algorithm for averaging phase angle values. An example of application to other signals is the measurements of chest wall vibrations caused by turbulence of air through the airways. In recent studies

on the respiration control system carried out in our laboratory, there are indications that measurement of vibrations on the chest wall caused by turbulence in air flow could be of some value in the assessment of airway resistance and tracheal blockage. If such measurements are to be studied as spatio-temporal signals, they will also be subject to similar problems of synchronization and variability. (The slow movement of the chest wall could again be retrieved from acceleration measurements by integrating the signals twice; the integration can be conveniently performed in the frequency domain). Figure 5.1 shows an example of the ensemble averaged displacement of the chest wall at various sites due to cardiac activity. The possible application of such measurements to the study of chest wall movements due to respiration is particularly interesting. If serial measurements are taken, the problem of synchronizing the measurements with respect to respiration phases can be approached using similar methods. Hence one can establish how the thorax moves with respiration and can be useful in the studies of developing respiration difficulties, especially of mechanical or myoneural origin.

The method of displaying the scatter of signal spectra, as demonstrated in figure 2.18 is a useful tool for displaying signals where both amplitude and phase spectra are of some importance. One example is the ensemble study of evoked response potential measurements. Sayers (1974a,b) discovered the dominant role of phase spectra in auditory-evoked response patterns and proposed the use of the grouping of phase values

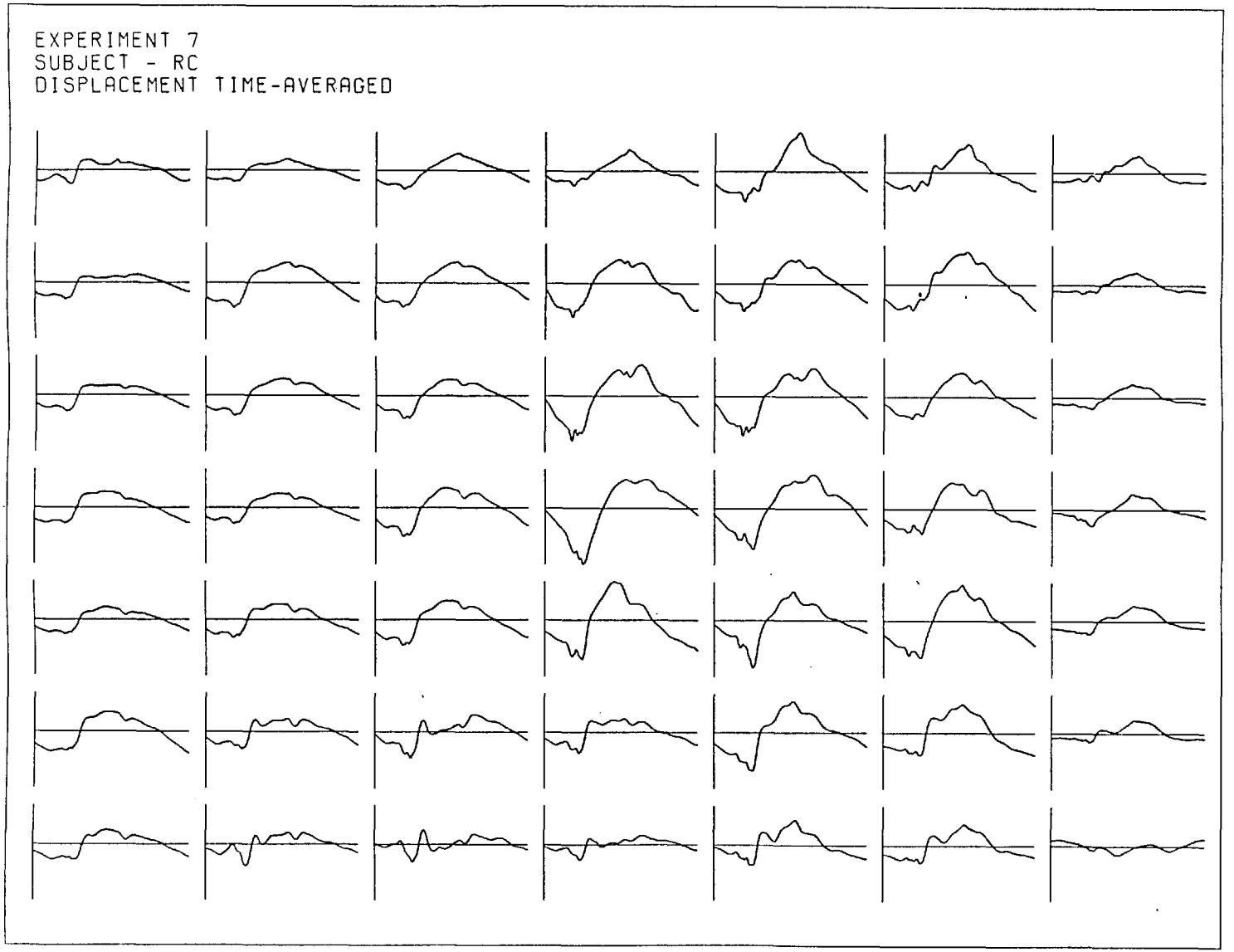

Figure 5.1 The ensemble averaged displacement signal obtained by double intergrating the acceleration measurements obtained in Experiment 1.

of individual frequency harmonics in an ensemble as an objective means of judgement of the presence of a response.

The phase dominant feature applies also to the vibration patterns; this suggests that characterising the signal phase spectra may be of some value. The simulation using transient oscillations has been helpful on this point by showing how to reproduce some of the features in the phase spectra of certain vibration patterns. However, closer study is needed into this relatively unexplored field before one can fully assess the usefulness of the phase spectra as means of characterisation.

The results of the various spatio-temporal analyses all point to the following possibilities:

1. The precordial vibrations are caused by multiple sources and are transmitted through different pathways to different sites on the precordium.
2. Different frequency groups of the vibrations spread differently over the precordium.

These suggest that the precordial vibrations measured at different sites can contain different information about cardiac mechanical activity. Theoretically, maximal information is obtained if the vibrations over the entire chest are measured. In practice, this is not possible and not necessarily profitable, because certain sites contain more 'information' than others. The optimal alternative is to measure the vibration only at those sites where the signals are 'informative'. It is therefore necessary objectively

to establish areas where useful information can be obtained.

Sainani et al., (1967-68) attempted to advance in this direction by mapping out on the chest wall the areas showing largest signals corresponding to loudest heart sounds in normal subjects and loudest murmurs and abnormal sounds in abnormal subjects. The work, while being very comprehensive from the clinical point of view, is subject to two objections from the engineering point of view. Firstly, the mapping was established by measurements at eight sites in normal subjects and 11-14 sites in abnormal subjects. The spatial sampling rate necessary to represent the spatial distribution adequately was not investigated. The sampling theorem demands a minimum spatial sampling frequency before one can be confident that no valuable spatial information is lost and no ambiguity imposed by aliasing. Secondly, the largest signals are not necessarily the most informative. Other sites where the vibrations are smaller in magnitude could also contain useful information different from that contained in the the loudest sites. The phase reversal of the second vibration measured on the upper right hand region of the chest, for example, would not have been noticed if only the largest signals were considered.

The methodology used by Hayashi (1973) also differs from ours in a number of ways. In his study the signal measured at different sites are synchronized by the onset of the QRS complex. The variation of delays between the

mechanical and electrical events were not taken into consideration. The signals were measured serially and compared directly with other measurements as if they were simultaneously acquired. The contour mapping were based on the maximal integrated value of the temporally-gated activity at each site; it therefore was not a true spatio-temporal study of the signal. The spatial measurements were made at 98 to 140 sites on the precordium and subsequently interpolated by linear interpolation; by using a more efficient method of interpolation, namely bi-cubic spline, we found that the number of measurement sites necessary to reproduce a reasonable spatial picture could be reduced.

Although we found that a spatial sampling rate of about one sample in three centimetres is sufficient for a regularly spaced grid (secion 3.2), it is however a very inefficient way of sampling. An examination of the spatial contour maps in figures 3.8 and 3.9 reveals that most of the spatial variations occur in areas near to the heart as one would expect. Therefore a non-uniform sampling grid as shown in figure 5.2 can yield equal spatial information with fewer samples. The sampling grid is defined by equal angle projections from the centre of the heart to the chest wall and gives increasing sampling distance on the chest wall as one moves away from the heart. The use of bi-cubic spline interpolation to reconstruct the spatial distirbution from such an irregular grid is straightforward. In fact, this constitutes a more efficient choice

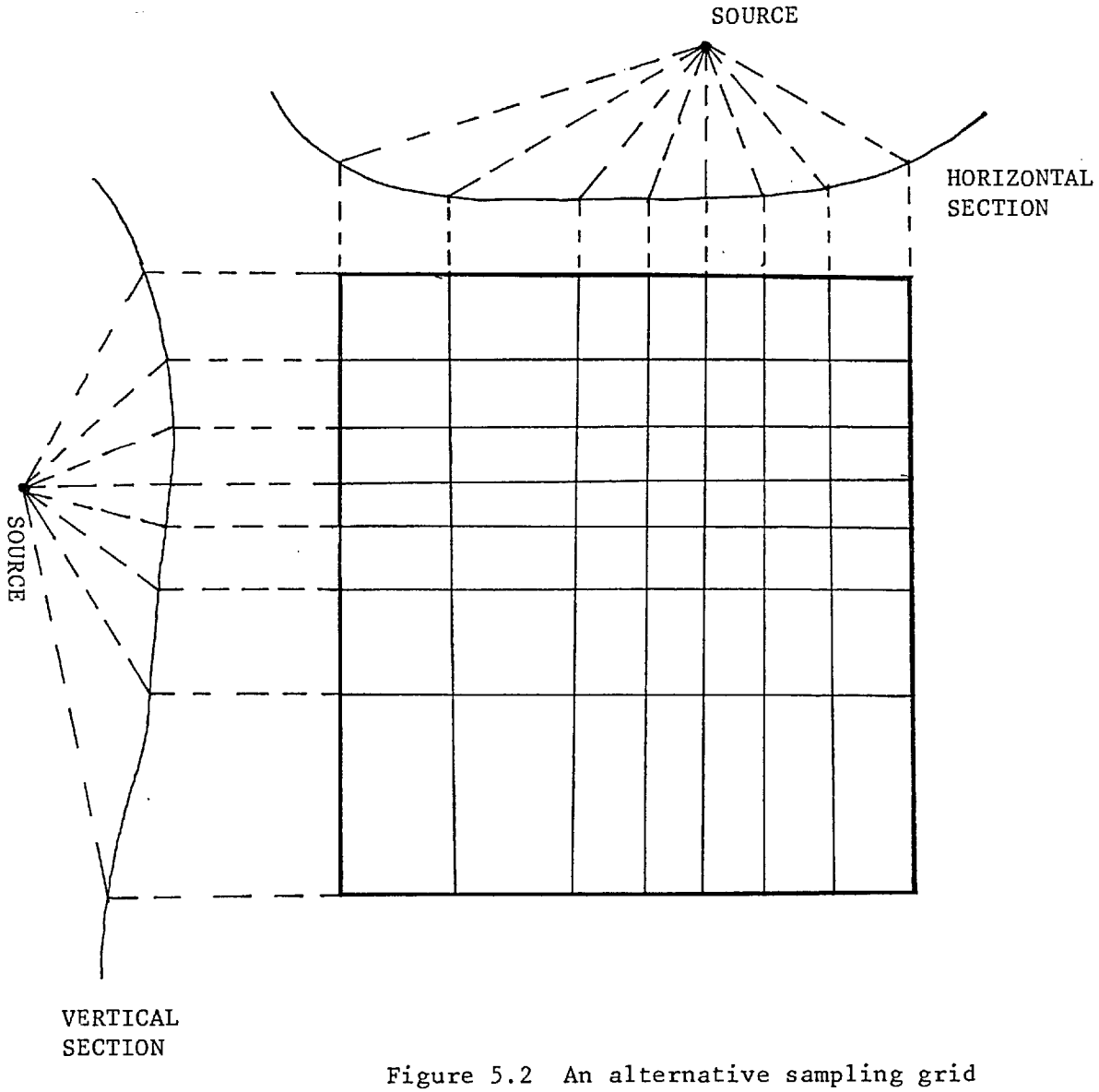

Figure 5.2 An alternative sampling grid based on equal angle projections of the source to the chest wall

of knots for the cubic spline polynomials than a regular rectangular grid.

The findings in section 3.3 also point to the fact that a minimum spatial sampling rate is necessary to represent the spatial variation of the precordial vibrations. One can, of course, question whether such spatial variation has any clinical significance - a question which is beyond the scope of the present work to answer - it is however important to realise that such minimum spatial sampling rate requirement should be considered in any spatial analysis of cardiac precordial vibrations.

The 'secondary source' model suggested by Faber (1962) does not seem to agree with our findings. The hypothesis that the vibration is first transmitted to a 'secondary source' on the surface and spread acorss the chest wall as Rayleigh waves cannot account for the large variations in the vibration patterns at different sites, including the doublereversal of phase in the second vibration. The deconvolution studies showed that there is no simple relationship between the transfer from the site with widest band signal to the other sites. On the other hand, the mechanical dipole representation proposed by Verburg (1975) agrees well with our findings. The double phase reversal reported here is regarded as a very positive indication that 'multiple dipoles' are necessary to represent the vibrations adequately.

As a result of the present work, a satisfactory procedure has been developed for the measurement of the

precordial vibration needed for these spatio-temporal investigations. By studying a larger sample of normal and abnormal subjects it should be possible to establish objectively exactly what kind of spatio-temporal differences between normal and abnormal signals can be expected and the locations where such differences in the signals can be observed. Although our study was limited to frequencies below 100 Hz, it can be easily extended to higher frequency bands using suitable accelerometers and high pass filters. In more extensive studies, measurement of individual sites separately will not be practical because of the time needed for the measurements. But using light-weight accelerometers one could measure a number of sites simultaneously and so reduce the time required for the measurements without introducing too much loading on the chest wall. A row of eight transducers can reduce a session of measurements at 64 sites for 2 minutes recordings to less than half an hour. The signals can be either recorded remotely on analogue tapes or digitized directly on-line by a small laboratory computer. The preprocessing and analysis of the digitized data can be performed efficiently on a larger computer.

Our attempt to solve the inverse problem achieved the purpose of establishing how the problem can be formulated. Although the constrained least square method has been shown to decrease the oscillation in the solutions obtained by the conventional least square method, there are still a number of difficulties associated with the inversion. Firstly, it is very difficult to assess the 'successfulness'

of the inversion. It has been shown that 'self-consistency' does not necessarily imply the goodness of the inversion as a representation of the sources. Secondly the various assumptions (homogeneity, infinite boundary etc) necessary for the simplicity of the associated mathematics are likely to cause large errors in the estimated transfer coefficients. However, it may be possible that instead of using the analytic method for the calculation of the transfer coefficient, the complexity of inhomogeneity and finite boundary can be included if the model is formulated using finite element methods. In this way, a more accurate model could be achieved.

In summary, it is argued that there are positive indications that spatio-temporal measurement and analysis of precordial cardiac vibrations can be valuable in extracting maximal information about the mechanical activity of the heart. An adequate procedure has been developed for such measurements, which can be a convenient starting point for investigations on a larger scale.

APPENDIX A

CALIBRATION OF THE ACCELEROMETER AND STRAIN GAUGE AMPLIFIER CIRCUIT

(1) A 10 Kg suspended mass was set into vibration by a shaker.

(2) The shaker was energized by a charge amplifier which derived its sinusoidal input from a Solatron frequency analyser.

(3) The vibratory force was transmitted to the mass via a force gauge which was known to have a flat frequency response up to 5 kHz.

(4) The accelerometer (JLT - BLA - 1) was glued to the suspended mass so that it monitored the horizontal vibration of the mass (figure A1).

(5) The input/output relationship (i.e. the reading of the force gauge and that of the accelerometer) was calculated using the Solatron frequency analyser over the frequency range from 2 Hz to 200 Hz.

(6) The amplitude and phase response of the accelerometer are shown in figure 2a & b (chapter 2).

(7) Figure A2 shows the circuit of the strain gauge amplifier.

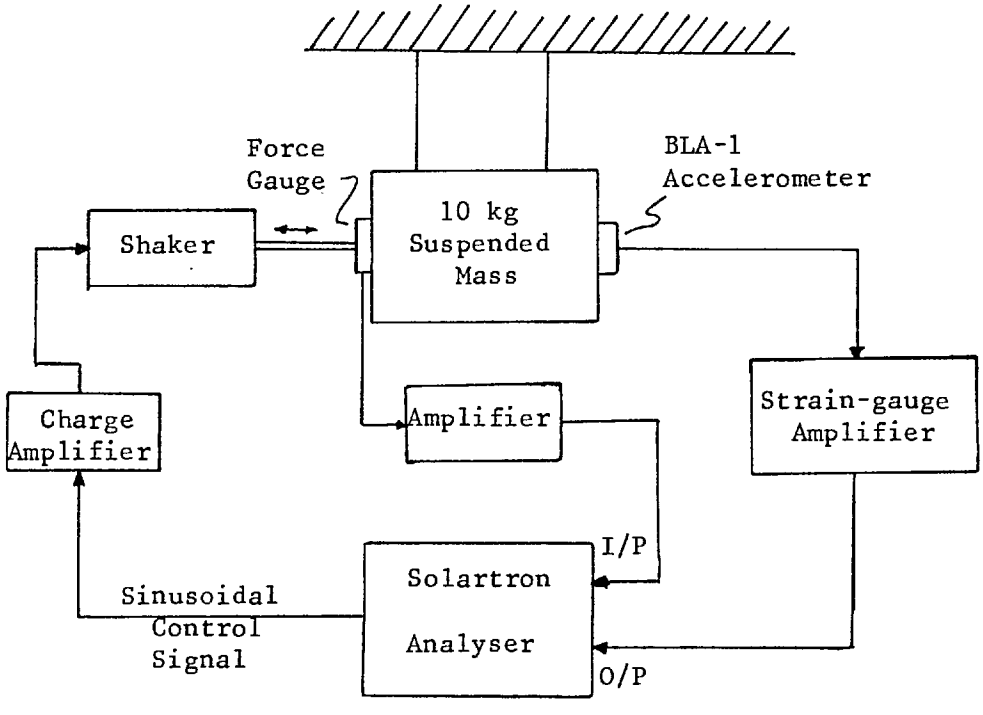

Figure A1 The calibration of the accelerometer

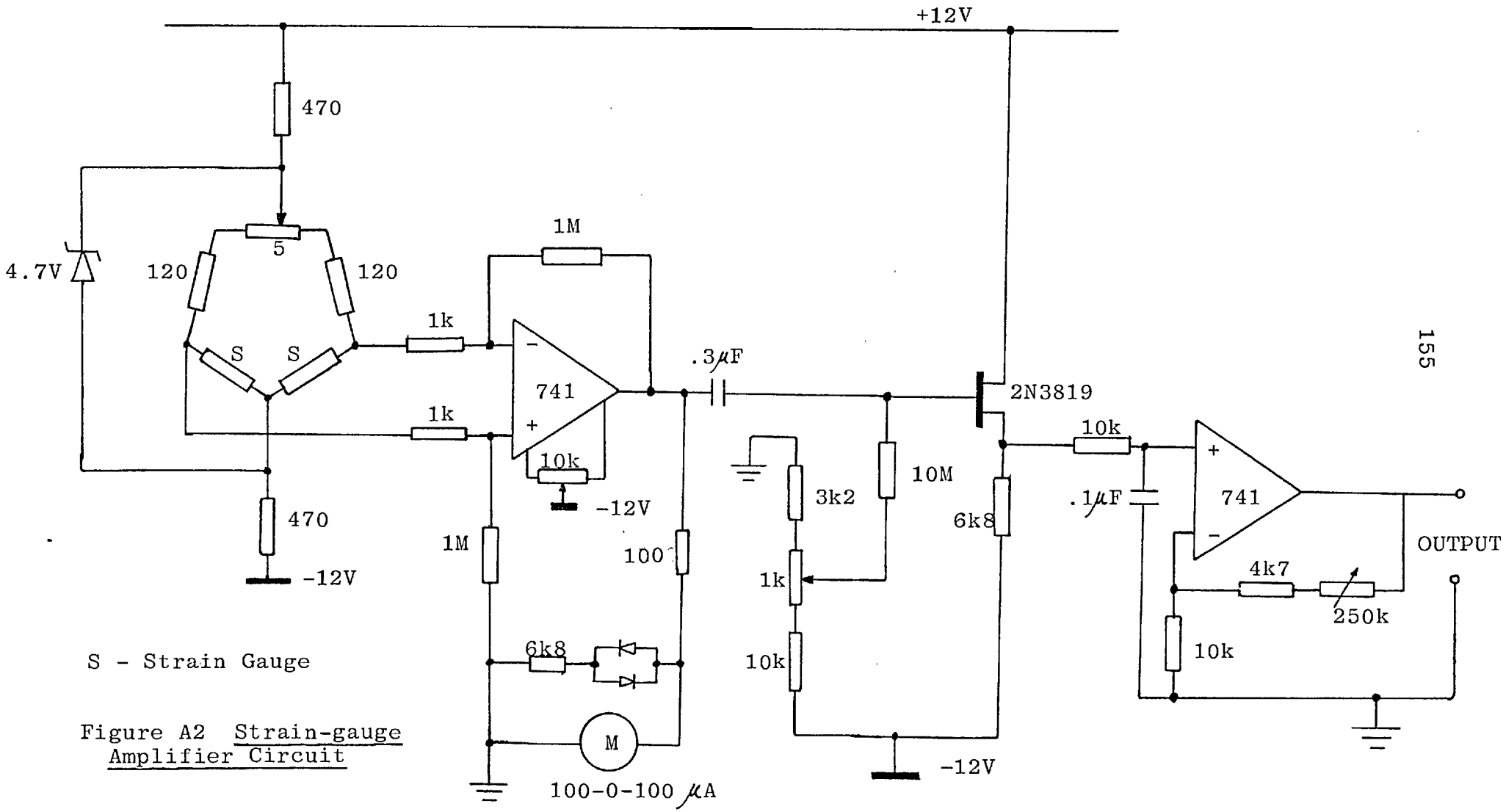

S - Strain Gauge

Figure A2 Strain-gauge Amplifier Circuit

APPENDIX B

SPECTRAL AVERAGING

B.1 Effect of Time Jitter on Coherent Averaging

Consider a template signal f(t) which is subject to a random time jitter δ_i. For simplicity, let us assume δ_i to be rectangularly distributed between $(-\delta, +\delta)$. By coherent averaging, we imply finding the signal

$$\bar{f}(t) = \frac{1}{N} \sum_{i=1}^{N} f(t+\delta_i) \quad \ldots\ldots\ldots\ldots\ldots\ldots \quad (B.1)$$

As N tends to infinity, this is equivalent to convoluting f(t) with the distribution function $p(\delta)$ (figure B1). This is the same as multiplying the spectrum of f(t) with that of $p(\delta)$ and hence causes smoothing. By the reciprocal relationship between the time and frequency domains, it is obvious that the wider the distribution function $p(\delta)$, (that is, larger time jitter), the sharper the filtering effect becomes.

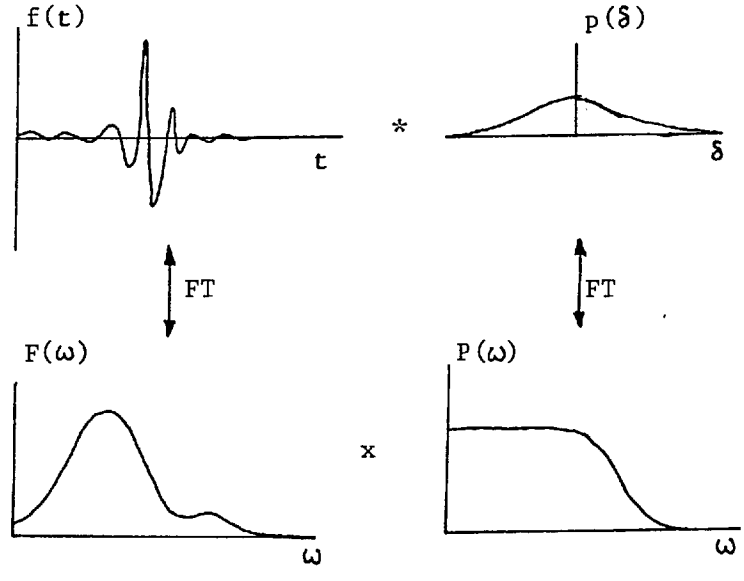

Figure B1 The filtering effect of time-jitter in coherent averaging

B.2 Spectral Effects of Time Shifting a Signal

Let $F(\omega)$ be the Fourier spectrum of the time-domain signal $f(t)$. Then,

$$f(t+\delta) \xleftrightarrow{FT} \int_{-\infty}^{\infty} f(t+\delta) \exp(-j\omega t)\, dt$$

$$= \int_{-\infty}^{\infty} f(t') \exp(-j\omega(t'-\delta))\, dt' \qquad \text{where } t' = t+\delta$$

$$= \exp(j\omega\delta) \int_{-\infty}^{\infty} f(t') \exp(-j\omega t')\, dt'$$

$$= \exp(j\theta)\, F(\omega) \qquad \ldots\ldots\ldots\ldots\ldots\ldots \quad (B.2)$$

where $\theta = \omega\delta = 2\,kf_o$ $\qquad$ k = harmonic number, f_o = fundamental frequency of the D.F.T.

$\ldots\ldots\ldots\ldots\ldots\ldots$ (B.3)

Therefore, the effect of time shifting a signal is to add a ramp to the phase spectrum of the signal leaving the amplitude spectrum unchanged. The slope of the ramp is proportional to the amount of jitter. For example, in our case where $f_o = 2.56$ Hz (100 sample points at a sampling rate of 256 per second), a shift of one sample point will give a slope of 3.59°/harmonic.

Conversely, if the phase spectrum of a signal has a ramp with

gradient g, this corresponds to a time shift of $\delta = g/2\ f_o$.

B.3 Effects of Spectral Averaging on Additive Noise

It is well known that coherent averaging an ensemble of N time synchronised signals has the effect of reducing any additive noise amplitude by a factor of $1/N^{1/2}$. The following section shows the effect fo spectral averaging on random additive noise component.

Consider a given frequency component, $F_i(\omega)$, of sweep number i of the ensemble such that

$$F_i(\omega) = S_i(\omega) + N_i(\omega)$$

where $S_i(\omega) = S(\omega)$ = invariant signal component

$N_i(\omega)$ = the random additive noise component

then

$$|F_i(\omega)| = |S_i(\omega) + N_i(\omega)|$$

$$= \left[|S_i(\omega)|^2 + |N_i(\omega)|^2 + 2\,|S_i(\omega)|\,|N_i(\omega)|\cos\theta_i \right]^{\frac{1}{2}}$$

Let $r_i(\omega) = \dfrac{|N_i(\omega)|}{|S_i(\omega)|}$

and assume that $|N_i(\omega)| \ll |S_i(\omega)|$

such that $r_i(\omega) \ll 1$

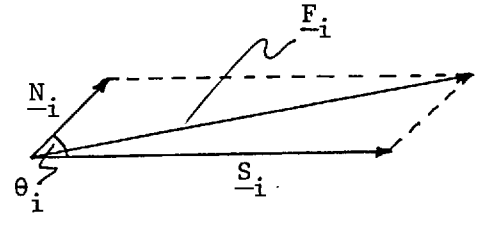

By dividing the expression by $|S_i(\omega)|$ and drop all ω, we obtain

$$|F_i| = |S_i| \left[1 + (r_i^2 + 2r_i \cos\theta_i) \right]^{\frac{1}{2}}$$

$$= |S_i| \left[1 + \frac{1}{2}(r_i^2 + 2r_i \cos\theta_i) - \frac{1}{8}(r_i^4 + 4r_i^3 \cos\theta_i + 4r_i^2 \cos^2\theta_i) + \ldots\ldots\ldots\right]$$

If $r_i \ll 1$, all terms higher than r_i^2 can be neglected, we obtain

$$|F_i| \doteq |S_i| \left[1 + \tfrac{1}{2}r_i^2 (1 - \cos^2\theta_i) + r_i \cos\theta_i\right]$$

Now, assume that θ_i is randomly and uniformly distributed between $+\pi$ and $-\pi$, which is the case for random noise (i.e. the noise component is not 'phase locked' to the signal component), averaging n such components gives,

$$|\overline{F}| = \frac{1}{n} \sum_{i=1}^{n} |F_i| = \frac{1}{n} \sum_{i=1}^{n} |S_i| \left[1 + r_i^2 \sin^2\theta_i + r_i \cos\theta_i\right]$$

As n becomes a large number, the last term on the R.H.S. averages to zero and the expression simplifies to,

$$|\overline{F}| \doteq \frac{1}{n} \sum_{i=1}^{n} |S_i| + \frac{1}{n} \sum_{i=1}^{n} \left(\tfrac{1}{2}\sin^2\theta_i \frac{|N_i|}{|S_i|}\right) |N_i|$$

averaged signal averaged residue noise

Since $\sin\theta_i$ is always less than 1, the averaging reduces the noise component from its average value of $\frac{1}{n}\sum N_i$ to the second term in the above expression.

Effect on Phase Spectrum

Let us assume that a particular harmonic component of the ensemble

consists of a signal and a noise component,

$$F_i(\omega) = S_i(\omega) + N_i(\omega)$$

Let us also, for the moment, assume that S_i has an invariate phase angle θ_s and the noise component N_i has a rectangularly distributed random phase angle between $\pm\pi$ with respect to θ_s. If the resultant component has a phase angle θ_i with respect to S_i, then

$$\theta_{F_i} = \theta_s + \theta_i$$

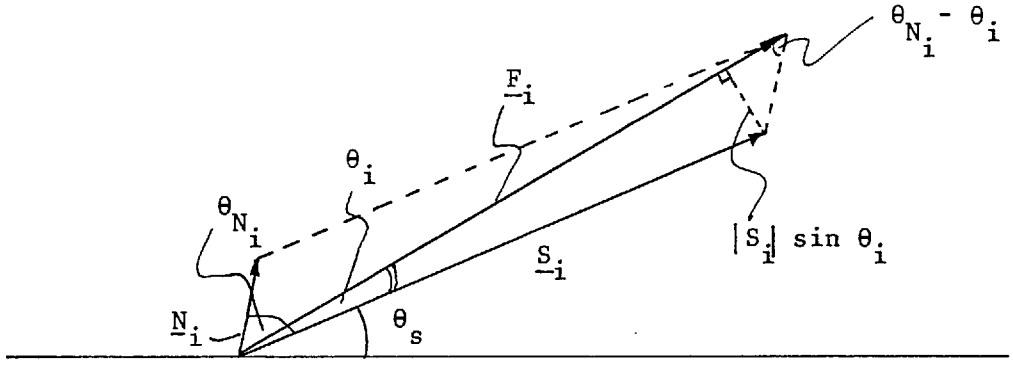

It can be shown that

$$|S_i| \sin \theta_i = |N_i| \sin (\theta_{N_i} - \theta_i)$$

$$\sin \theta_i = \frac{|N_i|}{|S_i|} (\sin \theta_{N_i} \cos \theta_i - \cos \theta_{N_i} \sin \theta_i)$$

if $|N_i| \ll |S_i|$, then $\frac{|N_i|}{|S_i|} \ll 1$ and $\sin \theta_i \to \theta_i \to 0$

$\cos \theta_i \to 1$

and $$\theta_i \doteq \frac{|N_i|}{|S_i|} \sin \theta_{N_i}$$

But $\theta_{F_i} = \theta_S + \theta_i$ or $\bar{\theta}_F = \theta_S + \bar{\theta}_i$

where $$\bar{\theta}_i = \frac{1}{n} \sum_{i=1}^{n} \frac{|N_i|}{|S_i|} \sin \theta_{N_i}$$

which tends to zero if n is large and θ_{N_i} satisfies the conditions mentioned earlier.

Therefore, the mean phase $\bar{\theta}_F$ will be an estimate of the true phase value θ_S of the signal at that frequency.

θ_S, however, need not be invariable but can be subject to statistical variation about a mean value $\bar{\theta}_S$. This is the case if the original signal in the time domain is subject to a random time jitter. Provided that θ_{N_i} is independent of θ_{S_i}, the above arguement still hold true and the mean phase in this case will be an estimate of the mean phase value of the signal for this particular component.

That is, $$\bar{\theta}_F = \bar{\theta}_S$$

APPENDIX C

FORMULATION OF THE CUBIC SPLINE INTERPOLATION

Consider a set of data values $(u_0,u_1,....,u_n)$ which are given at $(x_0,x_1,....,x_n)$, it is desired to fit a set of piecewise cubic polynomial functions to the data values such that the functions will have continuous first and second derivatives.

Let v(x) and w(x) be two typical consecutive piecewise cubic functions between $x_{i-1} \leqslant x \leqslant x_i$ and $x_i \leqslant x \leqslant x_{i+1}$ with the functional values u_{i-1}, u_i and u_{i+1} at the knots as shown in the diagram.

Also let $\Delta x_i = x_{i+1} - x_i$,

$\Delta u_i = u_{i+1} - u_i$

Then v(x) and w(x) and their second derivatives can be expressed as,

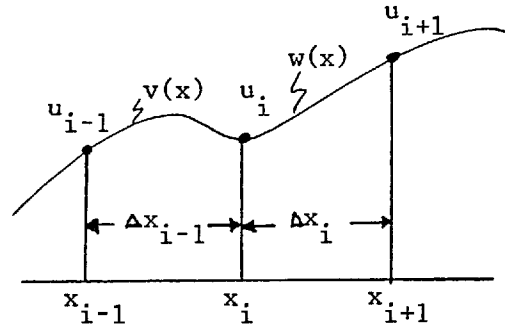

$$v(x) = a_0 + a_1 (x-x_{i-1}) + a_2 (x-x_{i-1})^2 + a_3 (x-x_{i-1})^3 \quad ..... \quad (C.1)$$

$$v''(x) = 2a_2 + 6a_3 (x-x_{i-1}) \quad ..... \quad (C.2)$$

$$w(x) = b_0 + b_1 (x-x_i) + b_2 (x-x_i)^2 + b_3 (x-x_i)^3 \quad ..... \quad (C.3)$$

$$w''(x) = 2b_2 + 6b_3 (x-x_i) \quad ..... \quad (C.4)$$

a_0,a_1,a_2,a_3 in equation C.1 can be solved in term of u_{i-1},u_i,u'_{i-1} and u'_i as,

$$a_0 = u_{i-1} \qquad a_1 = u'_{i-1}$$

$$a_2 = 3\frac{\Delta u_{i-1}}{\Delta x_{i-1}^2} - \frac{u_i' + 2u_{i-1}'}{\Delta x_{i-1}} \qquad a_3 = -2\frac{\Delta u_{i-1}}{\Delta x_{i-1}^3} + \frac{u_i' + u_{i-1}'}{\Delta x_{i-1}^2}$$

Similarly,

$$b_0 = u_i \qquad b_1 = u_i'$$

$$b_2 = 3\frac{\Delta u_i}{\Delta x_i^2} - \frac{u_{i+1}' + 2u_i'}{\Delta x_i} \qquad b_3 = -2\frac{\Delta u_i}{\Delta x_i^3} + \frac{u_{i+1}' + u_i'}{\Delta x_i^2}$$

Since $v''(x) = w''(x)$ at $x = x_i$, from equation C.2 and C.4, we obtain,

$$2a_0 + 6a_3\Delta x_{i-1} = 2b_2$$

Substituting a_2, a_3 and b_2 into the equation and simplify, we get,

$$\Delta x_i\, u_{i-1}' + 2(\Delta x_i + \Delta x_{i-1})\, u_i' + \Delta x_{i-1}\, u_{i+1}' = 3\,\Delta x_{i-1}\,\frac{\Delta u_i}{\Delta x_i} + \Delta x_i\,\frac{\Delta u_{i-1}}{\Delta x_{i-1}}$$

for $i = 1,2,.....,n-1$.

For equal spaced data, $\Delta x_i = h$ for all i, the equation simplifies to

$$u_{i-1}' + 4u_i' + u_{i+1}' = (3/h)\,(u_{i+1} - u_{i-1}) \quad ..... \quad (C.5)$$

This constitutes n-1 equations for the n+1 unknowns of u_i'. The other two equations needed to solve the problem are obtained from the boundary condition (section 4.2) that $v'''(x) = w'''(x)$ at $x = x_1$ and $x = x_{n-1}$. By differentiating equations C.2 and C.4 again and apply the boundary condition, we get

$$a_3 = b_3$$

Assuming equal interval, h, and substitute the expressions for a_3 and b_3

$$-2\frac{\Delta u_{i-1}}{h^3} + \frac{u'_i + u'_{i-1}}{h^2} = -2\frac{\Delta u_i}{h^3} + \frac{u'_{i+1} + u'_i}{h^2}$$

$$2\left(\frac{\Delta u_i}{h} - \frac{\Delta u_{i-1}}{h}\right) = u'_{i+1} - u'_{i-1}$$

By putting i = 1 and i = n-1, we get

$$u'_0 - u'_2 = -2/h\,(u_2 - 2u_1 + u_0)$$

$$u'_{n-2} - u'_n = -2/h\,(u_n - 2u_{n-1} + u_{n-2}) \quad \text{..... (C.6)}$$

The set of n+1 equations given by C.5 and C.6 can be expressed in matrix form as

$$\begin{bmatrix} 1 & 0 & -1 & 0 & 0 & . & . & . & 0 \\ 1 & 4 & 1 & 0 & 0 & . & . & . & 0 \\ 0 & 1 & 4 & 1 & 0 & . & . & . & . \\ . & . & . & . & . & . & . & . & . \\ . & . & . & . & 0 & 1 & 4 & 1 & 0 \\ 0 & . & . & . & 0 & 0 & 1 & 4 & 1 \\ 0 & . & . & . & 0 & 0 & 1 & 0 & -1 \end{bmatrix} \begin{bmatrix} u'_0 \\ u'_1 \\ u'_2 \\ . \\ u'_{n-2} \\ u'_{n-1} \\ u'_n \end{bmatrix} = \frac{3}{h} \begin{bmatrix} -\frac{2}{3}(u_2 - 2u_1 + u_0) \\ u_2 - u_0 \\ u_3 - u_1 \\ . \\ u_{n-1} - u_{n-3} \\ u_n - u_{n-2} \\ -\frac{2}{3}(u_n - 2u_{n-1} + u_{n-2}) \end{bmatrix}$$

The matrix is strictly diagonally dominant and can be solve conveniently by Gaussian elimination. Once u_i, u_{i+1}, u'_i and u'_{i+1} are known for the segment $x_i \leqslant x \leqslant x_{i+1}$, interpolation within the segment is trivial.

APPENDIX D

GENERAL CHARACTERISTICS OF WAVE TRANSMISSION IN A VISCOELASTIC MEDIUM

The propagation and attenuation properties of waves in body tissues had been studied by Oestreicher (1951), Franke (1951) and von Gierke (1952), taking into account elasticity, viscosity and compressibility of the medium. The medium can be described by its density ρ and the Lame's constants:

$$\lambda = \lambda_1 + i\omega\lambda_2$$
$$\mu = \mu_1 + i\omega\mu_2$$

where λ_1 = coefficient of volume compressibility,

λ_2 = coefficient of volume viscosity,

μ_1 = coefficient of shear elasticity,

μ_2 = coefficient of shear viscosity,

ω = circular frequency

The wave propagation in such medium is usually separated into the irrotational compression component and the equivoluminal shear component. For plane waves in the medium, the velocity and damping factor of the two components are given in terms of their wave numbers k and h such that (OESTREICHER, 1951):

v_c = velocity of the compression component = $\omega / R(k)$

α_c = attenuation of the compression component = $-I(k)$

v_{sh} = velocity of the shear component = $\omega/R(h)$

α_{sh} = attenuation of the shear component = $-I(h)$

where $k = \left(\frac{\rho\omega^2}{2\mu+\lambda}\right)^{\frac{1}{2}}$; $h = \left(\frac{\rho\omega^2}{\mu}\right)^{\frac{1}{2}}$

R(z) = real part of complex number z

I(z) = imaginary part of complex number z

The medium is obviously dispersive since the velocities vary with frequency. The damping factor is also frequency dependent. This implies that the vibration from the source will be distorted by the time it reaches the surface and the amount of distortion depends on the properties of the tissues on the transmission path. On the interfaces between different media or at free surfaces of the body, mixture of shear and compression waves call Rayleigh waves exist which has a velocity near that of the shear wave ($=0.91 v_{sh}$).

In the frequency range of our interest, the dispersion of compression waves is very small but the dispersion of shear waves is very marked. The shear waves have velocity much smaller than that of the compression waves but have a larger damping factor. They are, therefore, restricted to a region near the source. At low frequencies, the shear wave is dominated by μ_1 and as frequency increases, the viscosity μ_2 becomes more significant. Von Gierke (1952) had shown that λ_2 has no influence on the mechanical impedance of the tissues in the frequency range up to 20 kHz. With a large λ_1, the medium behaves as if it is incompressible.

APPENDIX E

IMPLEMENTATION OF THE SOLUTION TO THE FIELD EQUATION OF AN OSCILLATING SPHERE IN A VISCOELASTIC MEDIUM

E.1 The Solution

The field equation of an oscillating sphere in a viscoelastic medium had been solved by Oestreicher (1951). For a small oscillating sphere of radius a, oscillating sinusoidally along the x-axis with an amplitude of S_0, the solution is given as :

$$\underline{S} = \left[-A \operatorname{grad} \left(\frac{h_1(kr)}{kr} x \right) + B \left(2h_0(hr) \operatorname{grad} x - h_2(hr)\, r^3 \operatorname{grad} \frac{x}{r^3} \right) \right] S_0 \exp(i\omega t) \quad \ldots\ldots\ldots\ldots\ldots\ldots \quad (E.1)$$

where $\underline{S}$ = the displacement vector at any point with the cartesian coordinates (x,y,z) with respect to the cnetre of the sphere

r = the distance of the point (x,y,z) to the centre of the sphere
$= (x^2 + y^2 + z^2)^{\frac{1}{2}}$

h and k are as defined in Appendix D

and $h_n(p)$ is the spherical Hankel function of n^{th} order

The first term in the equation corresponds to the irrotational compression wave and the second term, the incompressible shear wave.

E.2 Spherical Hankel Functions

The spherical Hankel functions are given by Abramowitz (1968) as:

$$h_n(p) = j_n(p) - i\, y_n(p) \qquad \ldots\ldots\ldots\ldots\ldots \text{(E.2)}$$

where $j_n(p)$ and $y_n(p)$ are spherical Bessel functions of the 1^{st} kind. $y_n(p)$ can be calculated in terms of $j_n(p)$ by the following relationship,

$$y_n(p) = (-1)^{n+1}\, j_{n-1}(p) \qquad \ldots\ldots\ldots\ldots\ldots \text{(E.3)}$$

where $j_n(p)$ is, in turn, determined by the following recurrence relationships,

$$\begin{aligned} j_n(p) &= f_n(p) \sin p + (-1)^{n+1} f_{-n-1}(p) \cos p \\ f_0(p) &= p^{-1} \\ f_1(p) &= p^{-2} \\ f_{n-1}(p) + f_{n+1}(p) &= (2n+1)\, p^{-1} f_n(p) \end{aligned}$$

$\ldots\ldots\ldots\ldots\ldots$ (E.4)

From equations E.3 and E.4, $j_n(p)$ and $y_n(p)$ for n = 0, 1 and 2 can be obtained as :

$$\begin{aligned} j_0(p) &= \frac{\sin p}{p} \\ j_1(p) &= \frac{\sin p}{p^2} - \frac{\cos p}{p} \\ j_2(p) &= \left(\frac{3}{p^3} - \frac{1}{p}\right) \sin p - \frac{3}{p^2} \cos p \\ y_0(p) &= -j_{-1}(p) = -\frac{\cos p}{p} \\ y_1(p) &= -j_{-2}(p) = -\frac{\cos p}{p^2} - \frac{\sin p}{p} \\ y_2(p) &= -j_{-3}(p) = \left(-\frac{3}{p^3} + \frac{1}{p}\right) \cos p - \frac{3}{p^2} \sin p \end{aligned}$$

$\ldots\ldots\ldots\ldots\ldots$ (E.5)

using equations E.2 and E.5 and the relationship $\exp(ip) = \cos p + i \sin p$, the spherical Hankel functions for n = 0,1,2 can be expressed as,

$$h_0(p) = \frac{i}{p} \exp(-ip)$$

$$h_1(p) = \frac{(i - p)}{p^2} \exp(-ip)$$

$$h_2(p) = \frac{((3 - p^2)\, i - 3p)}{p^3} \exp(-ip) \qquad \ldots\ldots\ldots\ldots \quad (E.6)$$

An additional formula, the differentiation formula, is useful for the calculation of equation E.1 .

$$\left(\frac{1}{p}\frac{d}{dp}\right)^m \left[\, p^{-n} h_n(p) \,\right] = (-1)^m p^{-n-m} h_{n+m}(p)$$

For m = 1 and n = 1, we get

$$\frac{d}{dp}\left(\frac{h_1(p)}{p}\right) = -\frac{h_2(p)}{p} \qquad \ldots\ldots\ldots\ldots \quad (E.7)$$

E.3 Decomposition of the Solution

For the implementation of the solution given as equation E.1 on a digital computer, the equation has to be decomposed into its x-, y- and z-components. Using elementary vector algebra, the 'transfer function' in equation E.1 can be separated into three orthogonal components s_x, s_y and s_z such that,

$$\underline{S} = \left(s_x \underline{i} + s_y \underline{j} + s_z \underline{k} \right) S_0 \exp(i\omega t) \qquad \ldots\ldots\ldots\ldots \quad (E.8)$$

where

$$s_x = -A \frac{\partial}{\partial x}\left(\frac{h_1(kr)}{kr} x\right) + B\left[2h_0(hr) - h_2(hr)\, r^3 \frac{\partial}{\partial x}\left(\frac{x}{r^3}\right)\right]$$

$$s_y = -A \frac{\partial}{\partial y} \left(\frac{h_1(kr)}{kr} x \right) - B\, h_2(hr)\, r^3 \frac{\partial}{\partial y} \left(\frac{x}{r^3} \right)$$

..... (E.9)

and $s_z = s_y$ with y substituted by z (by symmetry).

By using equation E.7 and elementary calculus, the partial differentials can be simplified as the following,

$$\frac{\partial}{\partial x} \left(\frac{h_1(kr)}{kr} x \right) = - \left(\frac{x}{r}\right)^2 h_2(kr) + \frac{h_1(kr)}{kr}$$

$$\frac{\partial}{\partial x} \left(\frac{x}{r^3}\right) = \frac{1}{r^3} - \frac{3x^2}{r^5}$$

$$\frac{\partial}{\partial y} \left(\frac{h_1(kr)}{kr} x \right) = - \frac{xy}{r^2} h_2(kr)$$

$$\frac{\partial}{\partial y} \left(\frac{x}{r^3}\right) = - \frac{3xy}{r^5}$$

..... (E.10)

Substituting equations E.10 into E.9, we obtain

$$s_x = A \left[\frac{x^2}{r^2} h_2(kr) - \frac{h_1(kr)}{kr} \right] + B \left[2h_0(hr) - \left(1 - 3\frac{x^2}{r^2}\right) h_2(hr) \right]$$

$$s_y = \frac{xy}{r^2} \left[A\, h_2(kr) + 3B\, h_2(hr) \right]$$

$$s_z = \frac{xz}{r^2} \left[A\, h_2(kr) + 3B\, h_2(hr) \right]$$

..... (E.11)

The constant A and B can be calculated using the boundary condition that at the surface of the source, $x = y = r = a$, $s_z = 1$ and $s_y = 0$.

From equation E.11

$$1 = A \left[h_2(ka) - \frac{h_1(ka)}{ka} \right] + B \left[2h_0(ha) + 2h_2(ha) \right]$$

$$0 = A\, a\, h_2(ka) + B\, 3a\, h_2(ha)$$

By solving the simultaneous equations, A and B can be obtained as,

$$A = \frac{3ka\, h_2(ha)}{ka\, h_2(ka)\, h_2(ha) - 3h_1(ka)\, h_2(ha) - 2ka\, h_2(ka)\, h_0(ha)}$$

and $$B = -\frac{A\, h_2(ka)}{3\, h_2(ha)} \qquad \ldots\ldots\ldots\ldots\ldots \quad (E.12)$$

APPENDIX F

FORMULATION OF THE CONSTRAINED LEAST SQUARE METHOD

Consider a linear system described by the following matrix equation,

$$A\,\underline{f} = \underline{g} \qquad \ldots\ldots\ldots\ldots\ldots\ldots \quad (F.1)$$

It is desired to infer $\underline{f}$ from A and $\underline{g}$. Usually A is not exactly known and $\underline{g}$ is subjected to measurement errors. This may cause erroneous solution and redundancy is introduced such that A is a m x n matrix with $m > n$ (more equations than unknowns). However, the system of equations become incompatible and the least square method is used which effectively solve

$$A\,\underline{f} = \underline{g} + \underline{\epsilon} \qquad \ldots\ldots\ldots\ldots\ldots\ldots \quad (F.2)$$

with the condition that $\sum_{i=1}^{m} \epsilon_i^2 = \text{minimum.}$

This however often introduces 'oscillations' in the solution which, in many cases, are contradictory to some priori knowledge of the solution. Constraints are therefore introduced to the solution as suggested by Philips (1962) and Twomey (1965).

In our case, strict forward least square method has already been shown to be unacceptable. The source solutions are found to vibrate in such a manner so as to produce observations $(\underline{g} + \underline{\epsilon})$ which cancel each other and hence keep ϵ_i^2 minimum. An improvement is expected if $\underline{f}$ can be solved with the priori knowledge of a trial solution $\underline{p}$. The trial

solution was obtained by the method discussed in section 4.5 . In this way, instead of solving equation F.2 with the condition of minimizing $\sum_i \epsilon_i^2$, we would minimize the expression $\sum_j (f_j - p_j)^2$ with the auxillary condition that $\sum_i \epsilon_i^2$ = constant. The quantity to minimize becomes

$$\sum_j (f_j - p_j)^2 + \gamma^{-1} \sum_i \epsilon_i^2 \qquad \text{.....} \qquad (F.3)$$

where γ is a measure of the 'amount' of constraint applied.

Differentiating the expression with respect to f_j and set the derivative to zero, we obtain

$$2(f_j - p_j) + \gamma^{-1} \sum_{i=1}^{n} 2\epsilon_i a_{ij} = 0$$

for j = 1, 2,.....,m

In matrix form it is equivalent to,

$$\gamma(\underline{f} - \underline{p}) + A^T \underline{\epsilon} = 0 \qquad \text{.....} \qquad (F.4)$$

Eliminating ϵ from equation F.2 and F.4, we obtain

$$\gamma(\underline{f} - \underline{p}) + A^T (A\underline{f} - \underline{g}) = 0$$

$$\text{or} \quad \underline{f} = (A^T A - \gamma I)^{-1} (A^T \underline{g} + \gamma \underline{p}) \qquad \text{.....} \qquad (F.5)$$

Note that if $\gamma = 0$ we have

$$\underline{f} = (A^T A)^{-1} A^T \underline{g}$$

which is identical to the least square method and the amount of constraint

increases with the value of γ.

Instead of keeping $\sum_i \epsilon_i^2$ constant, we decided to set the criterion on the constraint by measuring the amount of cancellation of the source component using a quantity α called the norm ratio, the derivation of which is given in appendix G. Equation F.5 was solved for several values of γ iteratively until α reached the prescribed limits.

APPENDIX G

FORMULATION OF THE NORM RATIO

Let $\underline{R}_j(i)$ represents the contributions of source j to the precordial vibration at location i. It was desired to compute some quantitative measures which indicates how much these sources cancel one another in order to determine the amount of constraint needed for the inversion. If only two sources were considered (as in the case of the first vibration) the phase angle between the vectors representing the two sources is a convenient measure. But when three or more sources are present, the phase angle between the sources can no longer be used as a measure of the cancellation. Therefore a parameter called 'norm ratio' was used.

Let there be k sources and n observation sites. The ration $\beta(i) = \sum_{j=1}^{k} \left| \underline{R}_j(i) \right| \Big/ \left| \sum_{j=1}^{k} \underline{R}_j(i) \right|$ is a measure of how much do the sources cancel one another. If the sources cancel completely $\beta(i) \rightarrow \infty$ and if they are perfectly in phase, $\beta(i) \rightarrow 1$. However, the 'cancellation' of the sources contribution at a site where the signal is weak (and therefore noisy) should be less important than that of a location of stronger signal magnitude. Therefore a weighting factor, w(i), which is propertional to the square-root of the amplitude of the signal at location i was used where,

$$w(i) = \left| \sum_{j=1}^{k} \underline{R}_j(i) \right|^{\frac{1}{2}}$$

The norm ratio was then computed from the mean weighted value of β, that is,

$$\text{norm ratio, } \alpha = \frac{1}{n} \sum_{i=1}^{n} w(i) * (\beta (i) - 1)$$

It was found necessary to subtract 1 from β since β starts from 1 when the component are all in phase.

REFERENCES

Abramowitz, M. and Stegun, I.A. (1968). Handbook of mathematical functions. Dover Publications, New York.

Ahlberg, J.H., Nilson, E.N. and Walsh, J.L. (1967). The theory of splines and their applications. Academic Press, New York.

Bew, F.E., Pickering, D., Sleight, P. and Stott, F.D. (1971). Pixie-Cardiography:- Accelerometer applications to phonocardiography and displacement cardiography in childhood. Brit. Heart J. 33, 702.

Birkhoff, G. and Garabedian, H.L. (1960). Smooth surface interpolation. J. Math. and Phys., 39, 258.

Birkhoff, G. and De Boor, C.R. (1964). Piecewise polynomial interpolation and approximation. In: Approximation of function, Proceedings of the Symposium on approximation of functions, General Motors Research Laboratories, Warren, Michigan 1964. Edited by H.L. Garabedian. Elsevier Publishing Co.

Burton, A.C. (1971). Physiology and Biophysics of the Circulation. Year Book Medical Publishers Incorporated.

De Boor, C.R. (1962). Bicubic spline interpolation. J. Math. and Phys. 41, 212.

Dunn, F.L. and Rahm, W.E. (1952). Electrostethography II : New method for study of precordial transmission of cardiodynamics. Am. Heart J., 44, 95.

Eycleshymer, A.C. and Schoemaker, D.M. (1938). A cross-section anatomy. D. Appleton-Century Co. Inc., New York.

Faber, J.J. and Burton, A.C. (1962). Spread of heart sound over chest wall. Circulation Res., 11, 96.

Faber, J.J. (1963). Damping of sound of the chest surface. Circulation Res., 13, 352.

Franke, E.K. (1951). Mechanical impedance of the surface of the human body. J. Appl. Physiol., 3, 582.

von Gierke, H.E., Oestreicher, H.L., Franke, E.K. et al., (1952). Physics of vibrations in living tissues. J. Appl. Physiol., 4, 886.

Greville, T.N.E. (1967). Spline functions, interpolation and numerical quadrature. In: Mathematical method for digital computer, vol. II. Edited by A.R. Ralston and S.W. Herbert. John Wiley & Sons Inc.

Greville T.N.E. (1969). Theory and applications of spline functions. Academic Press, New York.

Quardo, R.A.L. (1972). The Multiple Series and Locus of the Equivalent Dipole representing Cardiac Activity in Man. Ph. D. Thesis. Engng in Medicine Lab., Imperial College, London.

Hayashi, R. (1973). Computer mapping for the equal intensity distribution of heart sounds and murmurs on the chest surface. Jap. Circ. J., 37, 1103.

Ikegaya, K., Suzumura, N. and Funada, T. (1971). Absolute calibration of phonocardiographic microphones and measurements of chest wall vibration. Med. Biol. Engng., 9, 683.

Lanczos, C. (1956). Applied analysis. Prentice-Hall, Inc., New York.

Laughlin, D.E. and Mahoney, R.P. (1972). New phonocardiographic transducers ultilizing the hot wire anemometer principle. Med. Biol. Engng., 10, 43.

Luisada, A.A. (1941). Variable interval between electrical and acoustic phenomena in auricular fibrillation. Am. Heart J., 22, 243.

Luisada, A.A. (1965). From auscultation to phonocardiography. Mosby, St. Louis.

Luisada, A.A., MacCanon, D.M., Coleman, B. et al., (1971). New studies on the first heart sound. Am. J. Cardiol., 28, 140.

Luisada, A.A. (1971b). The second heart sound in normal and abnormal conditions. Am. J. Cardiol., 28, 150.

Luisada, A.A. (1972). The sounds of the normal heart. W.H. Green, Inc., St. Louise.

MacCanon, D.M., Arevalo, F. and Meyer, E.C. (1964). Direct detection and timing of aortic valve closure. Circulation Res., 14, 387.

McKusick, V.A. (1958). Cardiovascular sound in health and disease. Williams & Wilkins Co., Baltimore.

Messer, A.D., Counihan, T.B., Rapraport, M.B., et al., (1951). The effect of cycle length on the time of occurrence of the first heart sound and the opening snap in mitral stenosis. Circulation, 4, 576.

Mori, M., Shah, P.M., MacCanon, et al., (1964). Hemodynamic correlates of the various components of the second heart sounds. Cardiologia, 44, 65.

Oestreicher, H.L. (1951). Field and impedance of oscillating sphere in a visco-elastic medium with an application to biophysics. J. Acoust. Soc. Am., 23, 707.

Philips, B.L. (1962). A technique for the numerical solution of certain internal equations of the first kind. J. Assoc. Comp. Mach., 9, 84.

Rotterdam, van A. and Vollenhoven, van E. (1967). Problems in relation to measurement of chest wall movement due to heart action. Med. & Biol. Engng., 5, 339.

Rushmer, R.F. (1971). Cardiovascular dynamics. W.B. Saunders.

Sainani, G.S. and Luisada, A.A. (1967). "Mapping" the precordium I : Heart sounds of normal subjects. Am. J. cardiol., 19, 788.

Sainani, G.S. and Luisada, A.A. (1968). Mapping of the precordium II : Murmurs and abnormal sounds. Acta Cardiol. (Brux), 23, 152.

Sayers, B. McA., Beagley, H.A. and Henshall, W.R. (1974). The mechanism of auditory evoked EEG responses. Nature, 247, 481.

Sayers, B. McA. and Beagley, H.A. (1974). Objective evaluation of auditory evoked EEG responses. Nature, 251, 608.

Shah, P.M., Slodki, S.J. and Luisada, A.A. (1964). A revision of the "classic" areas of auscultation of the heart. A physiological approach. Am. J. Med., 36, 293.

Sheppard, L.C. (1976). Correlation Analysis of Arterial Blood Pressure Responses to Vasoactive Drugs. Ph. D. Thesis. Engng. in Medicine Lab., Imperial College, London.

Takagi, S., Yoshimura, S. and Okamura, T. (1964). Trial and success in the technical realization of requirements for phonocardiographic microphones. Med. Biol. Engng., 2, 123.

Twomey, S. (1965). The application of numerical filtering to the solution of integral equations encountered in indirect sensing measurements. J. Franklin Inst., 279, 95.

Verburg, J. and Strackee, J. (1974). Phaseless recursive filtering applied to chest wall displacements and velocities using accelerometers. Med. Biol. Engng., 4, 483.

Verburg, J. (1975). Transmission of vibrations of the heart to the chestwall; Physics, physiological significance and ultility. In : Cardio-circulatory analysis of aspects of diagnosis, assist, therapeutic and prosthetic devices. 3, Part II. Delft Univ. Press.

Vollenhoven, van E., Wallenburg, J., Rotterdam, van A. et al., (1968). Calibration of contact microphones for phonocardiography. Med. Biol. Engng., 6, 71.

Vollenhoven, van E. (1971). Calibration of contact microphones applied to human chest wall. Med. Biol. Engng., 9, 365.

Wayne, H.H. (1973). Noninvasive technics in cardiology. Year Book Publishers, Inc.

Zalter, R., Hardy, H.C. and Luisada, A.A. (1963). Acoustic transmission characteristics of thorax. J. Appl. Physiol., 18, 428.